El-Sum Consultants

74 Middlefield Road • Atherton, California 94025 • (415) 324-3112

NASA CR-114636

AVAILABLE TO THE PUBLIC

DIAGNOSTIC TECHNIQUES FOR MEASUREMENT OF AERODYNAMIC NOISE IN FREE FIELD AND REVERBERANT ENVIRONMENT OF WIND TUNNELS

BY

H. M. A. EL-SUM AND O. K. MAWARDI

(MAY 1973)

Prepared under contract no. NAS2-6872

by

EL-SUM CONSULTANTS
Atherton, California

for

AMES RESEARCH CENTER
NATIONAL AERONAUTICS AND SPACE ADMINISTRATION

TABLE OF CONTENTS

		Page
FOREWORD		vii
SUMMARY		viii
GENERAL INTRODUCTION		1
	PART I	
	ACOUSTIC CHARACTERISTICS OF TURBOJET AS A NOISE SOURCE	
1.1	General Remarks for Free Field Sound Generation	5
1.1.1	Turbulent Jet Noise	5
1.1.2	Blade Passage Noise	9
1.2	Effect of Walls on Radiation Field	14
1.2.1	Quasi-reverberant Regime of Tunnel	14
	PART II	
	THE DETECTION OF DIRECT SOUND FROM A SOURCE IN A REVERBERANT BACKGROUND	
2.1	Introduction	21
2.2	Directional Microphones	21
2.2.1	Tubular Microphones	22
2.2.2	Linear Arrays	25
2.3	Correlation Detectors	31
2.4	Concluding Remarks on Direct Detection of Sound Source in a Reverberant Background	32
	PART III	
	OPTICAL DIAGNOSTIC METHODS	
3.1	Introduction	34
3.2	Holographic Interferometry	34
3.3	Acoustical Holography	36
3.3.1	Direct Acoustical Holography	36
3.3.2	Instantaneous Acoustical Holography	36
3.3.3	Spectral Analysis and Source Localization From Acoustical Holograms	37

TABLE OF CONTENTS (Contd)

Page

3.4 Optical Processing of Wideband Acoustic Signals 38
3.5 Concluding Remarks on Optical Diagnostic Methods 38

PART IV

DESIGN CHARACTERISTIC OF A HIGH DIRECTIVITY ACOUSTIC ANTENNA

4.1 Basic Considerations 39
4.2 Steering of Antenna 40
4.3 Beam Sharpening 47
4.4 Testing of Antenna 49
4.5 Evaluation of the Antenna and its Control 51
4.5.1 Procedure 51
4.5.2 Results 52

PART V

CONCLUSION AND RECOMMENDATIONS

5.1 Conclusion 71
5.2 Recommendation for Further Studies 72

BIBLIOGRAPHY 74

APPENDIX A: Earlier Study of the Project A-1

APPENDIX B: Acoustic Antenna, Electronic Steering Control (Model 909B) - Operating Manual B-1

LIST OF FIGURES

Number		Page
1.	Acoustic power level as a function of parameter ξ	7
2.	Normalized sound spectrum for a cold airjet	8
3.	Distribution of sound sources along jet	10
4.	Directivity patterns for fluctuating force terms in stator-rotor interactions	13
5.	Contours of equal acoustic pressure amplitude in a circular conduit	17
6.	Line or tubular microphone	23
7.	The directional characteristics of the microphone shown in Fig. 6 as a funetion of the ratio of the length of the line to the wavelength	23
8.	Tubular microphone with acoustic delays to effectively increase the length "ℓ"	24
9.	Effective directivity of line microphone with delay line as shown in Fig. 8	25
10.	Directivity pattern for $d/\lambda = 0.75$ and $L = 1/8$	29
11.	Connections for 13 microphones arranged in three batches	30
12.	Typical block circuit diagram for one of the batches of Fig. 11	31
13.	Geometry of antenna array	39
14.	Minor-lobe amplitude as a function of the length of the array	41
15.	Circuit diagram for one of the elements of phase shifter	44
16.	Calibration of delay line phase shifting network	45
17.	Steering calibration of antenna for d/λ values referred to 500 cps	46
18.	Interconnection for "A" channel	48

LIST OF FIGURES (Contd)

Number		Page
19.	Scatter in the characteristics of the phase shifters for the "A" channel	50
20.	Fifteen charts of runs made to evaluate the acoustical antenna performance	54
21.	Acoustical antenna response at 500 Hz	70
22.	Acoustic antenna secondary lobe dB drop and angular resolution at 6 dB vs frequency	71
A-1	Jahoda's scheme for density autocorrelation holographic mapping	A-18
-	Acoustic antenna electronic steering control, front and back views	B-ii
B-1	Geometry of acoustic antenna	B-3
B-2	Acoustic antenna, block diagram	B-5
B-3	Acoustic antenna, positions of selector switches for antenna steering	B-6
B-4	Acoustic antenna, calibration curve of steering dials	B-8

LIST OF TABLES

Number		Page
1.	Numerical values of sensitivity coefficients valid for $(d/\lambda) \geq 1/2$	28
2.	Phase shift for microphones in a linear array	42
3.	Tchebycheff correction (shading) for five transducers per linear array	47
4.	Summary of results of antenna evaluation	53
-	Noise sources from various flow regimes	A-10
-	Tchebycheff correction coefficients for acoustic antenna model 909B	B-7

FOREWORD

This is the final reporting on a one man-year study of techniques to analyze aerodynamic noise sources in a free field and in the reverberant environment of the 40 x 80 foot wind tunnel at Ames Research Center (ARC). The project was funded by ARC-NASA, under contract No. NAS 2-6872.

The goal of this project, in a broad sense, was to identify and define techniques for studying aerodynamic noise generating mechanisms without perturbing the flow. Identification and definition of noise sources entails localization of such sources and determination of their characteristics (spectrum, strength, coherence, phase, etc.) under various flow regimes. Both analytical and experimental investigations were to be conducted. The experimental task was to be done in the 40 x 80 foot wind tunnel at ARC; consequently, the adopted technique of measurement was to be capable of discriminating between the true aerodynamic noise sources and the reverberant or background noise in that tunnel.

SUMMARY

This report covers: (a) phase I, the theoretical analysis of the various diagnostic techniques to define and identify noise sources in free field and, more importantly in ARC 40 x 80 foot wind tunnel which is quite reverberant, and (b) phase II, the design and testing of an acoustic antenna with an electronic steering control. Such a scheme for noise diagnosis was agreed upon because of its relatively low cost, short time needed for its design and construction and its promised good performance. Two models (909 and 909B) of the acoustic antenna electronic steering control were built. The second model has higher directivity (10° half angular resolution at 6 dB) as well as higher frequency selectivity. The antenna utilizes two crossed linear arrays of microphones, (5 microphones in each array); each array can be steered independently from 0° to 180°. The other important feature of the design is that the steering is independent of the acoustic frequency. The output in the first model is the sum of the outputs of the two arrays; the second model measures the product of the two arrays.

In the course of study, the theory of the acoustic characteristics and reverberation modes of wind tunnels was developed to show that a wind tunnel is quasi-reverberant, having a characteristic length ℓ of the order of magnitude of a wavelength. For a point source, on the axis of the tunnel, approximately plane waves propagate beyond ℓ, and higher order modes attenuate rapidly within the volume specified by ℓ (Sec. 1.2.1). Extended and/or non-axial sources result in high order modes propagating down the tunnel.

In all cases, however, there is a quasi-reverberant field within the volume characterized by the length ℓ. Thus, estimating the true strength of a sound source radiating in the reverberant environment of wind tunnels requires measurement in extreme proximity of the source and hence highly directional schemes.

In addition, calculation was initiated to obtain the reflection caustics of various orders in the tunnel; however, the work was abandoned in favour of pursuing the wave theory to obtain the mode of reverberation and propagation.

Techniques (mainly optical) to correlate the results of the acoustical antenna noise measurements with the density fluctuations in a jet flow are pointed out for future implementation.

The theoretical phase of the study is detailed in parts I, II, III and Appendix A of the report. The discussion on the acoustical antenna and its electronic steering control is covered in part IV and Appendix B. Conclusion and recommendations for further extension of the project are expounded in part V. Two bibliographies appear following part V and Appendix A.

Units used throughout the report are the International System of Units and the customary units.

Valuable technical support in one aspect or another of this study was contributed by R. Bracewell, D. Bershader and P. Soderman, to whom the authors are indeed grateful.

GENERAL INTRODUCTION

In spite of recent advances in noise control engineering, it is good engineering practice[1] to perform full size noise tests on aircraft engines and/or components. These tests will allow the engineer to introduce final improving adjustments to the design, since our scaling laws for noise generation are not that precise.

Now, it is important to obtain the noise characteristics of these engines (or components) not only when the engine is idling on the ground, but also under flight condition. Whereas, engine testing in a wind tunnel provides satisfactory information about the aerodynamic behavior of the engine, unfortunately for the acoustical engineer conventional noise measurements in a wind tunnel yield data which are difficult to unfold for the purpose of extracting the free field noise characteristics of the engine being tested. When the engine is in a wind tunnel, the engine noise radiation pattern as well as its spectrum are both distorted. At low Mach numbers the acoustic power emitted by the engine, however, is not affected by its being placed inside the wind tunnel, if the tunnel test section is large enough so as not to affect the aerodynamic performance of the engine.

One of the main reasons which makes it difficult to obtain the free field noise radiation pattern from wind tunnel measurements is the interfering presence of the walls. Indeed, in addition to the noise signal directly radiated from the engine under test, a detector would pick up signals reflected from the walls. Since the walls of the wind

tunnel are fairly good reflectors, this reflector or reverberant signal can be comparable to the directly radiated signal. It is important to point out that had one used an acoustic wattmeter of highly directional characteristics, the directivity pattern of the source (i.e., engine under test) could have been obtained. Unfortunately, at the present, no acoustic wattmeters with such desirable highly directional properties are available, so that one has to resort to other means such as are described later in this report to measure the direct sound radiated. Another reason responsible for complicating the interpretation of wind tunnel noise testing is the noise created by the fans driving the air inside the tunnel. This broadband noise[2] not only represents a background noise, but it can interact with the source thus enhancing the noise signal sensed by the noise detectors (see pp. A-11, 12).

In order to achieve the main goals of this investigation, viz., the development of opto/acoustical diagnostic tools to study noise generation without perturbing the flow, first we have to understand the interpretation of the measurements made in the tunnel. Accordingly, we propose to select an engine whose aero-acoustic characteristics are fairly well understood. The general noise features of such an engine in the tunnel are then outlined. Now a turbojet run cold (say by moving the compressor blades by an external electric motor) meets many of our requirements:

(1) The acoustic characteristics of the resulting subsonic jet are well understood.[3]

(2) The noise produced by the blades of the rotating machinery of the turbojet is rich in harmonics and appears as discrete frequencies

superimposed over the wideband spectrum of the jet. The mechanism for this noise is that of the general class of axial flow compressor noise whose theory has been worked out in details.[4]

(3) A turbojet rather than a conventional jet flow is proposed because the discrete blade passage frequency of the turbojet can be used as a calibration signal for the diagnostic techniques we wish to use and will be explained later in this report.

A fundamental question we wish to emphasize here is that a highly directional microphone which can be used to discriminate between the direct sound radiated and the reverberant noise will allow us to evaluate the total acoustic power generated by the turbojet. As mentioned previously this acoustic power is unaffected by the presence of the walls of the tunnel.

Another important point is that the turbulent fluctuations in the jet also are unaffected by the presence of the walls. Consequently, the measurement of the physical properties of these fluctuations (mean square intensity, correlation, etc.) through an optical diagnostic method will lead us to an estimate of the equivalent strength and spatial extension of the acoustic sources whose radiated power is (presumably) known.

In part I of this report the general aero-acoustic features of the turbojet are described. In particular, we will summarize the scaling laws for noise production and the effect of the walls of the tunnel. In the second part of the report, we point out a suggested procedure for differentiating between the direct and reverberant and background noise. In the third part we discuss optical methods that will allow us to map the fluctuating (turbulent or coherent) part of the flow. Part IV deals

with the design characteristics of high directivity acoustic antenna and its electronic steering control. Two models of this antenna were built, tested and evaluated. The results of the evaluation are included in this section. Part V enumerates our recommendation of areas that needed further follow up.

To make this report thorough and complete, we reproduced earlier suggestions and technical analysis of this project in Appendix A. Appendix B is a copy of the operating manual of the acoustical antenna and its electronic steering control.

PART I

ACOUSTIC CHARACTERISTICS OF TURBOJET AS A NOISE SOURCE

1.1 General Remarks for Free Field Sound Generation

The noise generated by a turbojet engine is contributed by a number of processes, the two salient ones being the turbulent noise in the jet flow and that due to the blade-passage tones (from turbine, from compressor, etc.). The presence of any afterburner adds to the noise generation, through additional combustion noise. This latter contribution will be neglected here.

1.1.1 Turbulent Jet Noise

Extensive measurements[5] on turbojet noise have indicated that the jet noise has the following characteristics:[6]

(i) the efficiency of conversion of mechanical to acoustic energy is a slowly varying function of the Reynolds number at low mach numbers and follows an inverse fifth power law of the mach number. Actually, one has

$$P = K\left(\frac{V}{C_o}\right)^5 \left(\rho_o \frac{V^3}{2} d^2\right) \qquad (1)$$

where P is the acoustic power, V the exit velocity, ρ_o, C_o the density and velocity of sound at the ambient temperature and d the diameter of the jet nozzle. The constant K is typically of the order of 10^{-4}.

An empirical relation[7] which has been obtained from over two decades of data collection on turbojet noise yields the total acoustic

power as a function of a parameter ξ given by

$$\xi = W \left[1 + \left(\frac{.0136\ W}{Td}\right)^3\right] \text{ watts} \qquad (2)$$

where

$$W = \frac{d^2V^3}{(200)\ T}\ p \quad \text{watts} \qquad (3)$$

T is the exit temperature in degrees Rankine

V is the average exit velocity in ft/sec

p is the exhaust pressure in atmospheres

d is the diameter of the nozzle in inches.

The dependence of the acoustic power P on ξ is shown in graphical form in Fig. 1.

(ii) The sound spectrum is very broad and has an ill-defined peak. The peak frequency varies as V/d. The spectral density falls off on both sides of the peak and a generalized spectrum is shown in Fig. 2.[8]

(iii) The polar distribution for the intensity of the sound radiated follows a "butterfly" type configuration in which almost all the sound radiated is encompassed in an acute angle with the jet. The angle for the directional maximum is apparently a function of the frequency and of the mach number. Defining a Strouhal number fd/V, Lassiter and Hubbard[9] state that this angle varies from 30° to 40° for fd/V values of 0.4 to 1.5. For lower values of this ratio, the angle slowly decreases to 15° for a corresponding ratio of 0.2.

(iv) The mechanism for the generation of sound by turbulence becomes considerably more efficient in the presence of a mean shear.[10] This increase in efficiency can be explained by the fact that the

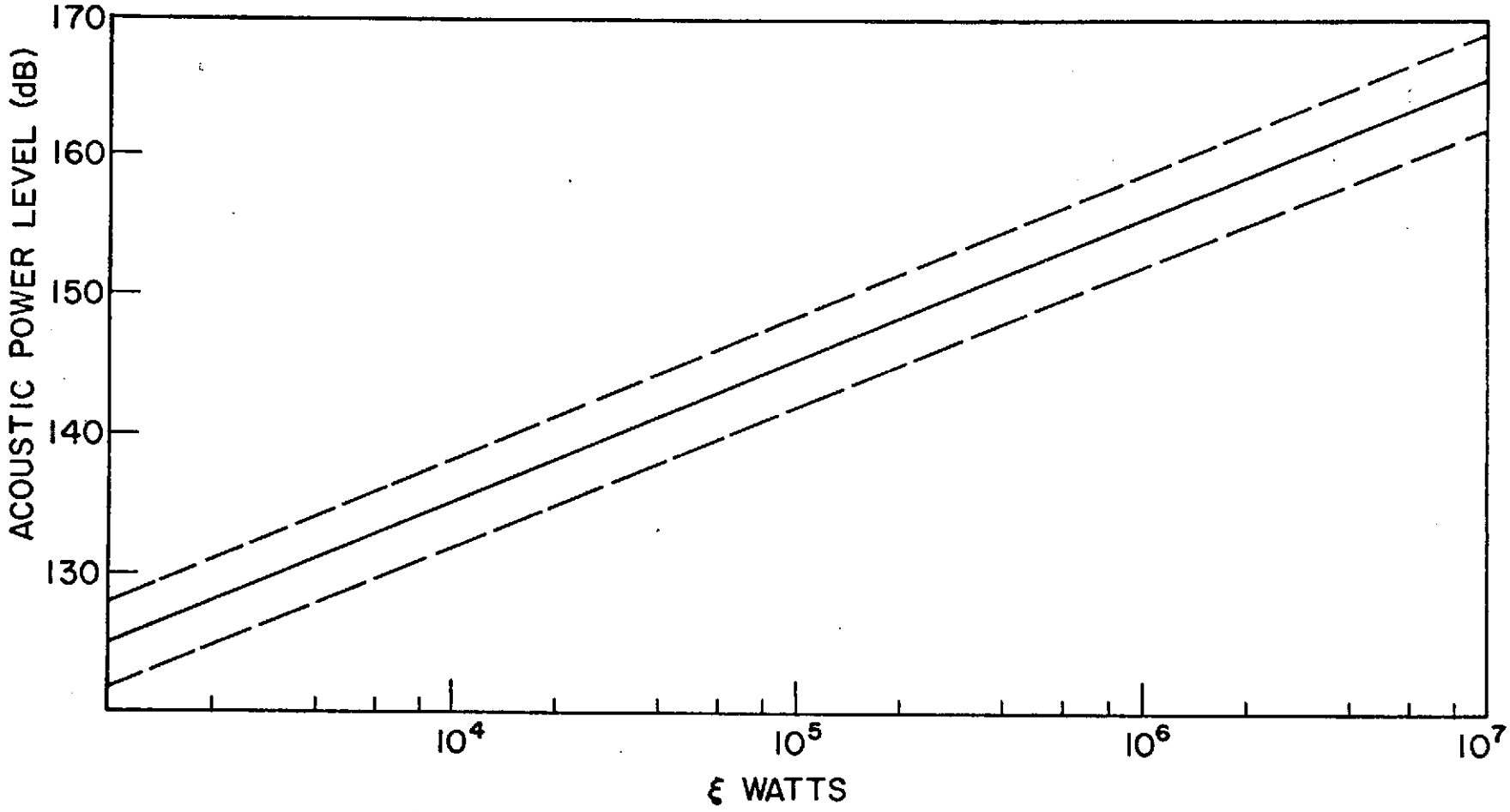

Fig. 1. Acoustic power level as a function of parameter ξ. Reference power level 10^{-13} watts (Ref. 7).

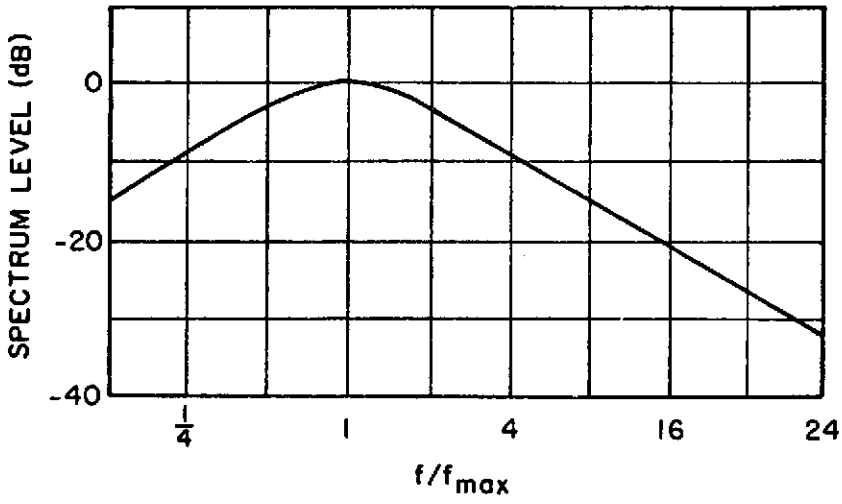

Fig. 2. Normalized sound spectrum for a cold air jet (Ref. 8).

momentum flux is considerably increased when it takes place in the direction of a large velocity gradient. Lighthill, using the result of Proudman[11] was able to show that the order of magnitude of the fluctuations of the gradient which contribute most to the rate of shear strain and hence to the sound production is about $8\left(\overline{v^2}\right)^{1/2}/L$, where L is the scale of the turbulence. Proudman had demonstrated that for isotropic turbulence the large nondissipating eddies contribute most to the sound production while the energy dissipating eddies of size much less than L do not radiate at all. In the presence of a mean shear the intermediate eddies become the dominant contributors to the sound production.

Ribner[12] was able to find, by combining Lighthill and Proudman theories to regions of similar flows for a subsonic jet, the spatial distribution of the equivalent noise sources along the jet. His calculations referred to the noise power emitted by a slice of jet indicate that

this power is essentially constant with distance (x) in the initial mixing region of the jet, then further downstream about 8 to 10 diameters from the nozzle the power falls off very rapidly with an x^{-7} power law. In this region of the jet the turbulence is fully developed (Fig. 3). The bulk of the noise is hence produced in this near region to the nozzle. These very important calculations are in substantial agreement with experimental observations.

1.1.2 Blade Passage Noise

It is clear that any detailed prediction of the noise generated by the turbine and compressor of a turbojet would require an accurate knowledge of the configuration of these components (i.e., profile of blades, aerodynamic performance, etc.). What we will do instead is to summarize the important features of the noise production in terms of design parameters. This point of view incorporates the results of intensive research on this subject. One of the investigations we have used extensively[13] in fact includes over 100 references on blade passage noise. The characteristic features of this noise are:

(i) The predominant radiation mechanism is through the fluctuating forces on the blades. The stator and rotor blades are equally important to the noise production. The coherent noise radiated is not only at the blades passage frequency but is rich in harmonics. Increasing the rotor-stator separation will preferentially reduce the higher harmonic radiation by the stator, while increase of stator-rotor separation will reduce all harmonics of the noise generated by the rotor.

(ii) The overall power and directionality of the noise radiated are determined by the source parameters, the rotational speed and blade/vane

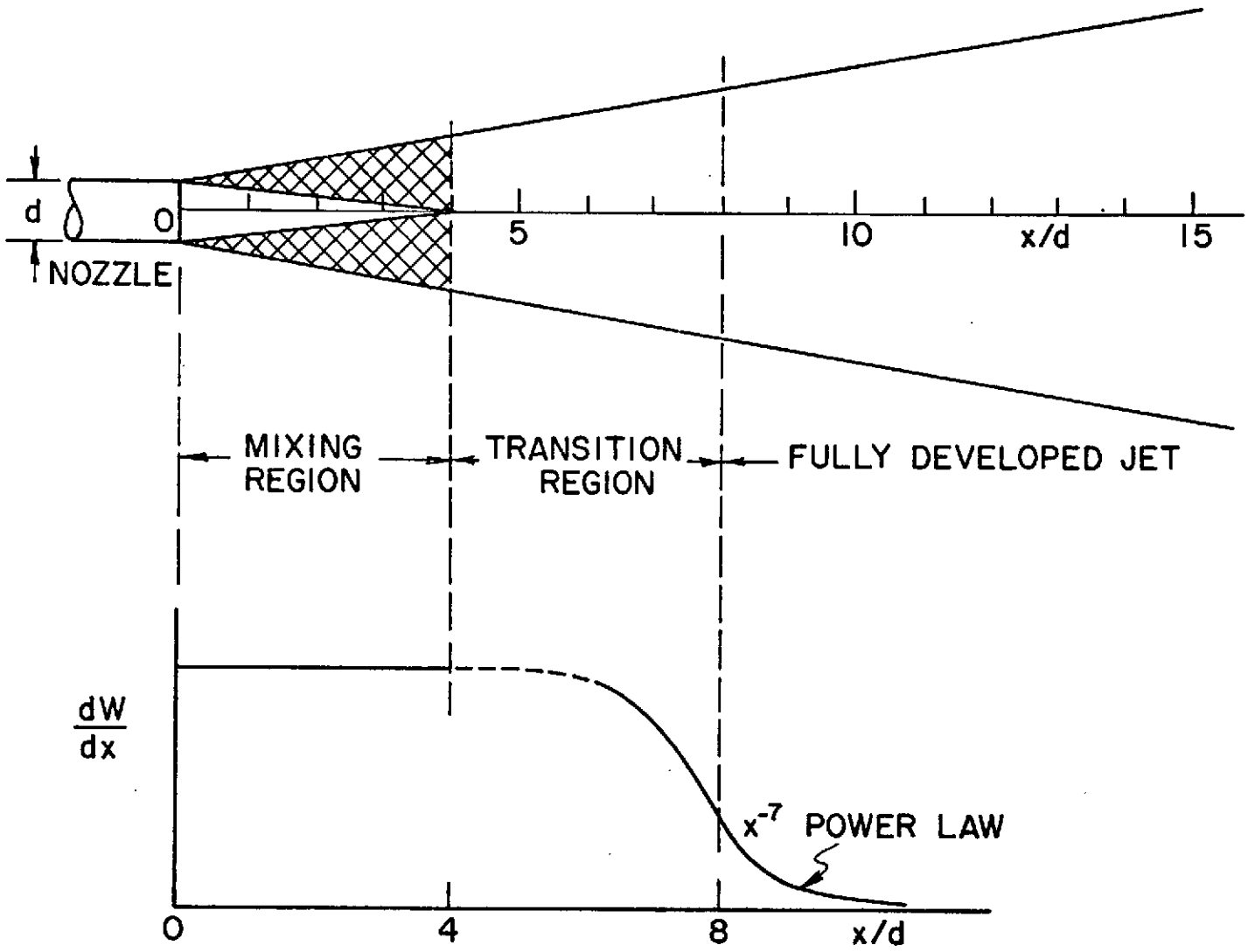

Figure 3. Distribution of sound sources along jet (from Ref. 12).

numbers. From a careful consideration of the fluctuating lift on the blades, Lawson[13] finds that the acoustic power radiated at the fundamental frequency of the blade passage frequency is given approximately by

$$W \approx \frac{\rho_o \, C_D \, B A_b^2 \, U_1^5}{128 \, A_e \, a_o^2} \tag{4}$$

where A_b is the total area of the blades

A_e is the effective area based on an effective radius R, i.e., $A_e = \pi R^2$

C_D is the aerodynamic drag coefficient for the blade

U_1 is the relative velocity at some effective radius

ρ_o, a_o are the density and sound velocity respectively for ambient conditions and

B is the number of blades.

Since it is more conventional to refer the noise production as a function of the mechanical tip speed V_T for the blades through the relation

$$U_1 = \frac{R \, V_T}{\sqrt{2} \, R_T} \tag{5}$$

where R_T is the tip radius, and when a 45° angle between U_1 and V_T is assumed, one finds that Eq. (4) reduces to

$$W = \frac{\rho_o \, C_D \, B}{128 \, a_o^2} \left(\frac{A_b}{A_e}\right)^2 \left(\frac{R}{R_T}\right)^3 \frac{\pi D^2}{4} \left(\frac{V_T}{\sqrt{2}}\right)^5 \tag{6}$$

For the above expression, $R_T = D/2$. It thus becomes apparent that the noise generation depends on the fifth power of the velocity and on the area of the blades. The above formula is in good agreement with

experimental observation. Indeed when it is compared to empirically derived formulas such as that of Beranek[14] which is

$$\text{PWL (re } 10^{-13} \text{ watts)} = 135 + 20 \log_{10} \text{HP} - 10 \log_{10} q \qquad (7)$$

one finds that Eqs. (6) and (7) are equivalent since

$$\text{HP} = \text{horsepower} \sim D^2V^3$$

and $$q = \text{compressor discharge in ft}^3/\text{sec} \sim D^2V.$$

Using reasonable values for the parameters such as

$$A_b/A_e = 0.5$$

$$R/R_T = 0.8$$

$$C_D = 0.2$$

one finds that Eqs. (6) and (7) have the same dependence on D and V. Equation (6) underestimates the power by a few dBs. This is expected since Eq. (6) is the power radiated for the fundamental only. When the contribution of the harmonics are added the agreement becomes very close.

(iii) An important property (to our study) of the blade passage tone is the directivity of the radiation pattern. This pattern is readily obtained from the fluctuating rotating forces on the blades. The equivalent sources turn out to be equivalent to a ring source. Consequently appreciable side lobes will appear whenever the ring size becomes comparable to the (Doppler-shifted) wave length. Because of the presence of the air flow, more sound is radiated forward (out of the compressor inlet) than rearwards.

Typical directivity patterns are shown in Fig. 4.

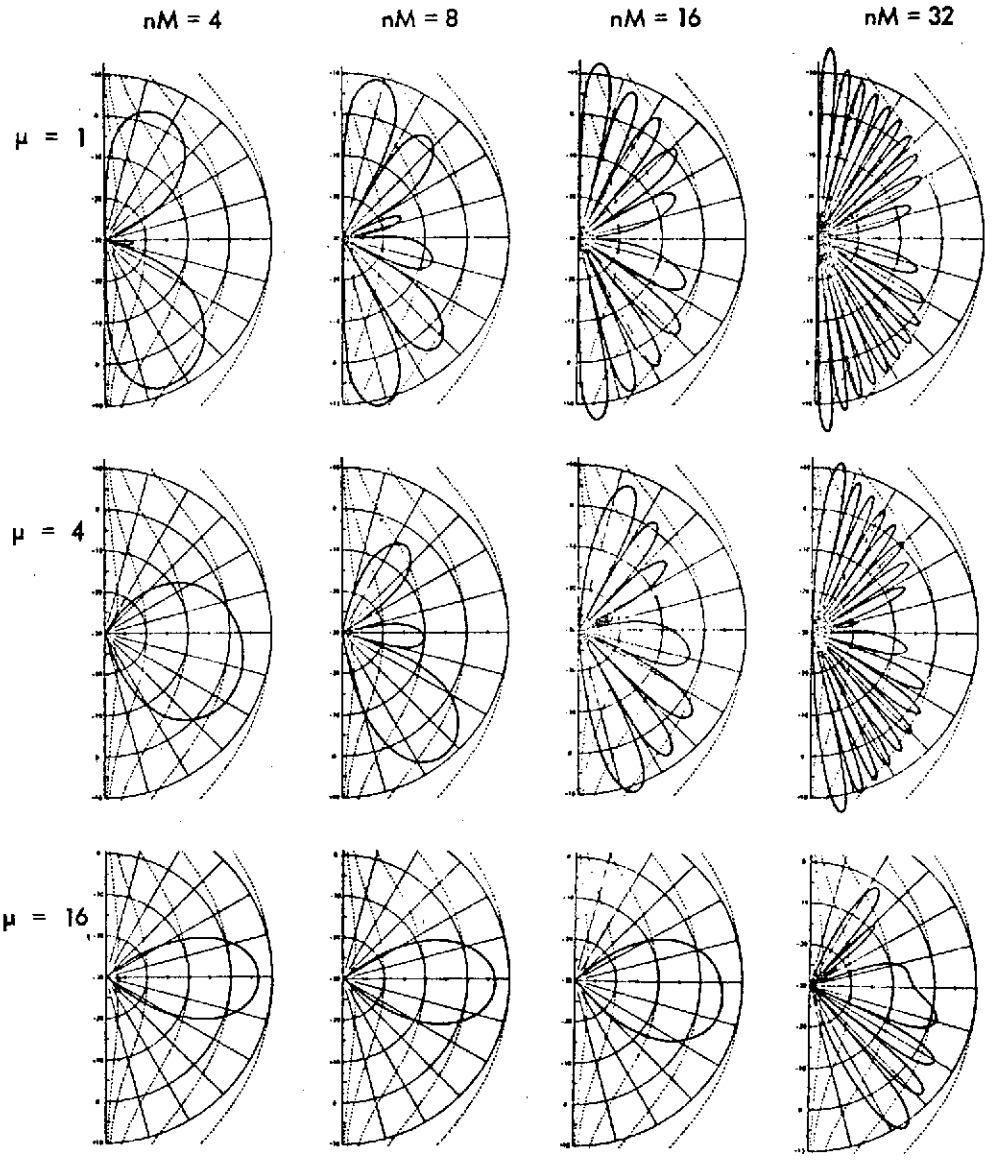

Figure 4. Directivity Patterns for Fluctuating Force Terms in Stator-Rotor Interactions. Up is forward and represents direction of flow. $M = \Omega R/a_o$ the rotational mach number of the rotor, n = sound harmonic number and the modal order μ = (mB-kV) where m is the order of the harmonic, B is the number of blades, k the wave number and V the velocity (from Ref. 13).

1.2 Effect of Walls on Radiation Field

Since the walls of the wind tunnel are fairly rigid and because the acoustic signals we are dealing with are mainly in the audible range, the walls of the tunnel behave as good acoustic reflectors.

The wind tunnel as an acoustic enclosure presents some specific peculiarities. In spite of its length, the tunnel cannot be visualized from an acoustic point of view as an infinitely long duct to a sound source located in the test section of the tunnel. Neither is the tunnel an ideal reverberant chamber in the sense that the excited acoustic normal modes of the tunnel are in equilibrium with each other. More specifically, the combination of sound source plus tunnel does not lead to a "diffuse" acoustic field, with a well defined uniform "reverberant" energy density. Instead, one expects a large number of modes to be excited. Some, whose $\underline{k}$ vector is along the axis of the tunnel will be akin to "travelling, hence nonreverberant modes", others will be standing modes with a likelihood of establishing a quasi-reverberant situation.

We are after all searching for diagnostic techniques that will allow us to differentiate between the direct and "reflected" sound in the tunnel. The question of paramount importance, therefore, is the estimate of a mode "mixing length". A corollary to this estimate is the criteria for mixing of lateral or cross modes of the tunnel.

1.2.1 Quasi-reverberant Regime of Tunnel

When a simple point source is placed in an enclosure, then under steady state conditions, a large number of normal modes are excited. In the limit of high frequency and if the source is not near a wall, so that

the different standing waves excited have their nodal surfaces distributed enough at random that one can use the average value of the intensity of these various modes, the reverberant sound intensity in the enclosure is[15]

$$\overline{W} = \frac{2\pi \rho_o Q_o^2 \nu^2}{a_o^2 \gamma} \tag{8}$$

where Q is the strength of the source

ν is the sound frequency of the source

γ is the average sound absorption of the walls, and

ρ_o, a_o are as before the density and velocity of sound, respectively.

Close to the sound source the wave behaves as if the source were in free space. Consequently, had one been interested in measuring the sound directly radiated from the source, a proximity measurement would yield the required information. On the other hand, when the source is extended in space proximity measurements are no longer adequate to allow one to determine the strength distribution of the sound source. A typical example to clarify this point is seen by considering the case of a dipole-like source: the nul point of the dipole would not be discernible in view of the background reverberant signal. It is clear, therefore, that some other method must be designed to map the source distribution.

But before we actually discuss an appropriate diagnostic technique it is important to establish whether it is indeed possible for a reverberant field to exist in an infinitely long conduit (highly idealized wind tunnel). To simplify the mathematical calculations we demonstrate

the existence of this reverberant field on a conduit of circular cross-section. The conclusions can be extended to a conduit with a different cross section, but obviously the criteria are bound to be numerically, but not qualitatively, different.

We begin by calculating the sound pressure field inside a conduit with rigid walls and due to a simple source placed on the axis of the conduit. It is readily shown from elementary acoustic theory, that when the source has unit strength the field is given by

$$p \sim \sum_{n=0}^{\infty} \frac{J_o(\beta_n r)}{\beta_n J_o^2(\beta_n a)} \exp\left(i\sqrt{k^2 - \beta_n^2}\,|z|\right) \qquad (9)$$

where k is the wave number $2\pi/\lambda$

$(\beta_n a)$ is the n^{th} root of $J_1(\beta a) = 0$, and

a is the radius of the conduit.

The field is described by means of a cylindrical coordinate system whose polar axis coincides with the axis of the conduit. Since the source is symmetrically located on the axis, there are no normal modes with azimuthal dependence.

Now Eq. (9) indicates that any mode of order n propagates whenever $k > \beta_n$, otherwise it is damped. The lowest mode for $\beta_o = 0$ corresponds to the dominant plane wave mode. Suppose we consider all frequencies with $k \leq \beta_1$. Consequently, all modes higher than the fundamental are attenuated. Figure 5 shows graphically the evolution of the pressure distribution from that due to a point source to that of a plane wave.

Now, in the interim region from the origin to a length ℓ which is determined on page 18, the higher order modes do not propagate, and classical theory indicates that the energy associated with these modes

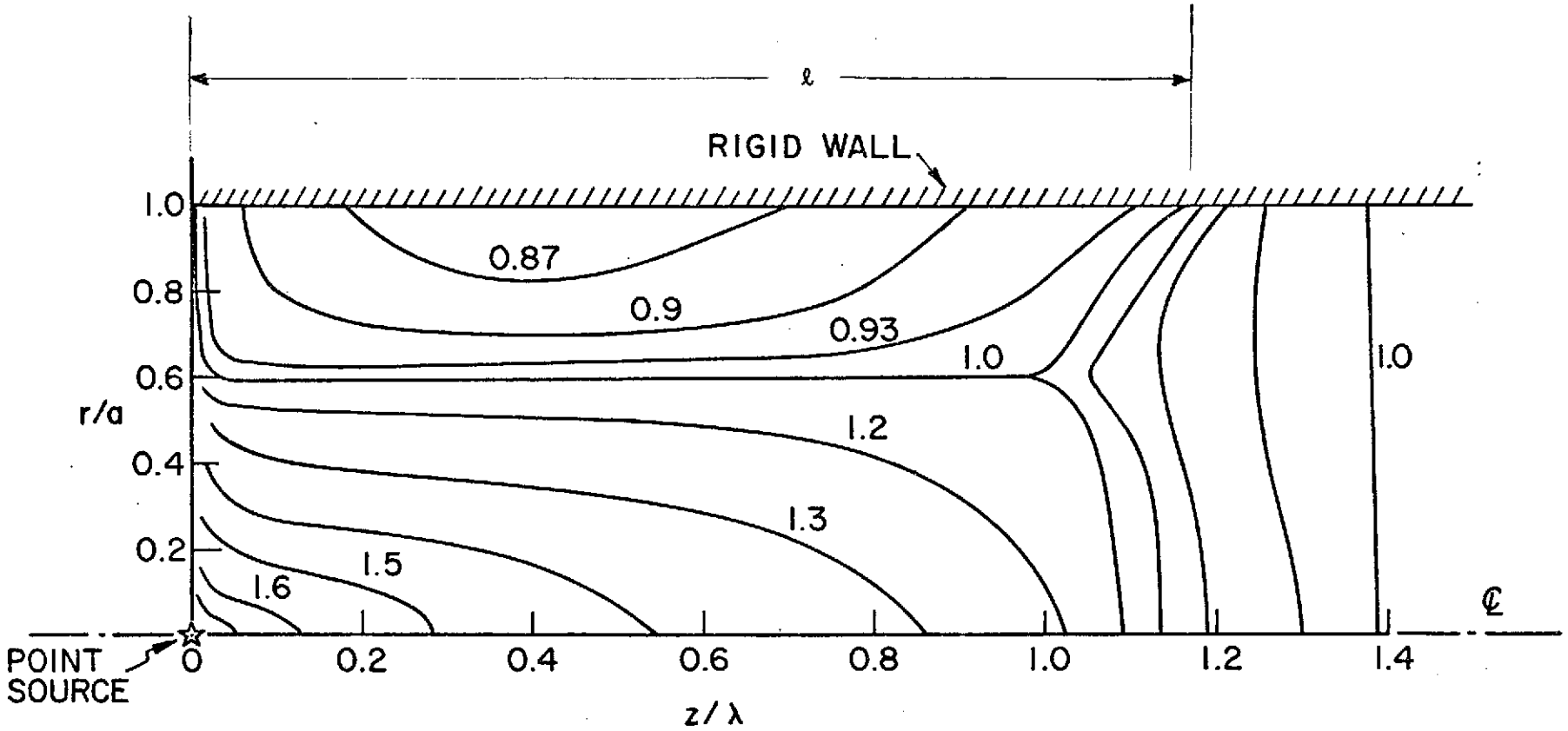

Fig. 5. Contours of equal acoustic pressure amplitude in a circular conduit. Notice that beyond $z/\lambda = 1$, a plane wave begins to emerge.

represent a reactive (nondissipative) energy. Actually, these modes are trapped and bounce back and forth off the walls of the conduit. But this is the usual situation for a reverberant field. Consequently, a reverberant field can be set up in a conduit. but it is restricted to the band of frequencies defined by $k < \beta_1$ within the characteristic length ℓ (a function of k).

An estimate of the length "ℓ" (a distance at which plane wave emerges) can be had by considering the exponent of Eq. (9). Manipulation of this quantity leads to

$$\sqrt{k^2 - \beta_n^2}\,|z| = \sqrt{(2\pi)^2 - (\beta_n a)^2 \left(\frac{\lambda}{a}\right)^2}\,\left|\frac{z}{\lambda}\right|$$

Since $(\beta_1 a) = 3.831$, the critical value for a/λ is

$$\left(\frac{a}{\lambda}\right) = \frac{3.831}{2\pi} = 0.61 \qquad (10)$$

If we require, on the other hand, for the n=1 mode to decay by a factor e over a wavelength, then we must have

$$\frac{a}{\lambda} = \frac{3.831}{\sqrt{1 + (2\pi)^2}} = .602 \qquad (11)$$

The characteristic length ℓ is then

$$\ell = \left(\frac{a}{.602}\right) \qquad (12)$$

i.e., this length is of the order of a diameter.

The above estimate for the characteristic length "ℓ" is conservative since it was reckoned on the basis of a symmetrically located source on the axis. If the source is off axis, normal modes with azimuthal dependence appear in Eq. (9) and the corresponding length ℓ becomes

longer. Furthermore, if instead of a simple source we had a dipole source, then a larger number of modes are excited.

The conclusion of these arguments is that in spite of the conduit like behavior, it is expected that the sound field in the test section of the wind tunnel to behave like a fully developed reverberant field. As we saw earlier, the sound source is approximately 8 to 10 turbojet nozzle diameters in extension and is equivalent to a mixture of lateral and longitudinal quadrupoles. Since the nozzle diameter is much smaller than the tunnel characteristic dimensions (40x80 ft), the sound field in the vicinity of the source is definitely reverberant in behavior. This does not apply, however, to the whole tunnel. We thus like to refer to the field as quasi-reverberant.

Before we close this phase of the discussion, we will make a few remarks concerning the mixing of cross-modes. The exciting of cross modes in the wind tunnel is very likely because of the rotating fluctuating lift forces on the blades of the compressor. The corresponding source term becomes a very efficient exciter of the higher order so-called "swirling" modes. This question is of importance to this study because any mixing of these modes would tend to accelerate the onset of reverberation conditions. We discussed above the situation for a jet alone. Now, when the compressor noise is introduced in the discussion we have to take into consideration the fact that the large number of coherent fluctuations associated with these swirling modes are in fact true sources; yet they could be mistaken for random reverberant noise.

One convenient way of treating this dilemma is to rely on a correlation for the spectral density of these modes. Bolleter and Crocker[16]

have studied this question at length and they were able to show that these higher order modes can interfere constructively or destructively depending on the frequency and the distance from the source. An axial interference "wavelength" L between an "mn" and a "pq" mode (the two numbers, refer to azimuthal and radial nodes order) can thus be found and which is given by

$$L = \frac{\lambda}{\left[1 - (\omega_{mn}/\omega)^2\right]^{1/2} - \left[1 - (\omega_{pq}/\omega)^2\right]^{1/2}} \qquad (13)$$

here ω_{mn}, ω_{pq} are the resonance frequencies of the modes and λ is the wave length in free space. The presence of "L" is an indication that such fluctuations are indeed associated with sources and do not represent a spurious noise signal.

PART II

THE DETECTION OF DIRECT SOUND FROM A SOURCE IN A REVERBERANT BACKGROUND

2.1 Introduction

As pointed out in Part I, the measurement of the direct sound radiated from a source in an enclosure can be done by sampling the sound field in the immediate vicinity of the source provided that the acoustic strength of the source is much higher than the equivalent strength of the reverberant sound in the background. If this criterion is not fulfilled, a correlation detection technique has to be used to be able to differentiate between the direct and background reflected sound.

Now the use of highly directional microphones allows one to measure the sound close to the source and this without having to place the microphone close to the source. We will show later in this part of the report that if a correlation procedure is to be used then the use of directional microphones has the very great advantage of enhancing the signal-to-noise figure of merit. Directional microphones are thus highly desirable instruments in measuring the direct sound. In the following sections we first discuss the design of directional microphones and in a subsequent section we outline a correlation detection method.

2.2 Directional Microphones

An extensive amount of investigation has been done towards developing a highly directional sound detector. The basic concept used has been

one of preferential wave interference to reinforce the reception in a particular direction more than in an another. Two methods have been used with success. In the first method, the sound collected from different places on a line is chanelled to a single microphone. Several devices have been employed[17,18,19,20] to adjust the acoustic delays in the separate channels so that interference between the signals from these channels would lead to the required directivity. A typical example of this class of microphones is the so-called "tubular or line microphone". In the second method, several microphones are arranged in an array[21] (linear or other) and the electrical output is mixed to allow the phase interference necessary to provide the directional response. Experience acquired in the design of directional antennas has been extended to the construction of equivalent acoustic detectors. We now proceed to discuss the design of these two types of microphones.

2.2.1 Tubular Microphones.

These consist of a microphone constructed out of a number of small tubes with the open end, as pick up points, equally spaced on a line. The other end is terminated in a velocity or pressure microphone. No matter which termination is used it is imperative that the small tubes are terminated into the correct acoustic impedance (ρC) to avoid the excitation of standing waves in the small tubes. It is readily shown that the directivity R_θ of such a microphone, Figure 6, is given by [Ref. 18]

$$R_\theta = \frac{\sin\left[\frac{\pi}{\lambda}(\ell - \ell \cos\theta)\right]}{\frac{\pi}{\lambda}(\ell - \ell \cos\theta)} . \qquad (14)$$

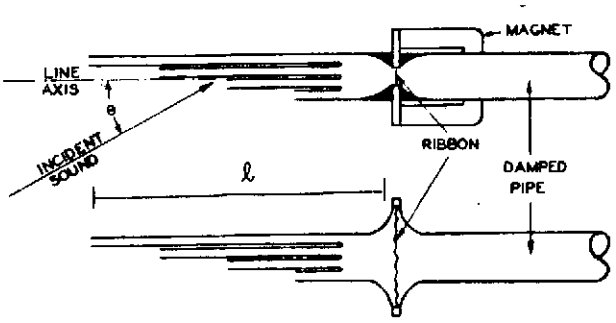

Fig. 6. Line or tubular microphone. Useful directivity on the line axis. This microphone consists of a large number of small pipes arranged in a line with the distance from the opening of each pipe to the common junction decreasing in equal steps. The system is terminated in a ribbon element and an acoustical resistance. Another alternative is to terminate the system in a pressure microphone. No damped pipe is then needed.

In the above expression ℓ is the length of the line. The directivity for a large number of small pipes ($n \to \infty$) is independent of n. The corresponding angular dependence is shown in Fig. 7.

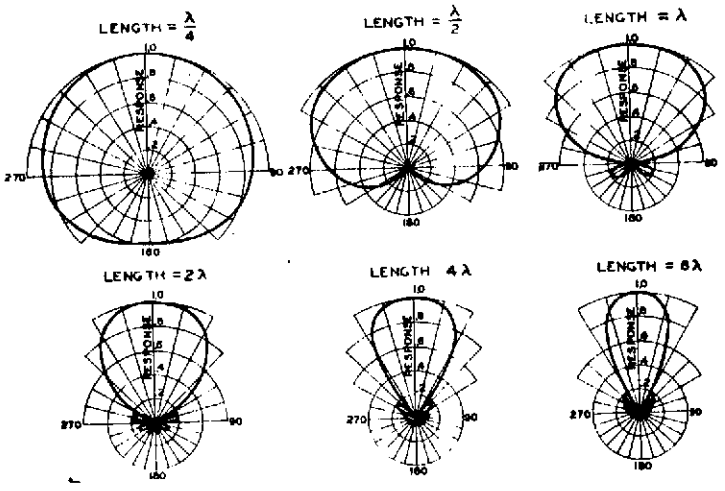

Fig. 7. The directional characteristics of the microphone shown in Fig. 6 as a function of the ratio of the length of the line to the wavelength. The polar graph depicts the output, in volts, as a function of the angle, in degrees.

In order to effectively increase ℓ and hence improve the directivity, Olson[18] has suggested to add a delay in each line. The amount of delay added is proportional to the distance from the pipe opening to the pickup point nearest the common termination (Fig. 8).

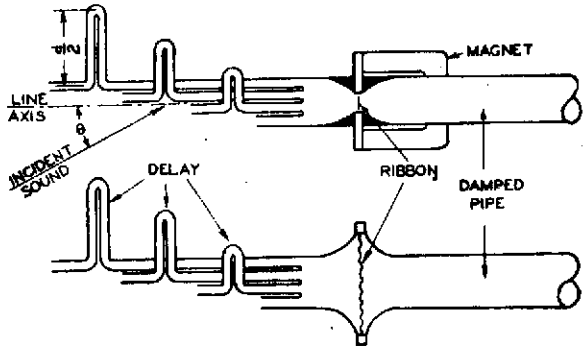

Fig. 8. Tubular microphone with acoustic delays to effectively increase the length "ℓ".

As one would expect it, the same directivity factor is used except that the length is now increased. In fact, one obtains

$$R_\theta = \frac{\sin\left[\frac{\pi}{\lambda}(\ell - \ell\cos\theta + d)\right]}{\left[\frac{\pi}{\lambda}(\ell - \ell\cos\theta + d)\right]} \qquad (15)$$

Here again R_θ has been calculated on the basis of $n \to \infty$. The behavior of Eq. (15) is shown in graphical form in Fig. 9.

The improved directivity of the microphone obviously does not represent the optimum that can be obtained with the present-day state of the art of antenna design. Furthermore it is seen that the sharpness of the directivity is very dependent on the ratio (ℓ/λ). Since at the low frequencies of the order of 100 Hz $\lambda \simeq 3$ meters, it is seen that a line microphone would be unusually unwieldy. Consequently a search for another diagnostic tool is desirable.

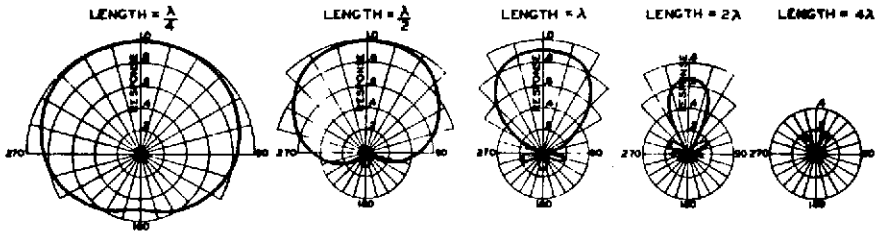

Fig. 9. Effective directivity of line microphone with delay line as shown in Fig. 8.

2.2.2 Linear Arrays

As mentioned above a linear array of identical (directional) microphones will have a response not unlike that of an ideal line or tubular microphone. In both cases, the phase mixing takes place. In one case it is with acoustic signals while in the other with the electrical (counterpart) signals. The advantage of the linear array, however, is that one does not have to be concerned with termination of a line as is the situation in the tubular microphone, where poor termination will cause mismatch and phase distortions. The drawback of the linear array is that one has to use several electro-acoustic transducers, hence they have to be compensated to make them identical. Furthermore, the cost is higher since one needs "n" transducers.

The directivity pattern of a linear array can be optimized by means of a number of methods[22] which have been developed over the years (Shading, Dolph-Tchebycheff correction, etc.). All these corrective procedures are much more easily adaptable to the electric circuits of the transducers, than to the all-acoustic network, so that there is an overall benefit in using an array of transducers.

Briefly summarized, the directivity of the array can be optimized on the basis of equal minor lobes pattern, by adjusting the spacing between the transducers, by altering the sensitivity of the transducers or by changing both. The other variables one has to consider are the number of transducers and the overall length of the array.

Now, Dolph[23] and Pritchard[24] have shown that the sharpest major lobe of a directivity pattern due to a linear array of equally spaced point elements is achieved when the elements sensitivity are such that all minor lobes in the pattern have the same relative amplitudes. It can also be shown that if the major half-width is specified, a maximum allowable spacing is uniquely defined independent of the number of elements or the specified minor lobe amplitude. The functional relation between the half-width, θ_L, and the spacing d_{max} was given by Pritchard[24] to be

$$\theta_L = \sin^{-1} \frac{1 - (d/\lambda)_{max}}{(d/\lambda)_{max}} \qquad (16)$$

If the spacing is made greater than $(d/\lambda)_{max}$, then the minor lobes no longer remain equal, neither is their relative amplitude small by comparison to the major lobe. It is clear, of course, that the sensitivity of the various elements on the area has to satisfy a dependence derived by means of a Tchebycheff optimizing technique. Indeed, if we use (2M+1) transducers equally spaced, so that one transducer is located in the center of the array, let us define the normalized sensitivity of the individual transducers by b_m. The directivity pattern function is expressed by

$$K_{2M+1}(\theta) = b_o + 2b_1 \cos\phi + \ldots + 2b_M \cos M\phi \qquad (17)$$

where $\phi = kd \sin \theta$. The conventional Tchebycheff procedure consists in first introducing the variable

$$x = \cos \phi,$$

the directivity of Eq. (17) is now rewritten as $K_{2M+1}(x)$. The required directivity pattern (i.e., one with equal minor lobes) is now found immediately from

$$K_{2M+1}(x) = LT_M(z) \tag{18}$$

where $z = (Ax + B)$ and T_M is the Tchebycheff polynomial of degree M. In the above expression L is the relative amplitude of the minor lobes (which are all equal) and A, B are constants. These constants are obtained by means of the following simple procedure. Let z_{oM} be the value of z which makes $T_M(z) = 1/L$, then

$$A = (z_{oM} + 1)/2 \quad \text{and}$$

$$B = (z_{oM} - 1)/2$$

The values of A, B and corresponding b_M for different M and L have been tabulated by Pritchard (Table I). In fact for L = 1/8 and M = 2 (i.e., 5 transducers), we have

$$\left.\begin{aligned} b_o &= 0.281\ 150 \\ b_1 &= 0.230\ 032 \\ b_2 &= 0.129\ 373 \end{aligned}\right\} \tag{19}$$

Now if we select θ_L of Eq. (16) to be about 10°, then $(d/\lambda)_{max} \approx 0.843$. Suppose we decide to have the maximum $(d/\lambda)_{max} = 0.750 < (0.843)$ then the directivity pattern is as shown in Fig. 10.

TABLE I

NUMERICAL VALUES OF SENSITIVITY COEFFICIENTS

VALID FOR $\left(\frac{d}{\lambda}\right) \geq \frac{1}{2}$ (After Pritchard, Ref. 23)

L dB	b_0	b_1	b_2
-39.7	0.340 206	0.247 423	0.082 474
-34.5	0.328 372	0.245 290	0.090 524
-29.8	0.314 516	0.241 936	0.100 807
-24.6	0.294 118	0.235 294	0.117 647
-22.0	0.281 150	0.230 032	0.129 393
-18.8	0.262 673	0.221 198	0.147 465
-16.9	0.250 000	0.214 286	0.160 714
-14.8	0.233 577	0.204 380	0.178 832
-13.8	0.225 513	0.199 154	0.188 090
-12.8	0.216 295	0.192 912	0.198 940
-12.0	0.208 450	0.187 387	0.208 388
-11.7	0.205 627	0.185 354	0.211 833
-10.6	0.193 090	0.176 053	0.227 402

Now, the linear array is needed to be used over the entire audio frequency range. Since this spectrum covers three octaves, the way we propose to build the array is to use one of the following alternatives.

1. Use 5 microphones whose sensitivities are weighted as indicated by Eq. (19). Between 0-100 Hz use a spacing of $d = 0.75\lambda = (0.75 \times 3.4) = 2.54$ m. Between 100-1000 Hz use a spacing of .254 m. Between 1000-10,000 Hz use a spacing of 0.0254 m. The way to achieve this arrangement is to have the microphones mounted on a track and the distances then adjusted from outside by a motorized system.

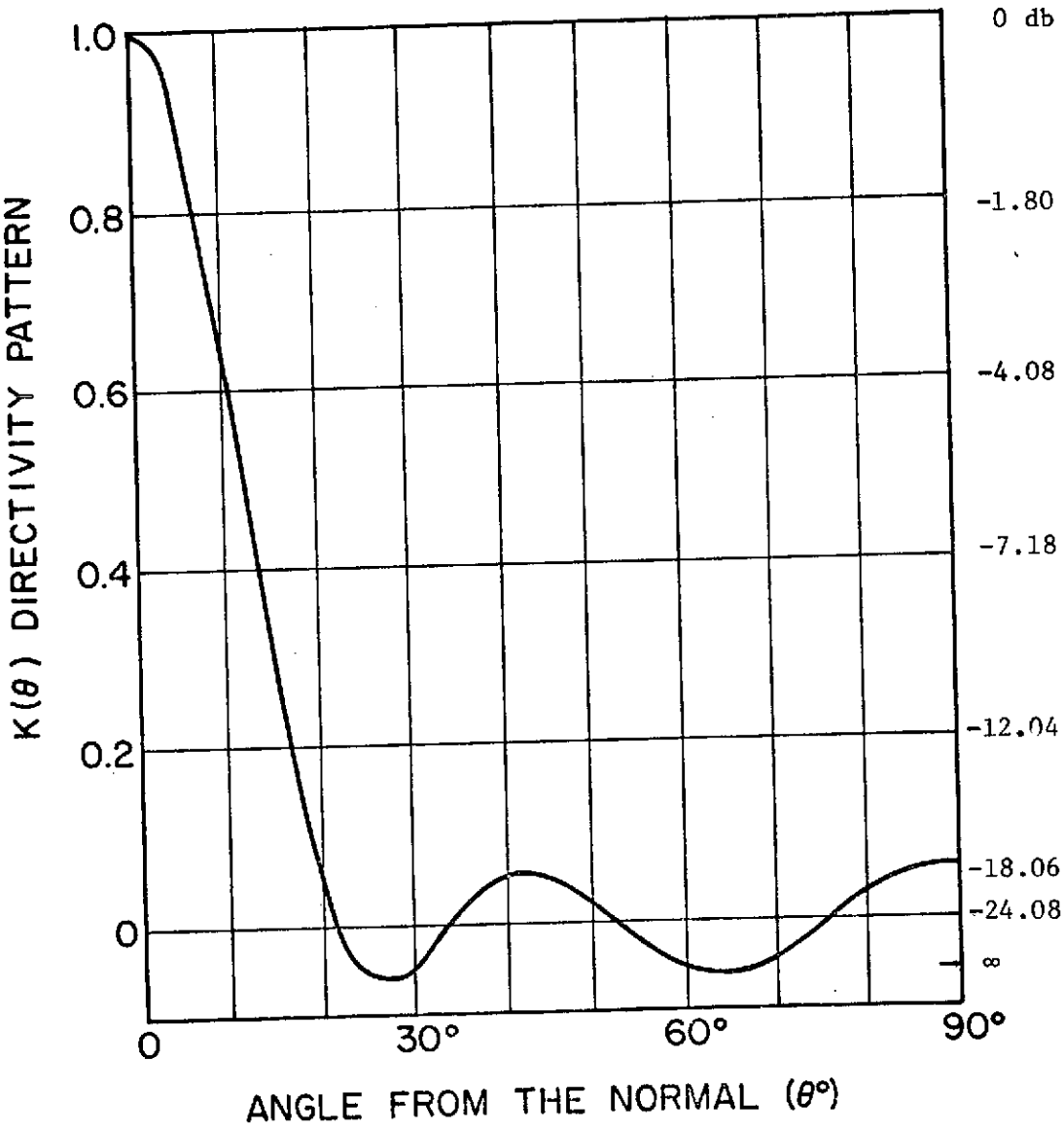

Fig. 10. Directivity pattern for $d/\lambda = 0.75$ and $L = 1/8$. Notice that as prescribed by the Tchebycheff criterion all minor lobes are of equal magnitudes.

The overall extension of the microphone is then 4x2.54 = 10.16 m or 30 ft. roughly in the maximum position. It is clear that with this arrangement we make the measurements in three steps, corresponding to three adjustments.

2. If it is decided to carry all measurements simultaneously, we use 13 microphones, spaced in three batches. The microphones are then connected as shown below in Fig. 11.

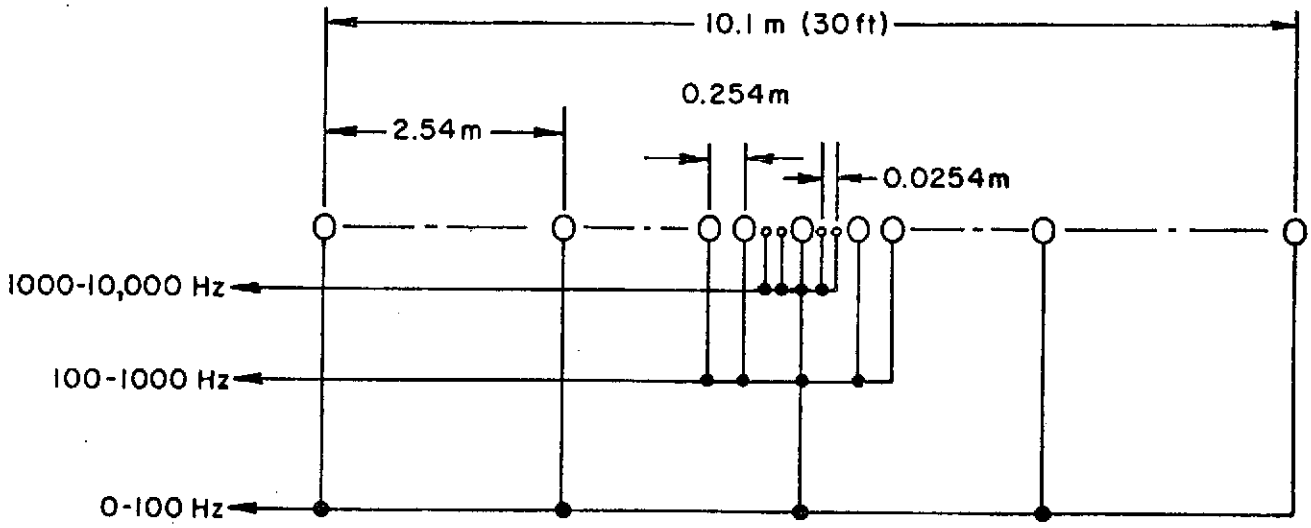

Fig. 11. Connections for 13 microphones arranged in three batches. Each batch has 5 microphones for the three frequency ranges 0-100 Hz, 100-1000 Hz or 1000-10,000 Hz. Microphones are separated by 2.54 m in the first batch, 0.254 m in the second and 0.025 m in the third.

It is to be understood that the weighting functions for the microphones must not be frequency dependent. This means that the adjustment is best done with purely resistive attenuating circuits. A typical arrangement is then as shown in Fig. 12. The criteria as to whether we use scheme ① or ② will depend on the cost and/or the need to have the measurements done simultaneously or not. This, of course, is set by the cost of running the wind tunnel, compared to the cost of microphones and circuitry.

We cannot complete this discussion without considering another method that has been used with considerable success in getting directivity through a correlation concept.

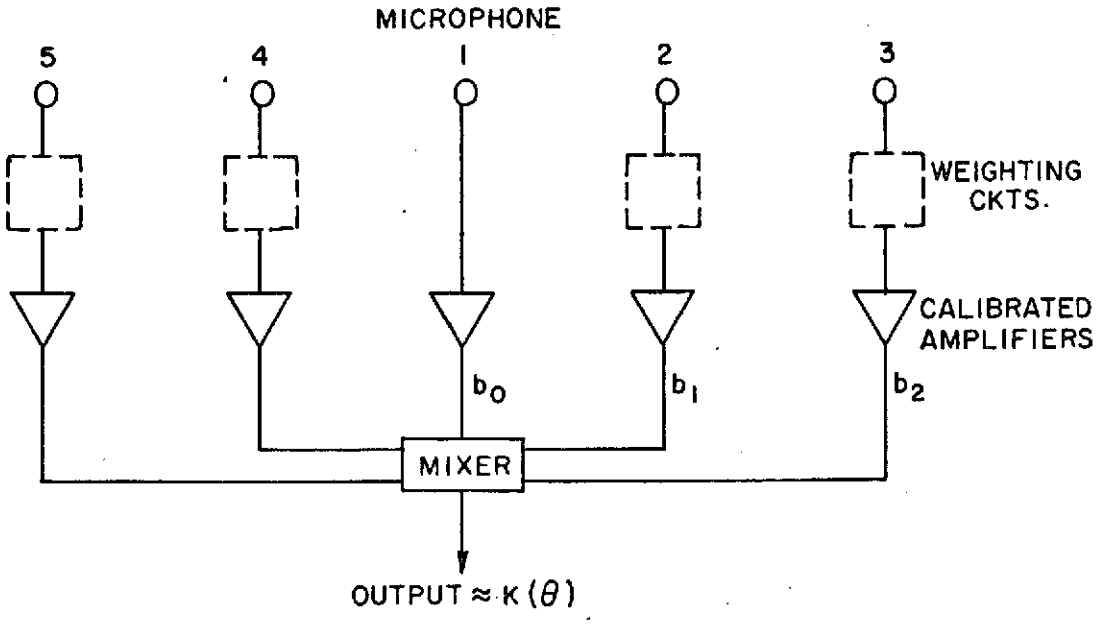

Fig. 12. Typical block circuit diagram for one of the batches of Fig. 11.

2.3 Correlation Detectors

The use of a correlator with a two-element array of directional receivers is one of the simplest arrangements of correlation detectors which has been used in radio astronomy investigations.[25] One of the chief advantages of such a system is that it is very insensitive to background noise from a distributed source (such as reverberant noise) allowing one to use greater recorder sensitivity than in the conventional sum-and-square law detector systems, thus making this technique specially suited to the detection of weak signals.

The output of the detector or correlator will, in general, consist of several components: a steady or d.c. component due to the signal; a steady component due to background noise; a fluctuating component due to the signal and a fluctuating component due to background noise. If the

third contribution is small compared to the last (i.e., small signal to noise input to detectors) we can neglect it. If we use a directional receiving system then in principle the signal (here the direct sound) should fall to zero as the signal source is removed from the principal axis of the receiving system. The d.c. output from the receiver thus corresponds to the background noise and this part could be biased off.

The effective response pattern of the system is improved. Indeed if the receiving pattern of one microphone is $K(\theta)$, the relative response of the correlation system is $K^2(\theta)\ \rho(d/c\ \sin\theta)$ where $\rho(\tau)$ is the normalized autocorrelation function of the signal. The delay $\tau = d/c\ \sin\theta$.

If one had used two tubular microphones, then the system can indeed pick up the direct sound and discriminate against the reverberant noise. Inspection of Figs. 7 and 9 indicate that the directivity of this microphone is poor by comparison to that of the linear array.

2.4 Concluding Remarks on Direct Detection of Sound Source in a Reverberant Background

The linear array appears to be the simplest of the various schemes we have discussed. It also displays the sharpest beam. For this reason we have decided to use it for measuring sound directly radiated from source.

To be sure, more complex (two dimensional) arrays can be found which would display an improved characteristic. We propose first to start with the linear array to demonstrate the feasibility of the technique.

So far we did not discuss the manner with which the array will be steered. In view of the physical size, it is clear that it is

much easier to steer it electronically. The procedure is quite straightforward.

Finally, as we pointed out above, two alternatives were suggested: (a) variable array length, and (b) fixed length many microphones used. We feel that the second alternative may be more costly in adding to the numbers of electro-acoustic channels, but the increased speed of performing the experiment more than outweighs the cost of the added equipment, through saving of personnel time and cost of operating the tunnel for longer periods.

The design that ARC approved is that for a crossed array, five elements per array. This is described in detail in part IV and Appendix B of this report.

PART III

OPTICAL DIAGNOSTIC METHODS

3.1 Introduction

The optical methods for the diagnosis of noise from a jet flow, which we proceed to expound, are based on the use of coherent optics and opto-acoustical techniques. These methods enable us to map the fluctuating (turbulent or coherent) part of the flow and hence measure small density variations and check the theories of mechanical to acoustical energy conversion. Furthermore, localization, spectrum analysis, background discrimination and optical processing of a wide-band signal will be facilitated.

These methods are grouped under holographic interferometry, acoustical holography and optical processing of wideband acoustic signals.

3.2 Holographic Interferometry

Fundamentals of holography are well known.[26,27] It is based on recording the interference between a known and an unknown wavefront. The latter can be reconstructed when the original recording (the hologram) is reilluminated by the known reference wave.

Holographic interferometry depends upon the interference between two reconstructed wavefronts. These wavefronts may have been recorded on the same hologram (double exposure) or on two different holograms, reconstructed in such a manner that the reconstructed waves coincide.[28]

Slight deviation between the two reconstructed waves is revealed in the form of three-dimensional interference fringes superimposed on the reconstructed image. The fringe data can be reduced to density information, as was done by Collins[29] who made use of Maldonado[30] line integral inversion scheme for the development of plasma emissivity. In this scheme, the fringe number functions that describe the interferometric data $g(y',\xi)$ is used to obtain the density-related function $f(x,y)$ by inverting the integral

$$g(y',\xi) = Q \int_{x_1'}^{x_2'} f(x,y)\, dx' \tag{20}$$

where

$$Q = \rho_\infty / \lambda \rho_s \tag{21}$$

$$f(x,y) = \rho(x,y)/\rho_\infty - 1 \tag{22}$$

$$n = 1 + \beta\rho/\rho_s \tag{23}$$

ρ_s = reference density at p°C and 760 mm Hg

β = dimensionless constant related to Gladstone-Dale constant

n = index of refraction

Collins and his co-workers reported that the fringe data may then be reduced to density information by expressing the density in a series of orthogonal polynomials and inverting the fringe-density integral equation by a computer program in the manner described in Ref. 29. Their scheme in brief consisted of using Q-switched laser to take double exposure holograms (20×10^{-9} sec. exposure) to freeze the jet flow. The two

exposures were taken before and after the jet was turned on. The fringes in the reconstructed images were then analyzed and the computer program was used to determine the density distribution.

A different arrangement was used by Jahodo[31] to map the auto-correlation of the density. The arrangement is based on taking an in-focus-diffused hologram of the flow. The density distribution is revealed as light intensity variation within the field of view.

3.3 Acoustical Holography

3.3.1 Direct Acoustical Holography

The acoustical field may be mapped into an optical one by making an acoustical hologram which is reconstructed optically. There are several ways of making such a hologram, which are summarized in Ref. 26. In this project, the information obtained by using the linear acoustical detectors (Section 2) may be used to construct a hologram of any region of the jet flow. This hologram, reconstructed optically, will then reveal the coherent sound sources as visible images in the right location with the correct intensity. In brief, this approach is rather another way to analyze the data obtained by the linear detectors array described in Section 2.

3.3.2 Instantaneous Acoustical Holography

Two superimposed pulsed holograms of the jet flow are made within a quarter of an acoustical cycle. The reconstruction of such a compound hologram reconstructs the acoustic field optically, indicating both the location and intensity of the coherent acoustic sources within the field

of view. This is an all optical technique where no acoustical transducers are needed. However, it is limited to the detection of purely coherent sources of known frequency; furthermore, it is rather costly, due to the need for strong double pulsed laser and good optical components capable of spreading the laser beam to a large extent (100 cm or more).

3.3.3 Spectral Analysis and Source Localization From Acoustical Holograms

When the acoustic field is mixed with a reference signal of fixed frequency f, and scanned by an acoustical detector with a constant velocity v, the resultant hologram reconstructs the acoustic field at an offset angle θ given by

$$\text{Sin } \theta = \frac{\Delta f}{f} \cdot \frac{C}{v} \qquad (24)$$

where C is the sound velocity and Δf is the frequency difference between the unknown source and the reference signal. Thus, it is easy to see that discrete sources of different frequencies will be reconstructed at different angles θ. In other words with this simple approach noise sources may be localized and their fundamental frequencies determined. Each technique, however, is valuable for stationary sources having single characteristic frequencies. Information on other types of sources, however, can be obtained but with difficulty and less accuracy.[26] A more serious drawback, though, is the needed stability of the acoustic field during the recording of the whole field. Again, an acoustical detector is needed and the linear array described in Section 2 can be used to form such a hologram. Better still, two crossed linear arrays,

if available, will be very useful and time saving.

3.4 Optical Processing of Wideband Acoustic Signals

An elegant method to determine the power spectrum of acoustic signals, using coherent optical techniques, was developed by Markevitch.[32] The principle of the technique is simply to transfer the recorded acoustic signal to a two dimensional photographic transparency in the form of an appropriate raster. An optical Fourier transform of the transparency will then reveal the spectrum of the recorded signal. Spectral resolution of 0.5 Hz is easily obtained and 0.05 Hz was demonstrated. Signals of 30 dB below the background noise was detected and 50 dB below background noise is hoped for.

The equipment to carry out the analysis is rather very expensive to build, especially just for this project. Instead, already existing equipment can be used to analyze a tape recording of the noise by special arrangement.

3.5 Concluding Remarks on Optical Diagnostic Methods

In addition to the linear detectors array described in Part II, availability of (a) pulsed laser, (b) CW laser and (c) appropriate optical components and mounts are needed to make and reconstruct either optical or acoustical holograms. The analysis of the data may be done directly by optical means and by computer.

By special arrangement, the detected signal from the linear array may be tape recorded and analyzed by the coherent optical processes.

Measurement of the density fluctuations in the flow by other optical means are discussed in Secs. 3.2.3 to 3.2.6 of Appendix A.

PART IV

DESIGN CHARACTERISTIC OF A HIGH DIRECTIVITY ACOUSTIC ANTENNA

4.1 Basic Considerations

The response of a planar microphone whose transduction efficiency is $w(x, y)$ can be shown to be proportional to

$$\iint w(x, y)\exp ik(x \cos \alpha + y \cos \beta)dxdy \tag{25}$$

where the interpretation of the various geometric symbols are readily found from Fig. 13.

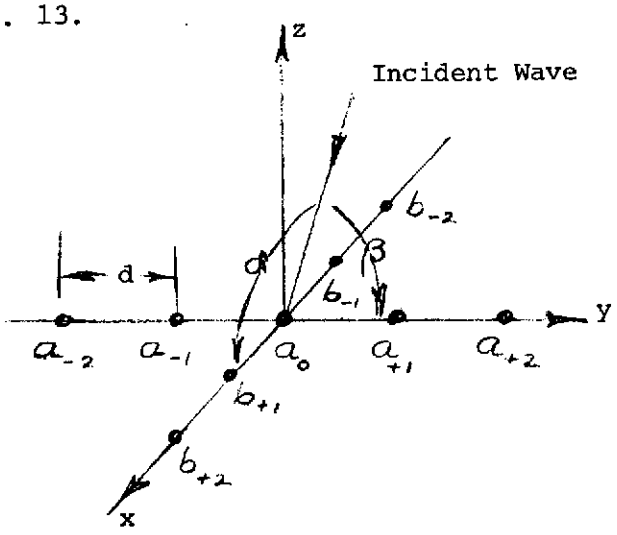

Fig. 13 Geometry of Antenna Array.

For a distribution of point microphones, the response is proportional to a quantity which reduces the double integral to a double summation, viz.,

$$\sum_n \sum_m w_n w_m \exp ik(x_n \cos \alpha + y_n \cos \beta) \tag{26}$$

where w_n, w_m are the individual sensitivities of the microphones and n, m are the number of microphones in the x and y directions respectively.

4.2 Steering of Antenna

When the antenna is tilted by α (or β) there is an acoustic phase difference of $\frac{2\pi f d_x}{c} \cos \alpha$ (for $\beta = 0$, say) between neighbouring microphones, where d_x = distance between microphones in the x-direction, f is the frequency and c the velocity of sound.

In order to steer the antenna by electronic means, one has to introduce a relative phase shift between the outputs of the different microphones. To produce an effective rotation of the (x-arm) by an angle α , the relative electronic phase shift must be $(\frac{2\pi f d_x}{c} \cos \alpha)$. Similarly a rotation of the (y-arm) by an angle β would require a phase shift of $\frac{2\pi f d_y}{c} \cos \beta$.

The important design parameters which have to be decided upon in order to provide the design criteria for the electronic circuitry are: the number of microphones to be used and the separation distance d between the microphones. Of course the separation in the x direction could be different from that in the y-direction. For equal sharpness in the x and y direction the separations $d_x = d_y = d$ say. The actual magnitude of d will depend on the Tchebycheff design criteria which was discussed in Sec. 2.2.2.

The number of microphones to be used is set by the directivity sharpness desired together with cost considerations. Figure 14 shows that the gain in sharpness from a (15°) to a (5°) sharp beam would entail an increase in the number of microphones from 5 to 15 per direction (i.e. from 9 to 29 total for the same discrimination of 26 db.) This gain in directivity represents an appreciable increase in capital investment which is not warranted. Since the total number of microphones available was thirteen which would have

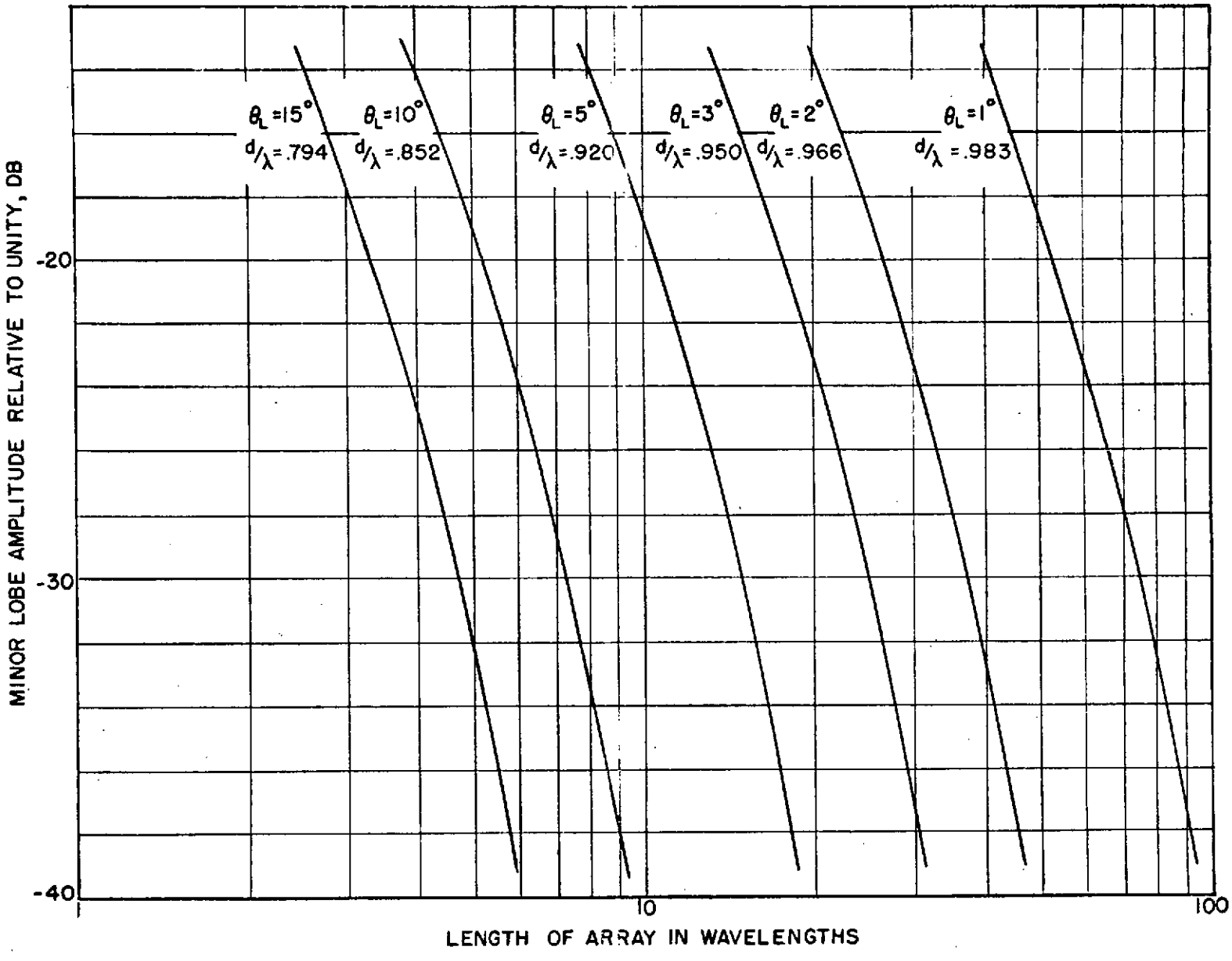

Fig. 14 Minor-Lobe Amplitude as a Function of the Length of the Array. The angle θ_L refers to the half angle of the beam. The actual number of microphones can be deduced from the ratio d/λ .

yielded an array of 7 microphones per direction, it was decided to use a total of 9 microphones (i.e. 5 per direction). This decision was justified on the grounds that the gain from 25 dB to 36 dB microphone was not appreciable.

As was discussed earlier, Section 2.2, the Tchebycheff correction is d/λ dependent. Concentrating on the frequency range 100 Hz to 1 kHz with a $d/\lambda = 0.75$, the maximum electronic phase shift will occur at a frequency of 1 kHz. Denoting the various microphones by a_{-2}, a_{-1}, etc. ... and b_{-2}, b_{-1}, etc. ..., we have typically (d = 25.4 cms)

TABLE II

Station	Phase Shift	Phase Shift for $\alpha = 0^{o}$ at f = 1 kHz
a_{-2}	0	0
a_{-1}	$\frac{4.7\ f}{10^3} \cos \alpha$	4.7 radians
a_{0}	2 (")	2 x 4.7
a_{+1}	3 (")	3 x 4.7
a_{+2}	4 (")	4 x 4.7

The phase shifters are all-pass networks designed to provide a phase shift of 4.7 radians at 1 kHz. A typical such network is shown in Fig. 15. The phase shift for an all-pass network is a linear function of the frequency and is in fact proportional to the time constant RC for the circuit. But the phase per unit (as shown in Fig. 13) is limited to about 40^{o}. Consequently 8 similar units connected in cascade are needed to provide the required phase shift, and one can express the electric phase shift θ by

$$\theta = \omega F(RC) \tag{27}$$

where F is a complicated function of RC and $\omega = 2\pi f$.

Now, we equate the acoustic phase shift to the electric phase shift, i.e.,

$$\omega F(RC) = \frac{2\pi fd}{c} \cos \alpha$$

or

$$\cos \alpha = \cos^{-1}[F(RC) \frac{c}{d}] \qquad (28)$$

We thus notice that the steering angle α is a function of (RC) the electric time constant of the circuit and of the separation between the microphones, but is independent of the frequency.

Consequently, the steering is obtained by changing the value of the resistance R, which in the circuit of Fig. 15 corresponds to the resistance of the FET. By using a simple feedback control circuit, all the FET's in one phase shifting block can be made to change together by changing the voltage on the FET. There will be, of course, individual variations for the phase shift produced by the different units because of the unavoidable variations of the characteristics of the FET. By trial and error of hundreds of FET, the $(2x8x9) = 144$ FET's with the best match were selected.

The calibration of the instrument i.e., dial reading vs. average electric phase shift is shown in Fig. 16, while the transformation of Fig. 16 by means of Eq.(28) gives the steering angle for different values of d (compared to $(\frac{d}{\lambda} = \frac{3}{4})$ at 500 cps.) Fig. 17.

Because the FET's cannot be made to reach an infinite resistance (by removing the applied voltage), it is not possible to satisfy $F(RC) \to 0$, i.e., the zero phase shift point cannot be attained with the FET's alone. Consequently, relays have been added to by-pass the outputs from the microphones to be added via the

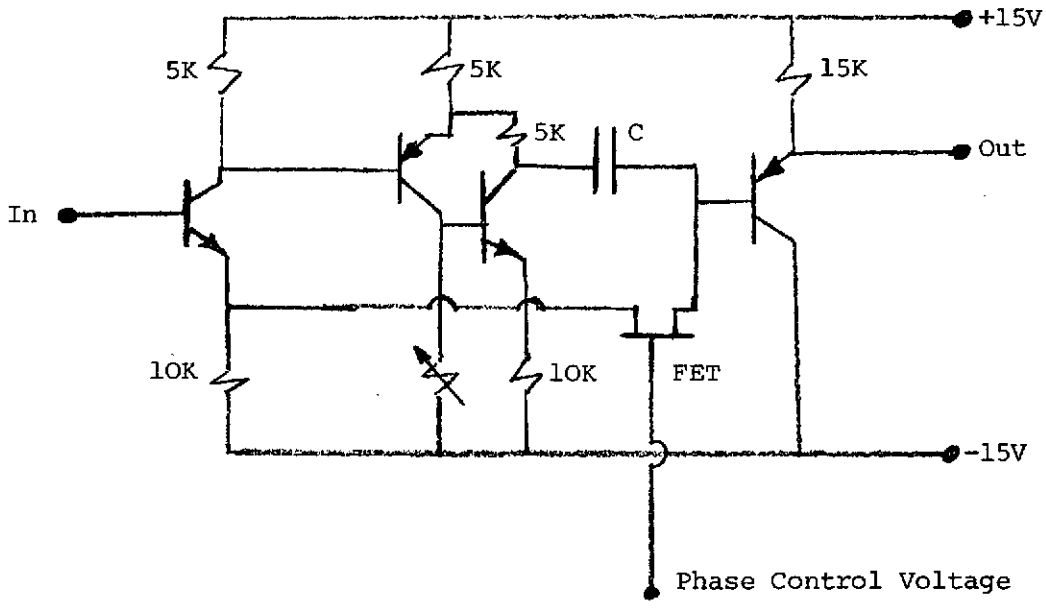

Fig. 15 Circuit Diagram for One of the Elements of Phase Shifter.

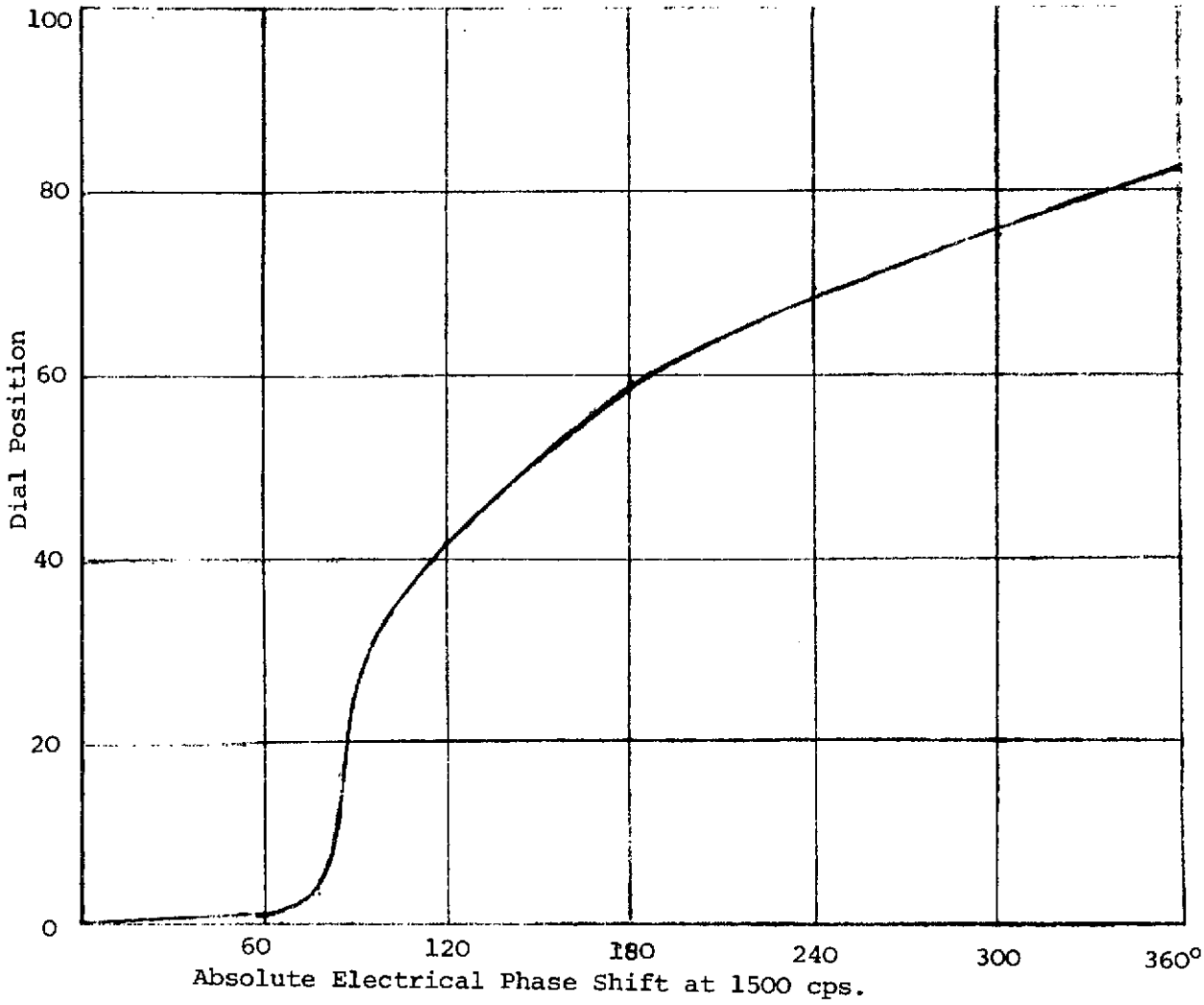

Fig. 16 Calibration of Delay Line Phase Shifting Network

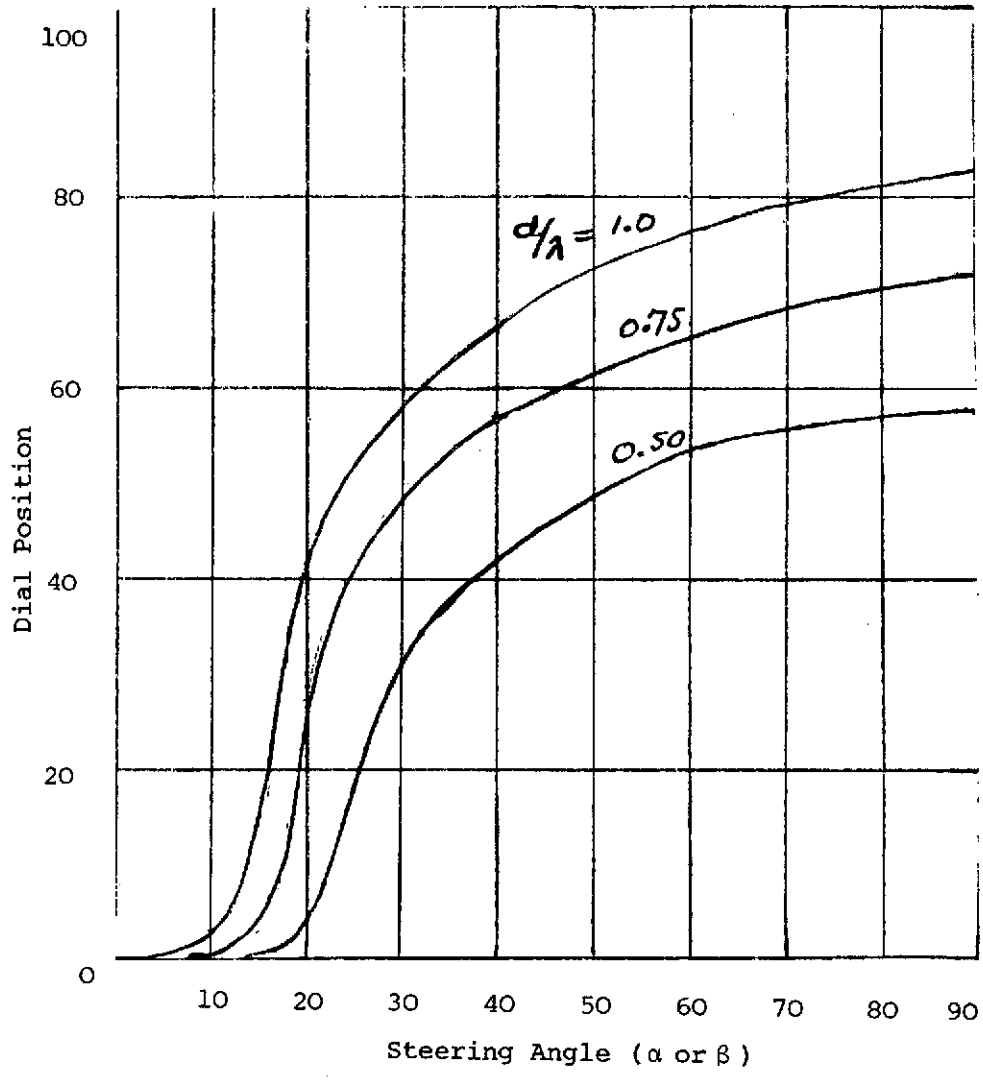

Fig. 17 Steering Caliberation of Antenna for d/λ values Referred to 500 cps.

operational amplifiers without any phase. The arrangement shown in Fig. 18 is self-explanatory.

4.3 Beam Sharpening

The shading of the microphone sensitivities has been described in details in Section 2.2.2. For 5 transducers per arm, the weight of the coefficients are as indicated below

TABLE III

$$b_{-2} = b_{+2} = 0.46 = a_{-2} = a_{+2}$$

$$b_{-1} = b_{+1} = 0.82 = a_{-1} = a_{+1}$$

$$b_o = a_o = 1.0$$

The Tchebycheff corrections reduces the minor lobes but does not sharpen the main lobe.

A simple procedure to achieve this sharpening is to use an elementary (integrated circuit) multiplier. The multiplier which effectively performs the operation $(\sum_n a_n) \times (\sum_m b_m)$ sharpens the beam by 6 db at the half power point. The disadvantage of the multiplier is that its output is at double the frequency. It is possible, however, to use an automatic gain control amplifier to restore the output at the same frequency, but with an amplitude proportional to $(\sum a_n) \times (\sum b_n)$ thus preserving the beam sharpness. The multiplication scheme obviously necessitates tuning the outputs of each array to a single frequency.

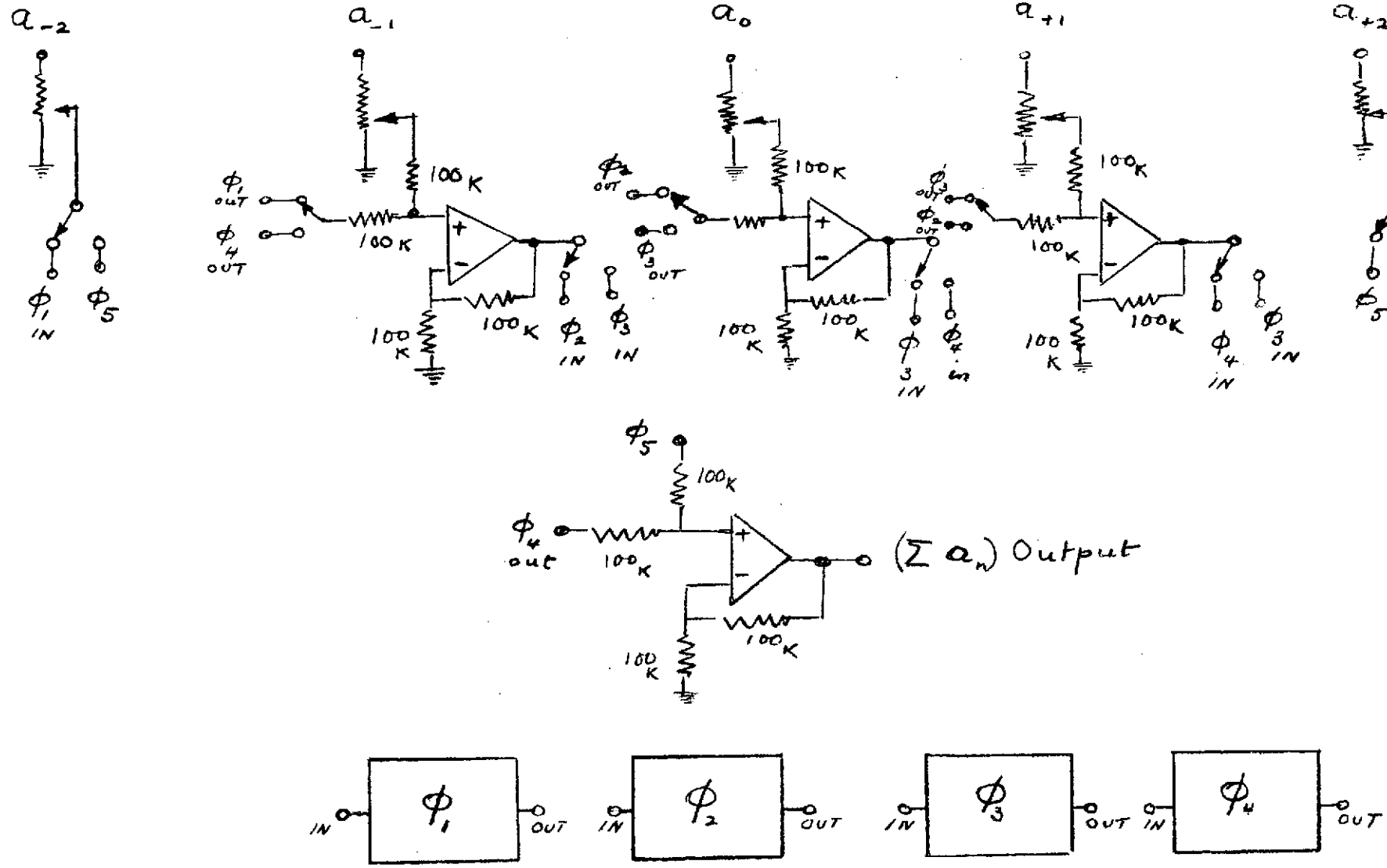

Fig. 18 Interconnection for "A" Channel. An identical circuit is used for the "B" channel. Notice the circuit used for the adding operational amplifiers so as to yield unity gain.

4.4 Testing of Antenna

A series of tests were performed, before delivery of the antenna control, to check on the operation of the system. These are described below.

1. Phase Shift. The individual phase shifts produced by the 8 delay lines (phase shifters) have been checked. Typical phase shifts produced have been shown in Fig. 19.

2. Linearity of Delay Lines. Keeping any one delay line fixed at a particular frequency, the amplitude of the input to the delay line was varied until a 1% occurred at the output. This limiting amplitude was found to be 50 mV. It is important to stress that all operational amplifiers gains have been adjusted so that their gain was always unity. The amplitude of the signal at the microphone plugs is therefore identical to that at the delay line input even though it goes through a series of amplifiers.

3. Linearity of Amplifiers. By connecting all the test points in parallel, one can effectively add the inputs of the amplifiers. Using the "A" channels alone and "B" channels separately it was checked that the signal $\sum_n a_n$ (or $\sum b_n$) did in fact increase with n, when the gain of all the channels as fixed by the potentiometers was made identical.

4. Linearity of Multipliers. Setting the phase shifts of the delay lines to zero, it was checked that the output $(\sum a_n) \times (\sum b_n)$ increased linearly with either $(\sum a_n)$ or $(\sum b_n)$. Furthermore, it was checked that the product went to zero if either $(\sum a_n)$ or $(\sum b_n)$ went to zero.

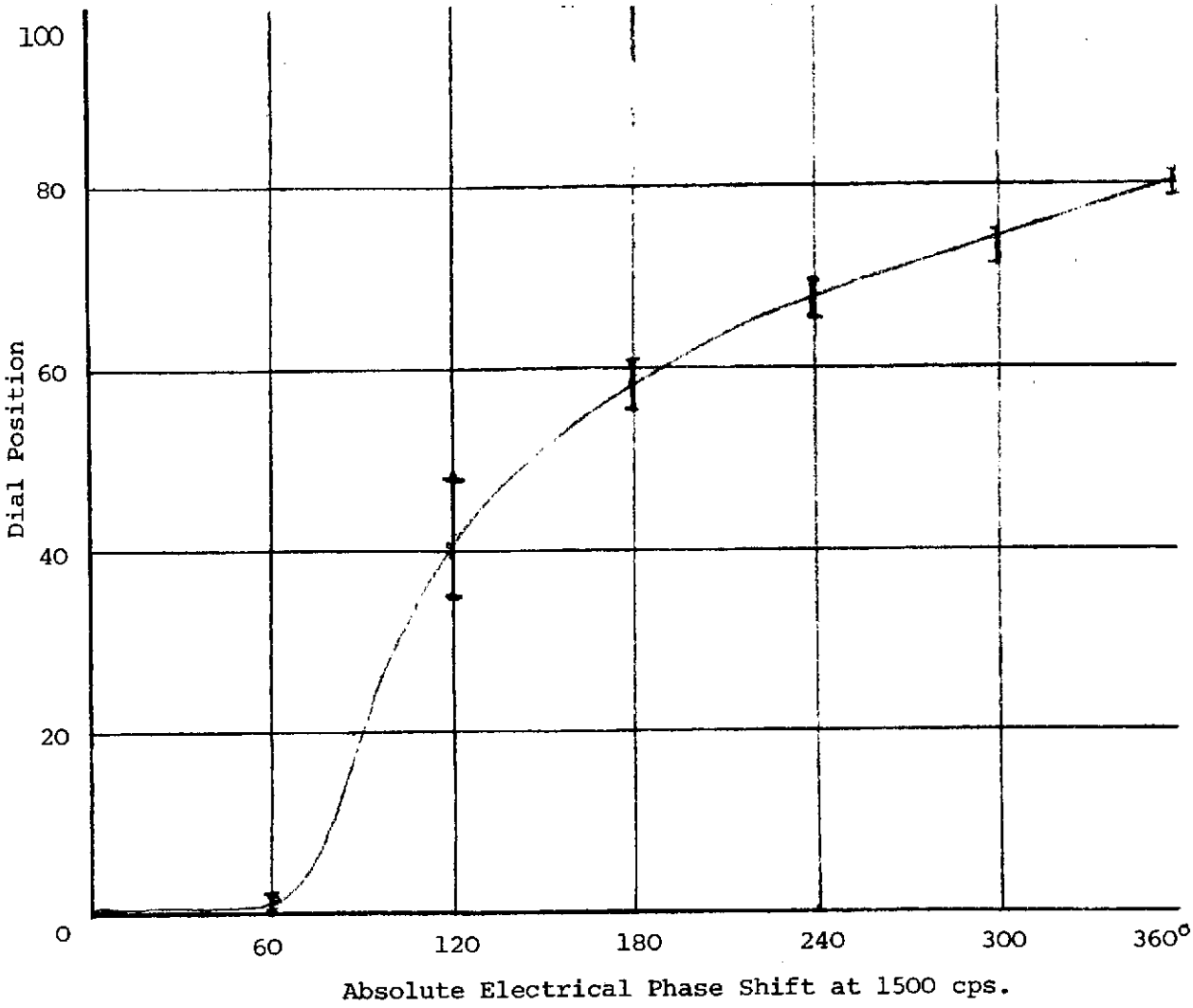

Fig. 19 Scatter in the characteristics of the phase shifters for the "A" channel. The curve drawn is the average for all the delay lines.

It was also found that the multipliers begin to distort when the signal length at the input of the system exceeds 30 mV. For this reason the signal from the microphone should be kept to less than 30 mV.

4.5 Evaluation of the Antenna and its Control

4.5.1 Procedure

With the cooperation of Mr. Paul Soderman of Ames Research Center, the following tests were made at ARC anechoic chamber to evaluate the performance of the acoustical antenna and its electronic steering control.

Nine omnidirectional microphones were mounted on two crossed arms A & B, 5 microphones per arm (Fig. 13), 45.7 cm (18") apart. This antenna was placed at one end of the anechoic chamber, facing a loudspeaker at the other end, about 6 m (20 ft) away. The antenna could be rotated around its vertical axis through 360°, in synchronism with a chart recorder. The connections and shading of the microphones followed the instruction manual, reproduced in Appendix B.

(a) In one series of tests, an acoustic frequency was selected; no shading was made; the controls of the electronic steering of A and B were switched off to simulate a (0,0) position of the antenna; the antenna was then rotated mechanically in synchronism with the chart recorder which plots the output. This was repeated at various other selected frequencies.

(b) The same set of runs were made after the microphones have been shaded.

(c) A third set of runs were made (with and without shading) when the distance between the microphones was changed to 22.9 cm (9").

(d) Another test was made which confirmed that the output of each arm alone is the sum of the outputs of the microphones on such arm.

(e) To confirm the insensitivity of the equipment to frequency, an electronic signal, simulating the acoustical one, was applied to all the microphones. The output then was seen to be the same regardless of the frequency of the input signal, or the steering controls.

(f) Finally a few runs were made to test the electronic steering, by leaving the antenna in the stationary position and plotting point by point the output versus the steering angle as read from the position of dial A alone. (Changing dial A alone simulates rotation of the antenna around a vertical axis.)

4.5.2 Results

Fifteen samples of the results of tests (a) to (d) of the previous section, Sec. 4.5.1, are enclosed. A summary of the analysis of these runs is tabulated below (Table IV). From these results, three main observations are made:

1. The antenna is indeed directional.

2. Shading improves the discrimination between the main and secondary lobes, but also widens the angular field of view.

3. When the antenna is adjusted for an optimum d/λ at a certain frequency, lower frequencies can be tolerated more than high frequencies which confirms our theoretical finding on page 26. At high frequencies, the amplitudes of secondary lobes increase and confuse their discrimination from the main lobe. Optimizing (d/λ) at 500 Hz gives reliable measurements in the range from about 200 to 750 Hz (see Fig. 22); if (d/λ) is optimum at 1000 Hz, measurements will be reliable from about 550 Hz to 1400 Hz (see Fig. 22).

4. Experimental results agree with the theoretical results as evident from comparing, for example, angle θ and the positions and amplitudes of

maxima and minima of run #7 (Fig. 20) with the theoretical calculations (Fig. 21).

TABLE IV

SUMMARY OF RESULTS OF ANTENNA EVALUATION

Symbol No.	Frequency f Hz	Mic. Separation d cm (in)	Shading	Main Lobe Angle θ° at		Diff. between main lobe and secondary lobe. Amplitudes DB
				Half Width	6 db drop	
(4)	560	46 (18)	No	8	7	9
	300	46 (18)	No	17	17	12
(1)	200	46 (18)	No	17		5
(1)	800	46 (18)	No	8		5
	560	46 (18)	Yes	18	11	19
(2)	1000	46 (18)	Yes	10	6	16
(3)	200	46 (18)	Yes	36	35	19
(4)	1000	23 (9)	No	12	10	14
(3)	350	23 (9)	No	37	32	22
(2)	2000	23 (9)	No	7	7	14
	1000	23 (9)	Yes	12	10	17
	560	23 (9)	Yes	30	21	17
	200	23 (9)	Yes			
(2)	1500	23 (9)	Yes	11	8	18
(1)&(2)	2000	23 (9)	Yes	5	4	17

Symbol: (1) Measurements are approximate.

(2) Amplitude of high order lobes reaches that of main lobe.

(3) High order lobes are indistinguishable.

(4) Optimum $(d/\lambda) = 0.75$.

The results of the electronic steering test (f) described in Sec. 4.5.1 were not quite conclusive. There was indeed an indication of steering, but the high sensitivity of the steering dials A & B at low angles made the evaluation rather difficult.* Further lengthy tests requiring fixing the dials A and/or B at a specific angle and repeating tests (a) to (d) were not done.

*In a new model, the phase shifters are so designed that the amount of cascading of the control resistance is a function of the steering angle. This equalizes the sensitivities of the dials thoughout the steering range.

Fig. 20 Fifteen charts of runs made to evaluate the acoustical antenna performance. The main parameters (separation d between the microphones, the frequency of the acoustical wave, and whether the microphones are shaded or not) are indicated on every chart. All the runs are made with the electronic steering control dials A&B in the off position simulating a (0,0) directivity position. (See Appendix B.)

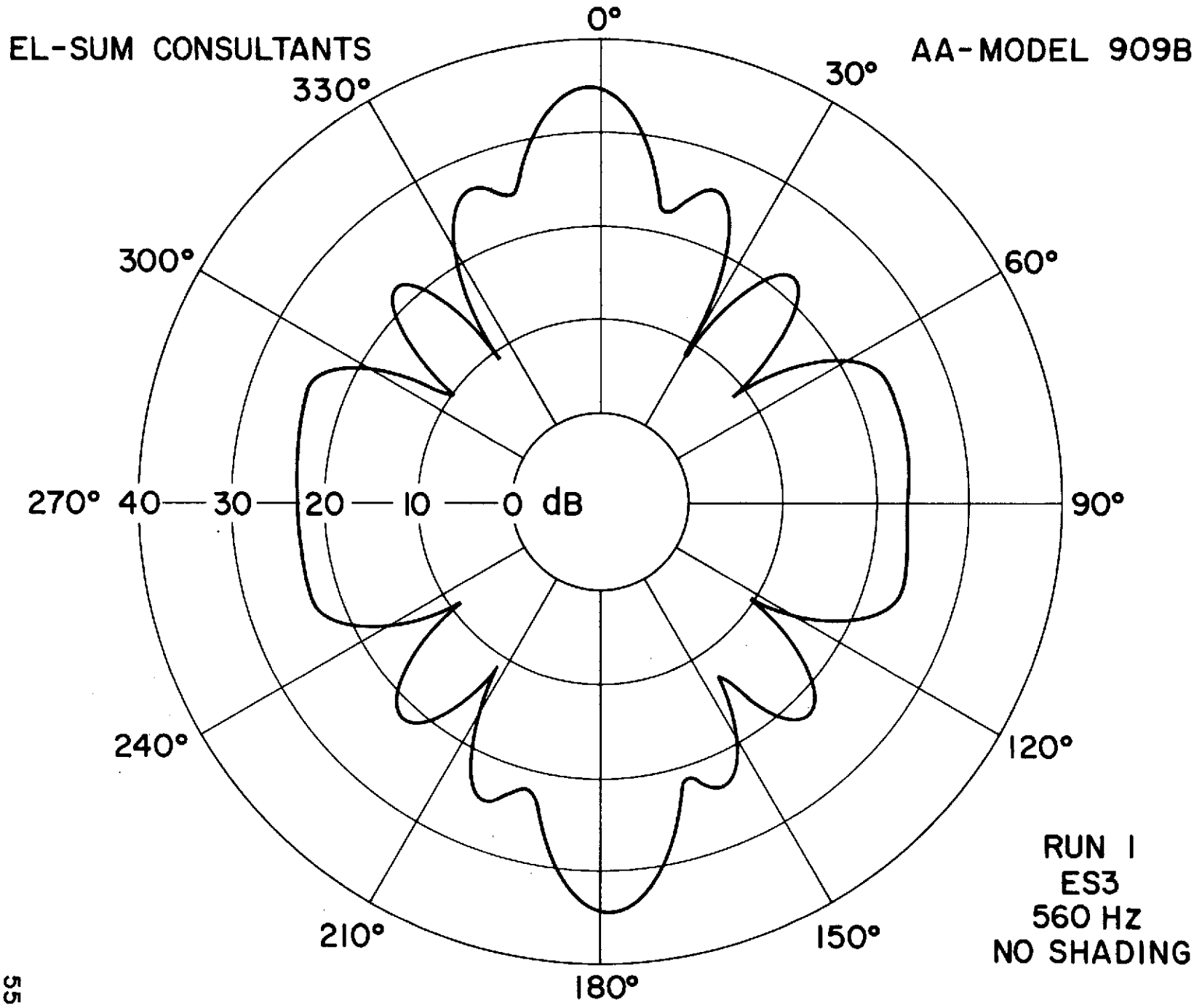
EL-SUM CONSULTANTS
AA-MODEL 909B
0°
30°
60°
90°
120°
150°
180°
210°
240°
270°
300°
330°
40
30
20
10
0 dB
RUN 1
ES3
560 Hz
NO SHADING

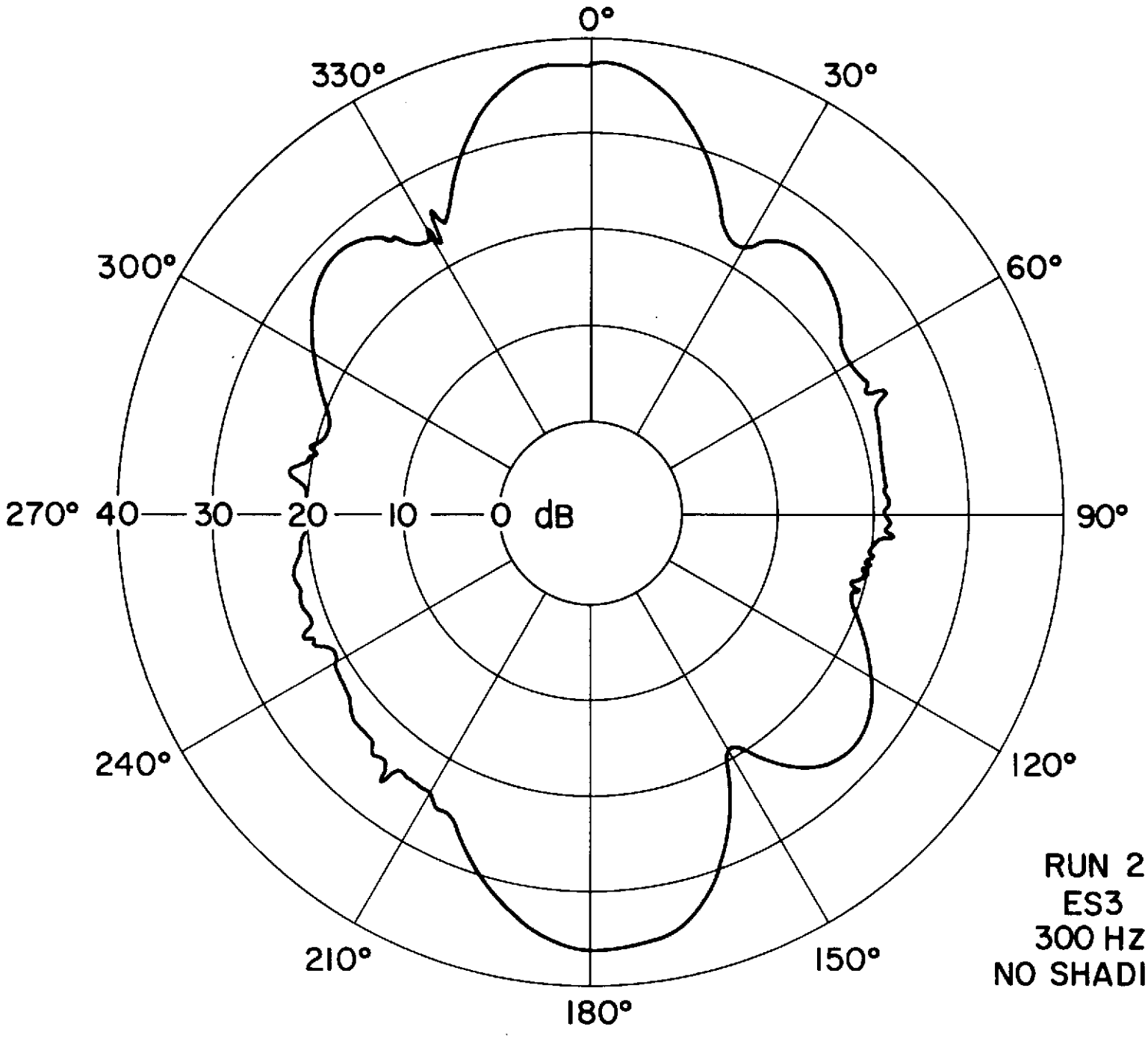

RUN 2
ES3
300 Hz
NO SHADING

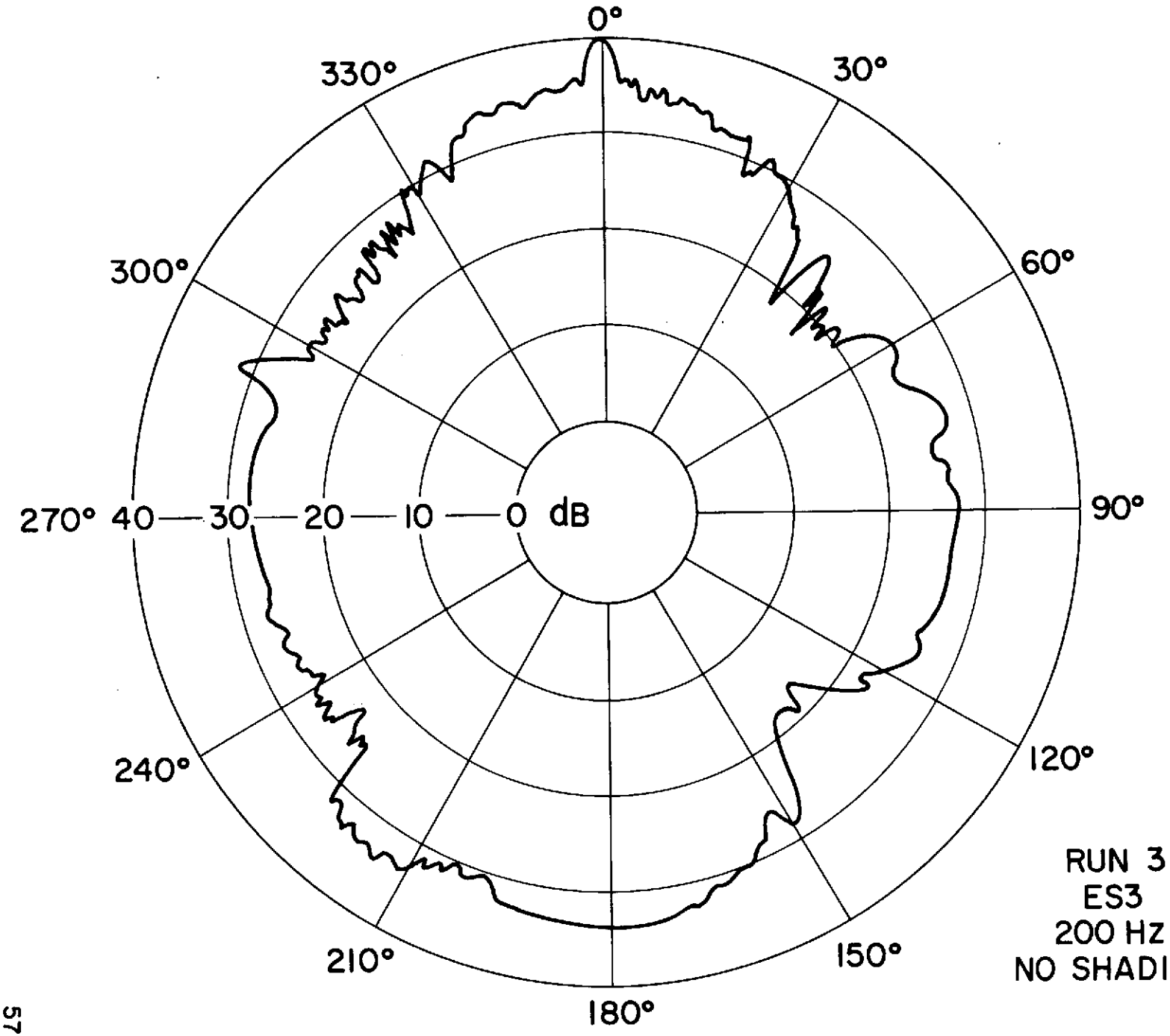

RUN 3
ES3
200 HZ
NO SHADING

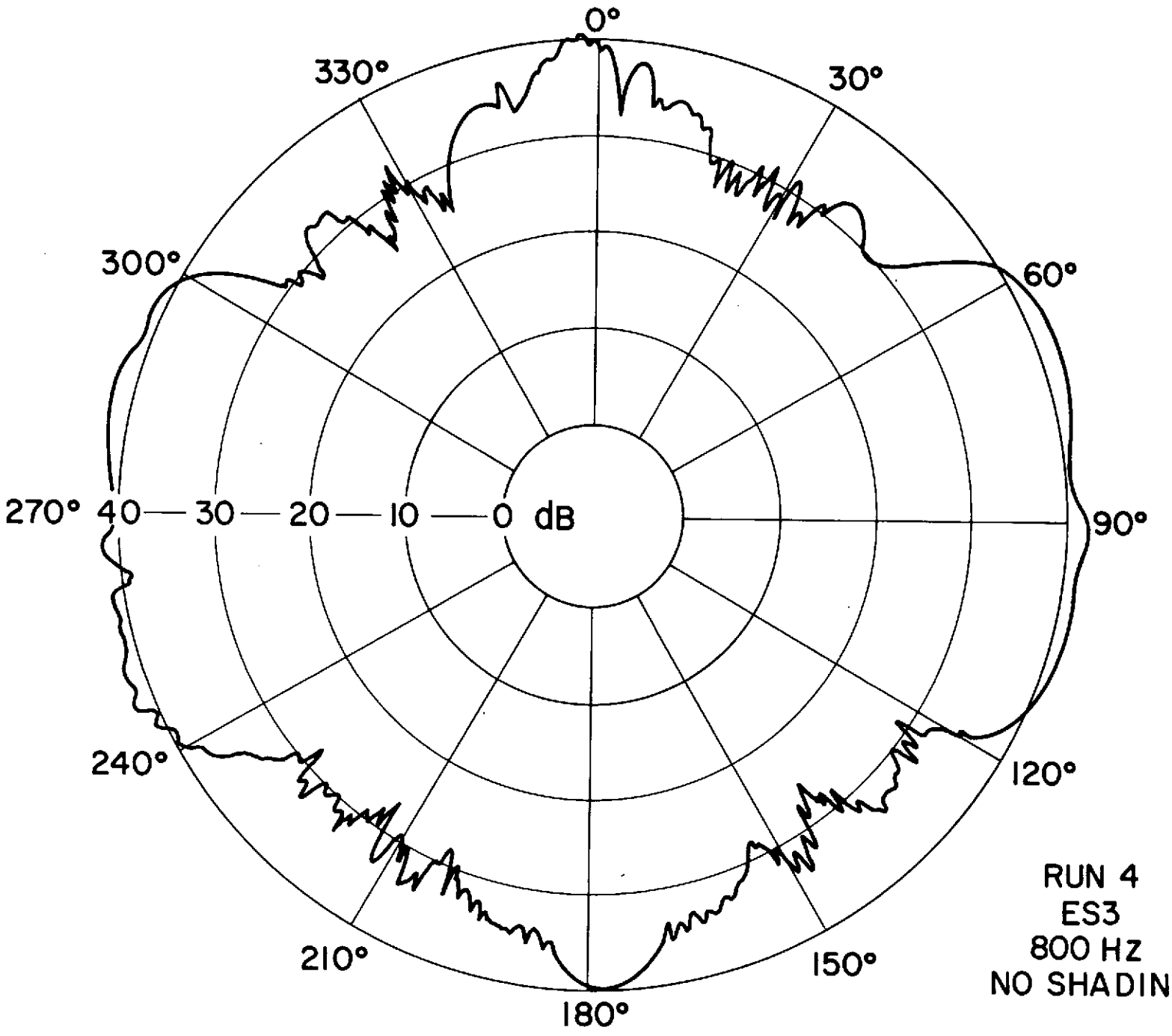

RUN 4
ES3
800 HZ
NO SHADING

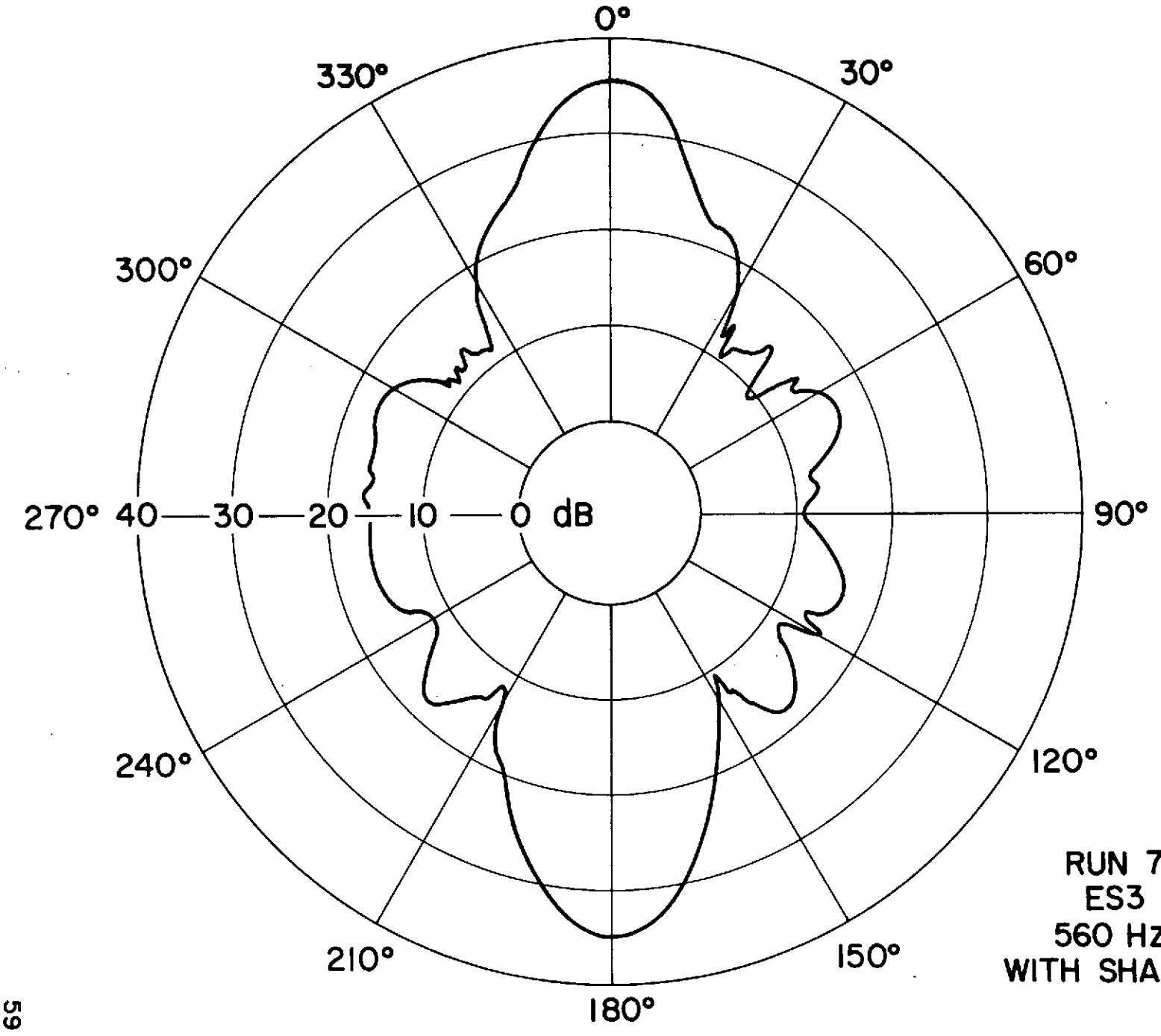

RUN 7
ES3
560 HZ
WITH SHADING

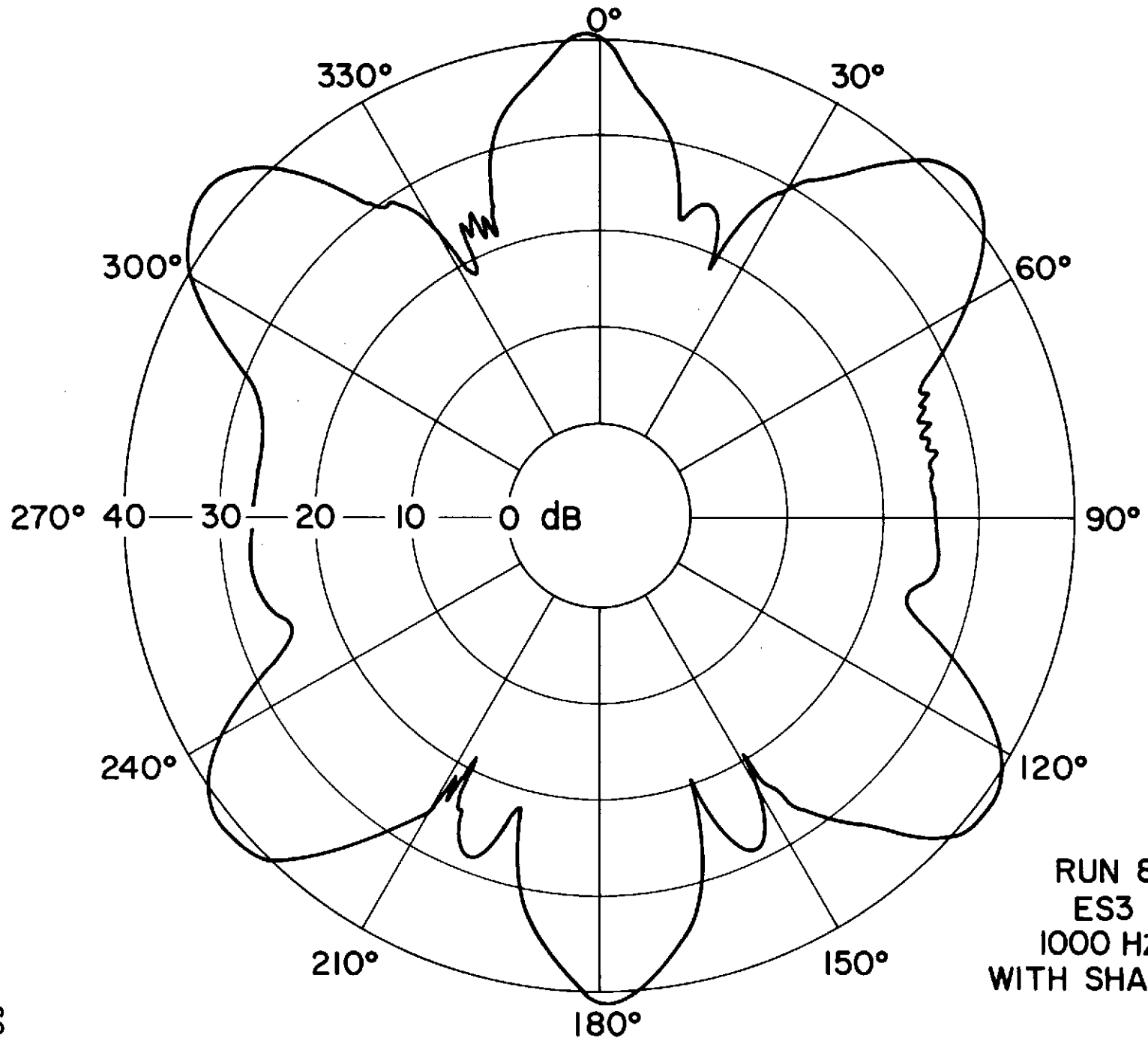

RUN 8
ES3
1000 HZ
WITH SHADING

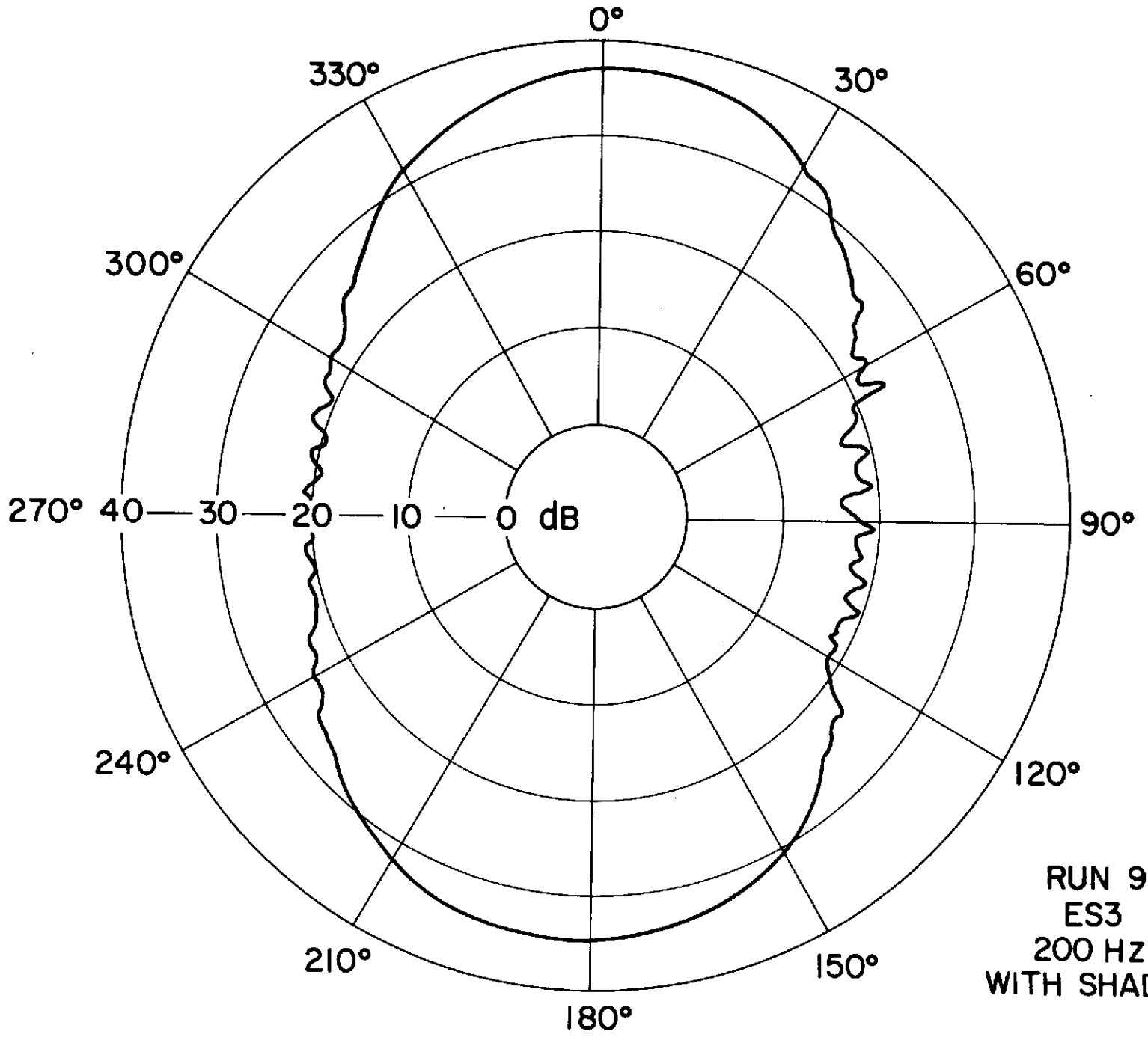

RUN 9
ES3
200 HZ
WITH SHADING

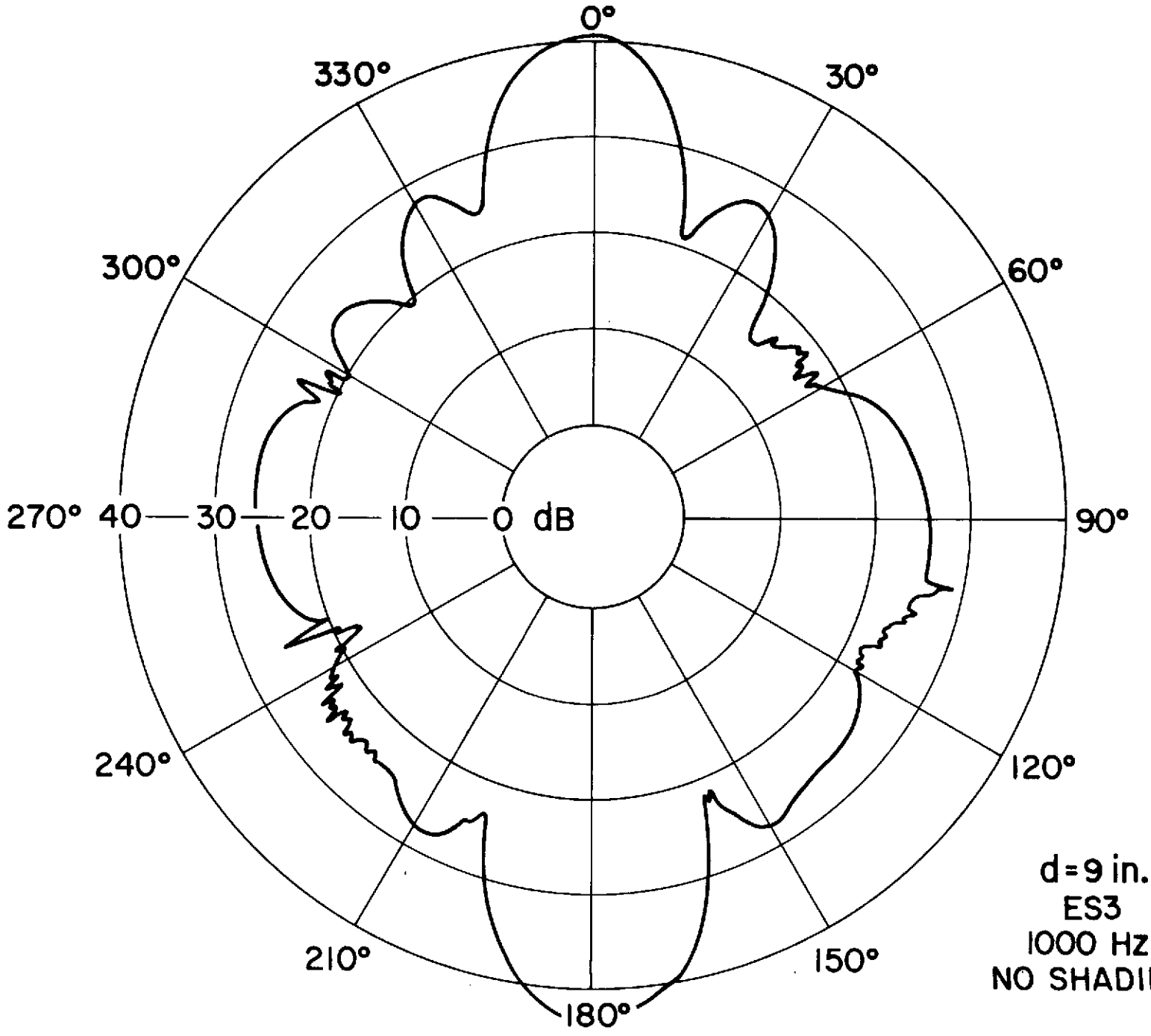

d=9 in. (23 cm)
ES3
1000 Hz
NO SHADING

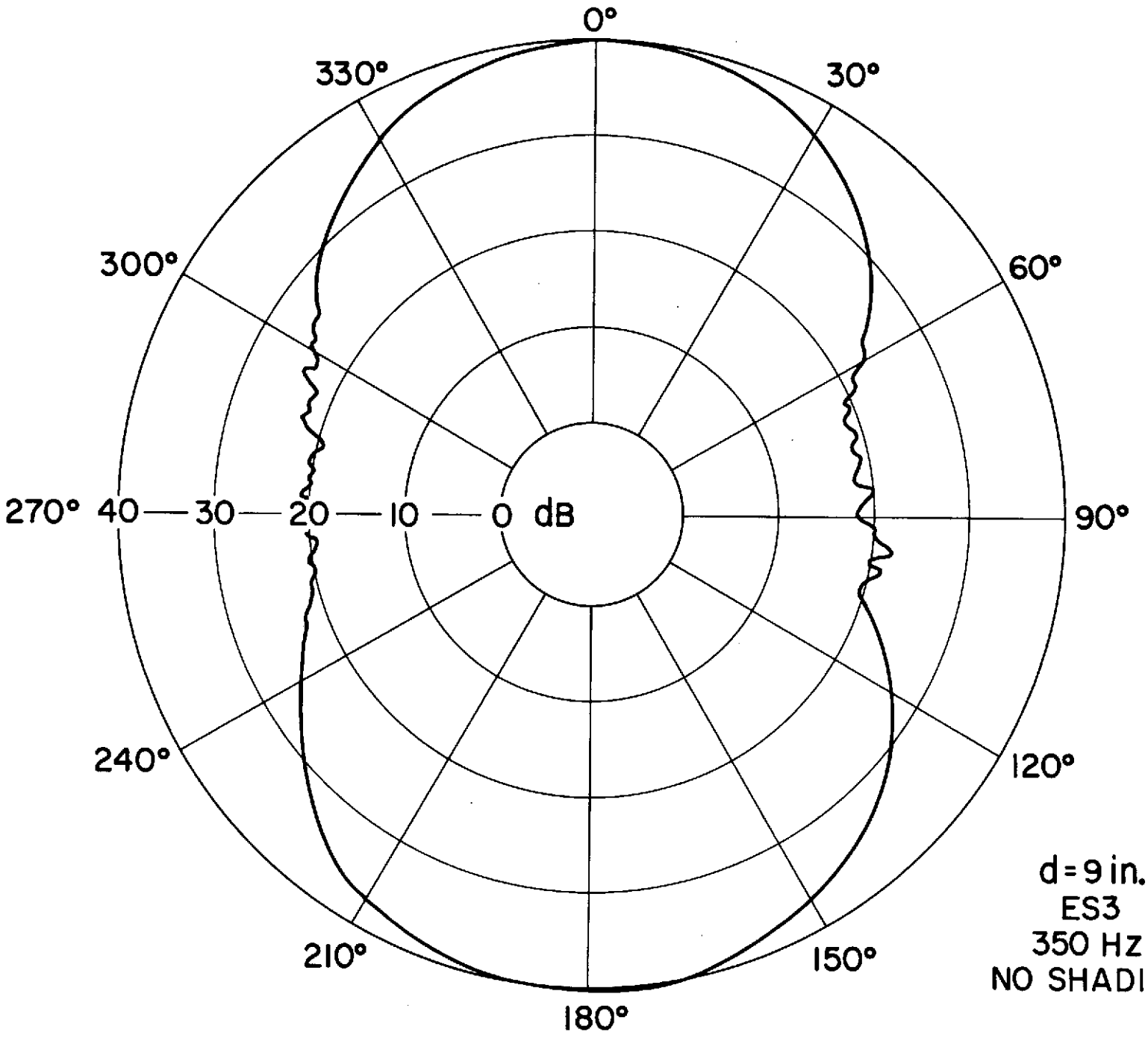

d = 9 in. (23 cm)
ES3
350 Hz
NO SHADING

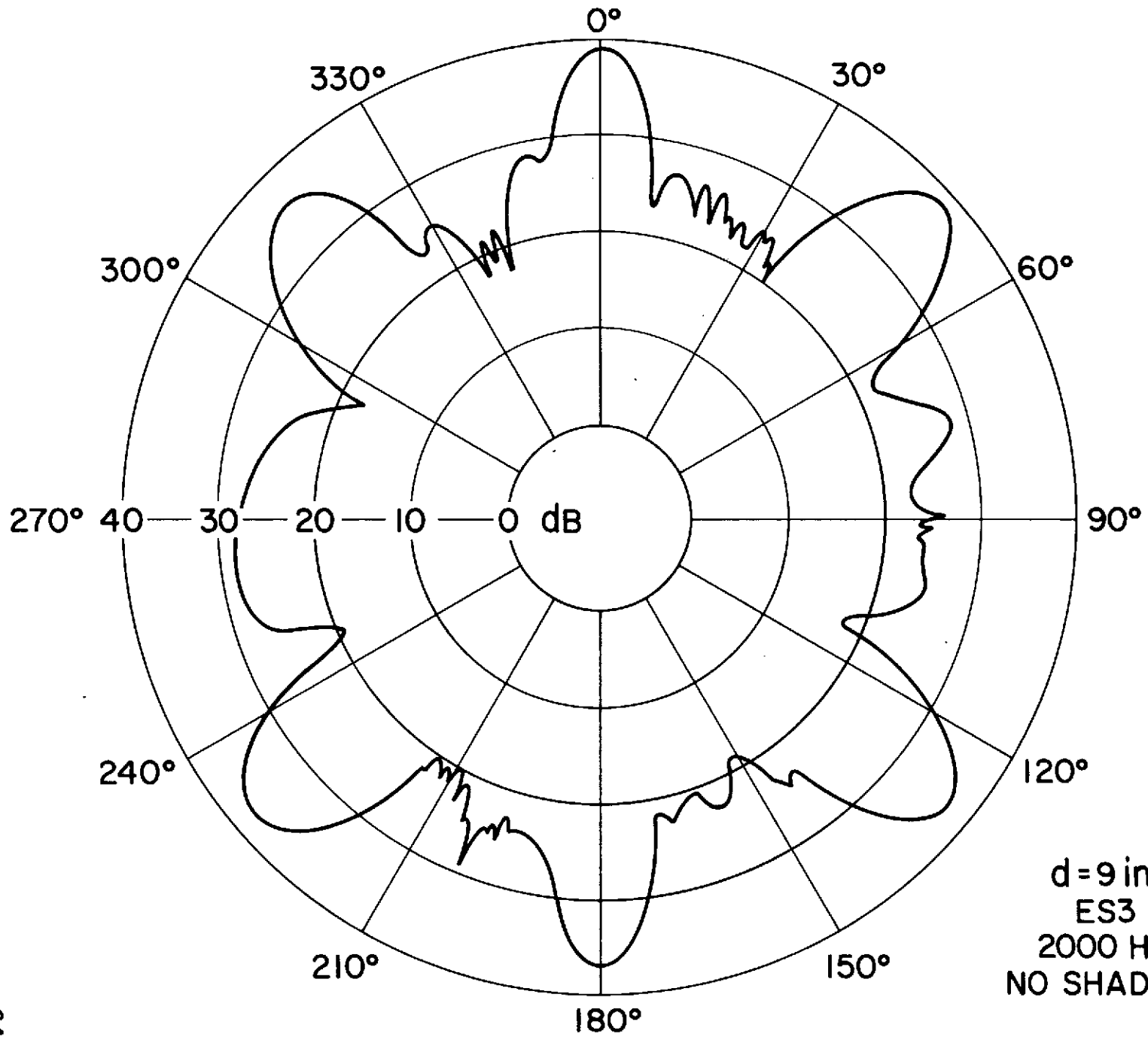

d = 9 in. (23 cm)
ES3
2000 HZ
NO SHADING

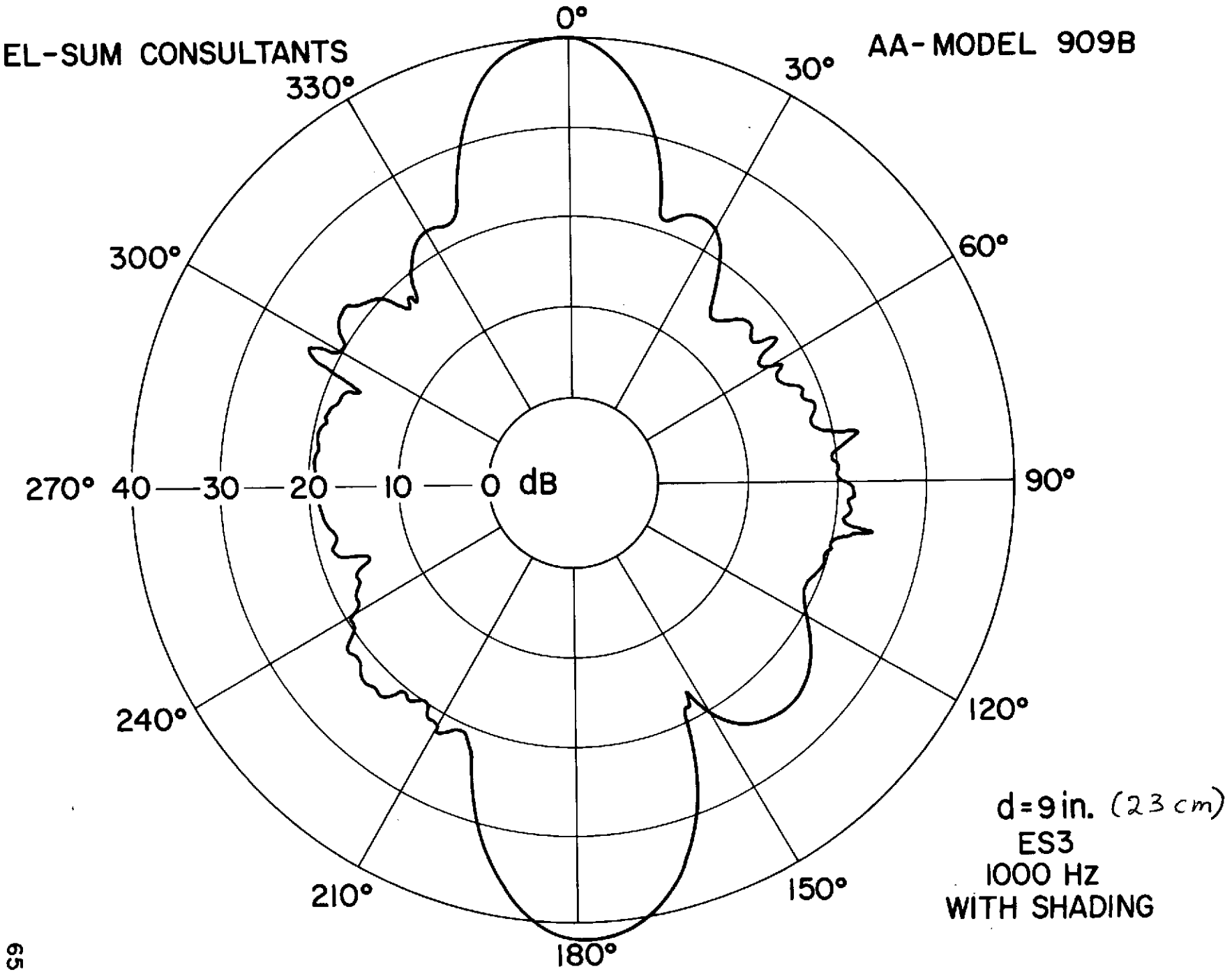
EL-SUM CONSULTANTS
AA-MODEL 909B
0°
30°
60°
90°
120°
150°
180°
210°
240°
270°
300°
330°
40
30
20
10
0 dB
d=9 in. (23 cm)
ES3
1000 Hz
WITH SHADING

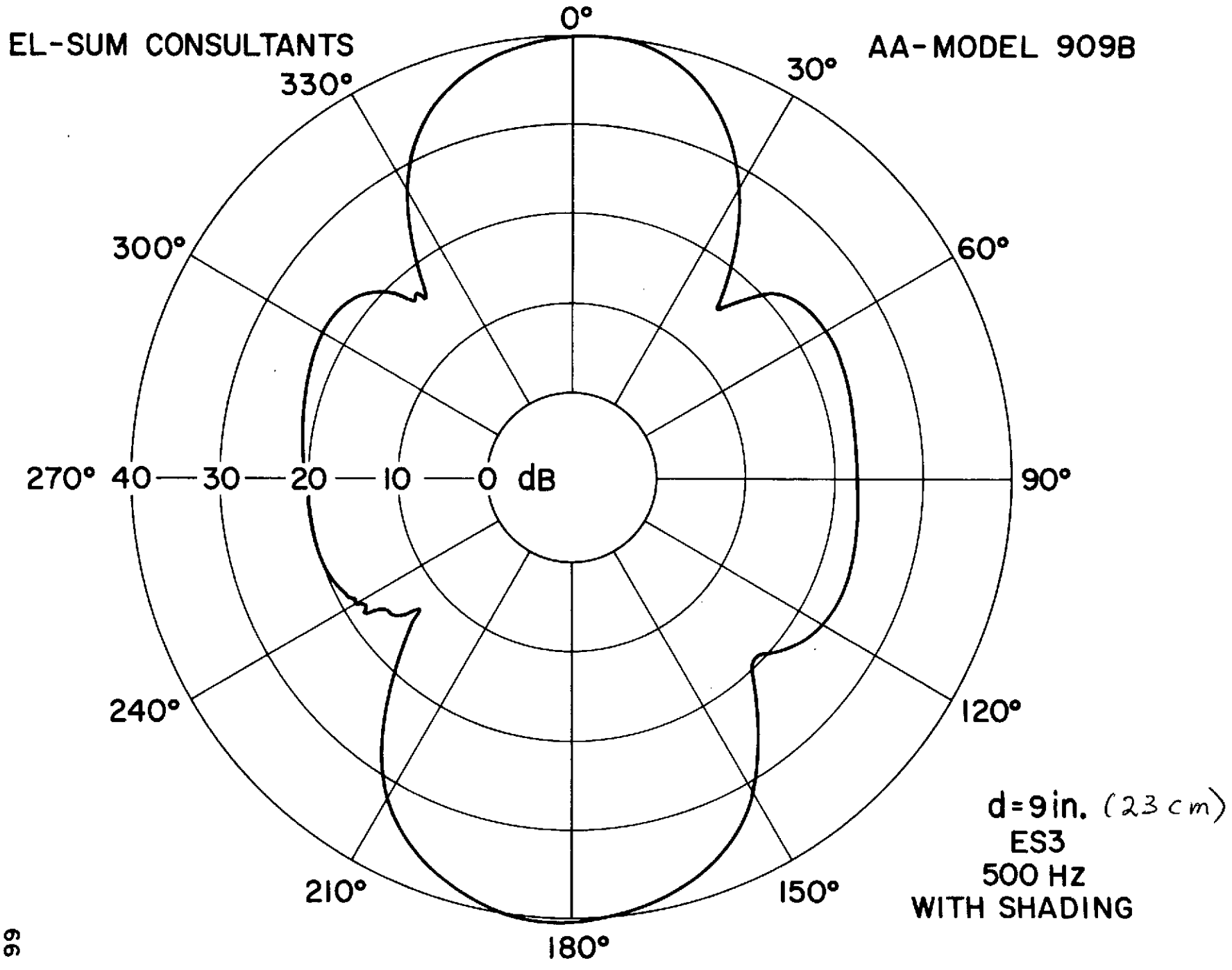
EL-SUM CONSULTANTS
AA-MODEL 909B
0°
30°
60°
90°
120°
150°
180°
210°
240°
270°
300°
330°
40
30
20
10
0 dB
d=9in. (23cm)
ES3
500 HZ
WITH SHADING

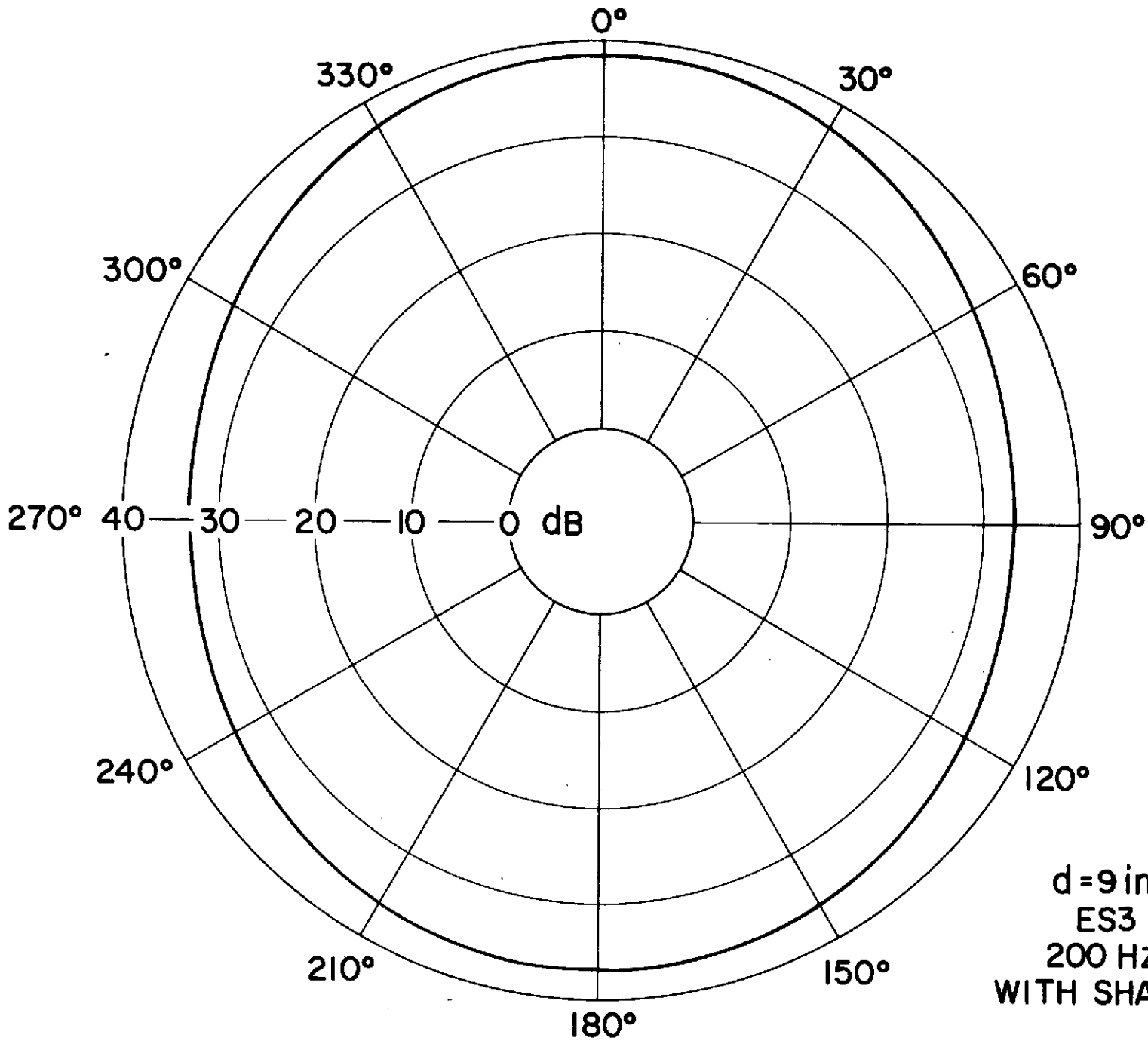

d = 9 in. (23 cm)
ES3
200 Hz
WITH SHADING

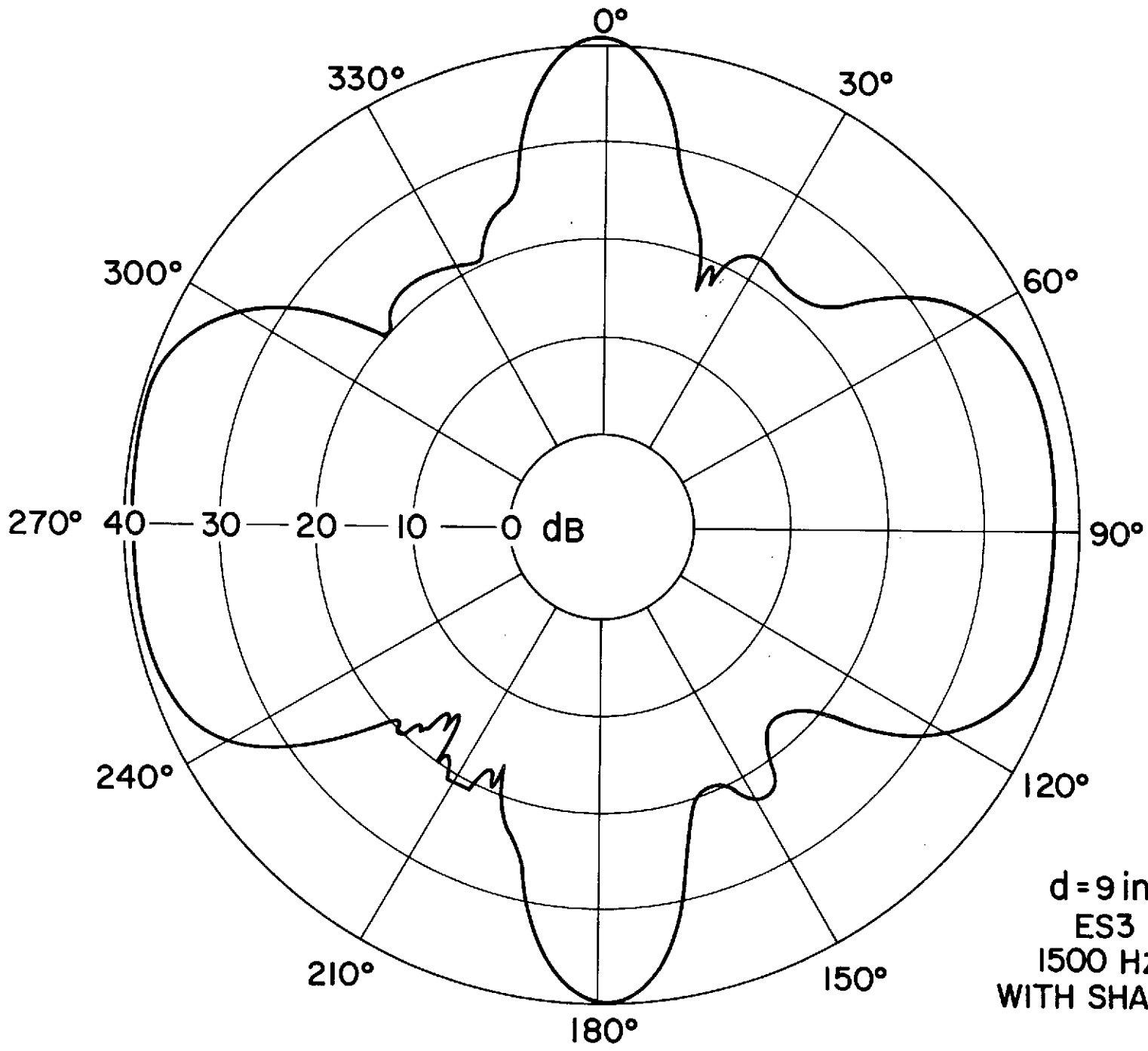

d = 9 in. (23 cm)
ES3
1500 Hz
WITH SHADING

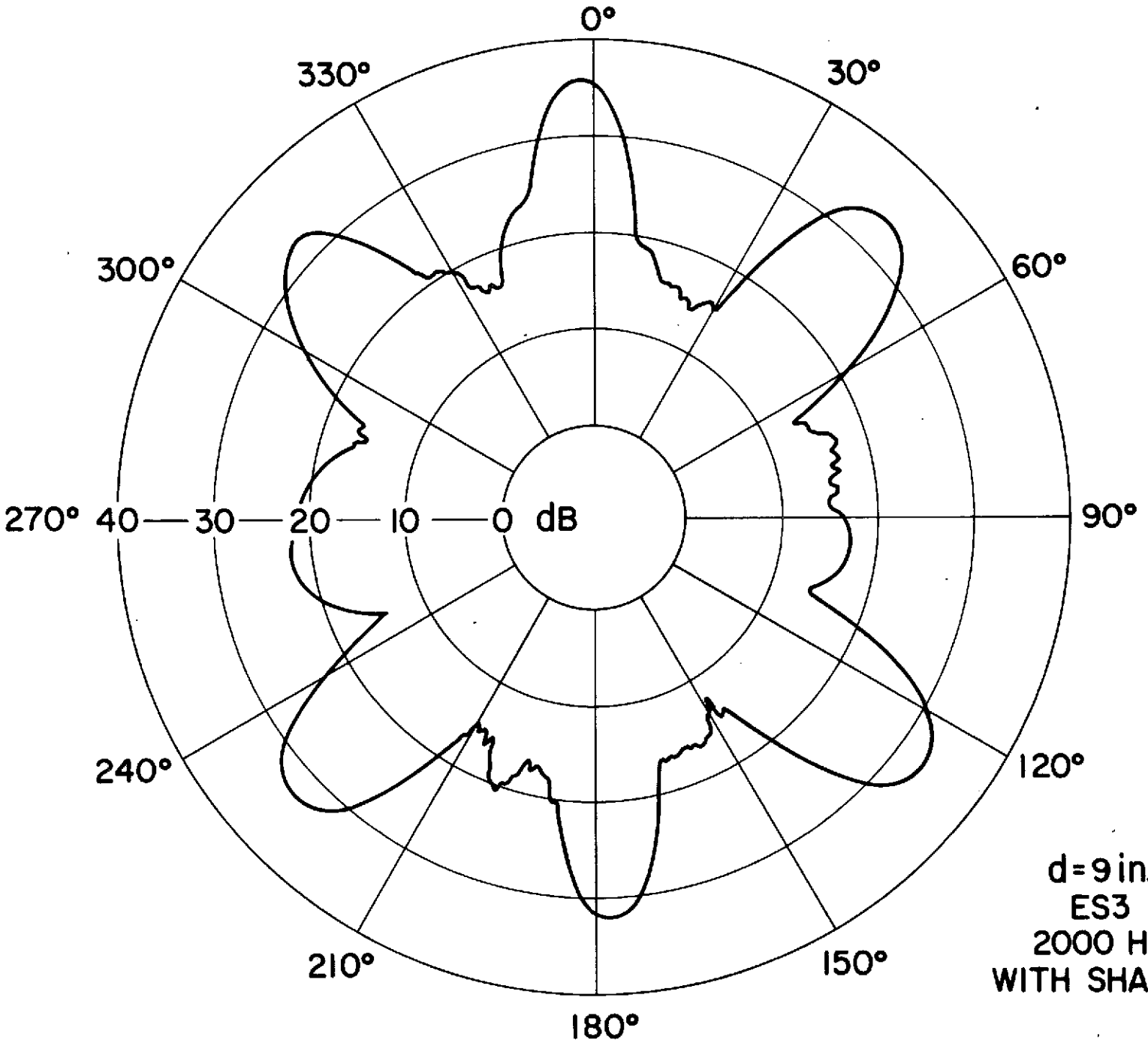

d=9 in. (23 cm)
ES3
2000 Hz
WITH SHADING

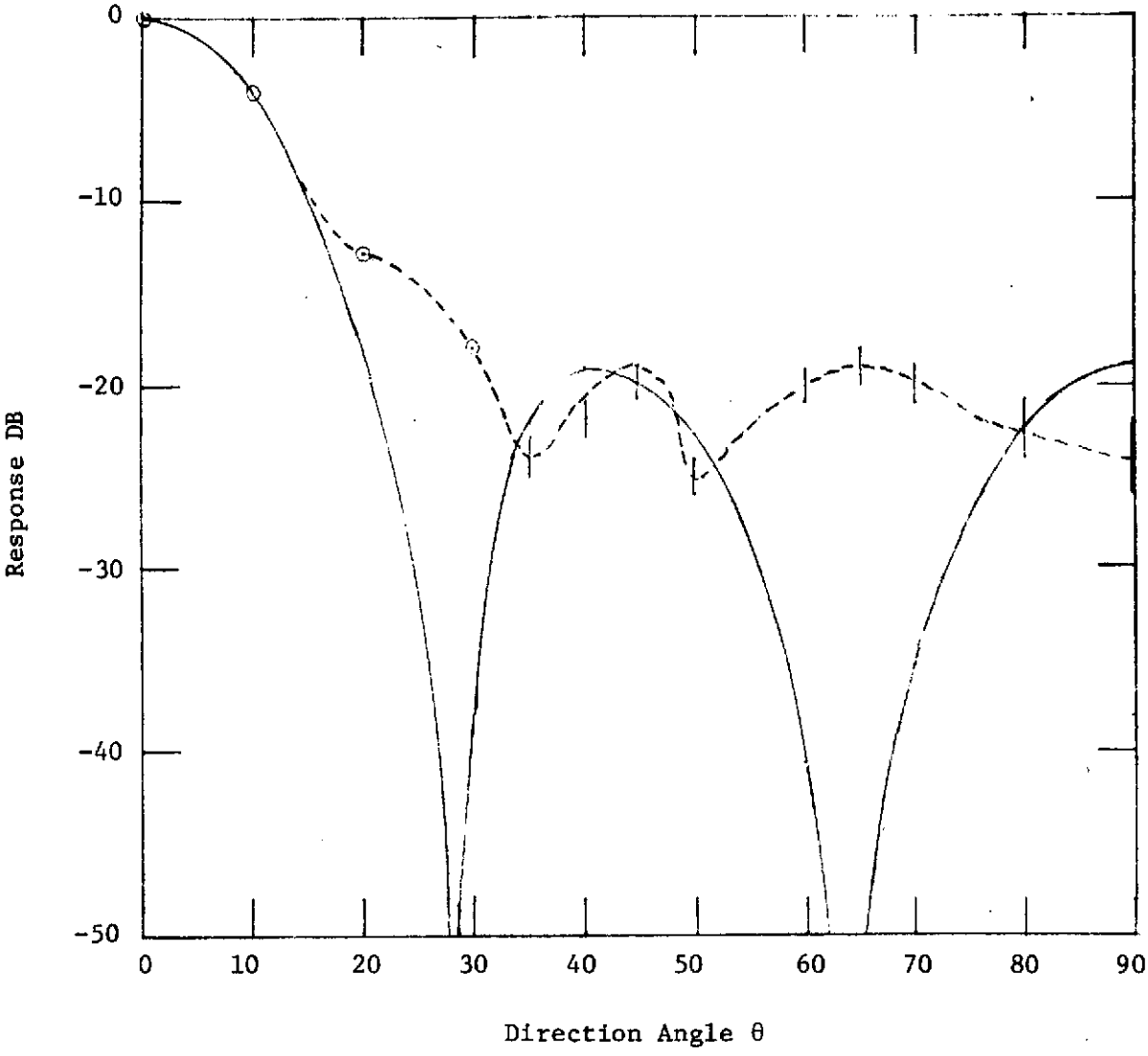

Fig. 21 Acoustical antenna response at 500 Hz (five shaded microphones per arm, placed 18" *apart). The output is the product of the two arms of the antenna. Solid curve is theoretical; dotted curve is experimental. Both curves agree for θ at half maximum (6 db), and for the difference (19 db) between the main and minor lobes. Shift in position of high order lobes in the experimental curve and lack of cancellation at the minima indicate possible poor phase matching between microphones, misalignment of the antenna (not working exactly in the far field), possible difference between individual microphone responses, and existence of white noise.

*46 cm

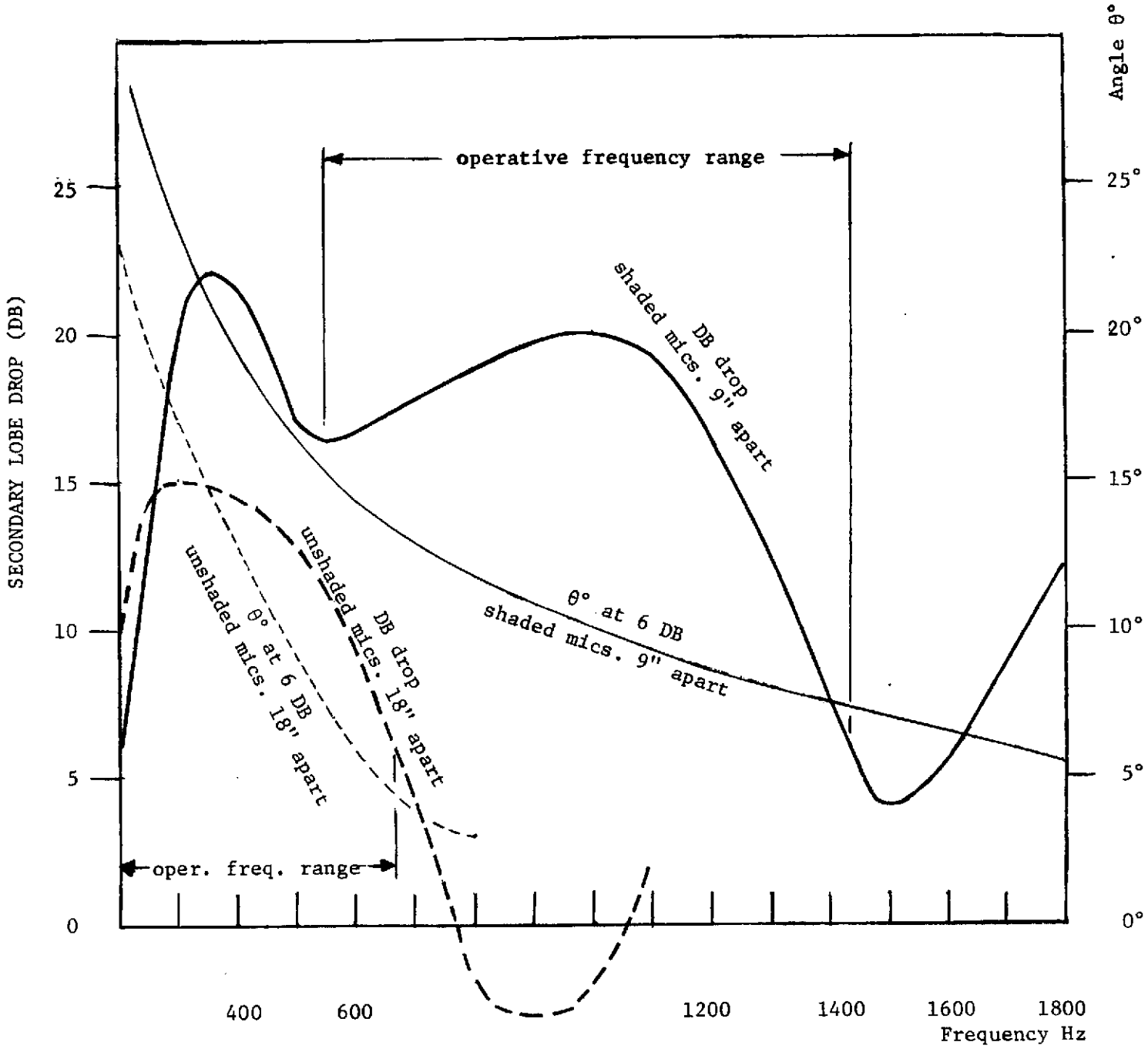

Fig. 22 Drop between the main lobe and secondary lobes as a function of frequency for acoustical antenna with microphones 9" *(solid curve) and 18" *(dotted curve) apart; $d/\lambda = 0.75$. Also, the semi-angular resolution θ° at 6 dB for the two cases are shown. For a minimum of 6 dB drop and to avoid confusion with antenna characters, the 9" microphones separation is operative within 550-1400 Hz, and the 18" microphones separation is operative within 200-750 Hz.

*23 cm

*46 cm

PART V

CONCLUSION AND RECOMMENDATIONS

5.1 Conclusion

The feasibility of measuring aerodynamic noise in a reverberant environment (e.g., the 40x80 foot wind tunnel at ARC) without disturbing the flow has been shown. Of the various techniques which can be used for this measurement, purely acoustical methods (specifically, acoustical antennas), were adopted because of the availability of many of the needed components. Equipment was built and evaluated to carry out such measurements. Other techniques including purely optical or opto-acoustical approaches requiring either more sophisticated, less available, or more expensive equipment, are still needed to supplement the acoustic antenna results for complete mapping of the acoustic field and correlate it with the theories of noise generating mechanisms in an aerodynamic flow. In brief, the acoustical antenna scheme which has been built is able to:

(a) localize the noise sources with an angular resolution of about 10° at 6 db,

(b) determine the frequency and strength of such sources,

(c) discriminate between the source and reverberant background,

(d) do all the measurements without disturbing the jet flow,

(e) steer the acoustic antenna electronically without disturbing the spatial position of the antenna, its components, or readjustment of the electronics of the control circuit,*

(f) measure various frequency ranges with the same electronic equipment, by merely changing the separation between the antenna microphones, or using other sets of microphones which are prearranged (Sec. 4.5.2 (3), p. 52 and Sec. 2.2.2 (2), p. 30), and

---

*Microphones are assumed to have flat characteristics from 0 to $\pm 90°$ only; otherwise the tunnel wall behind the antenna should be covered with absorbing material to prevent back reflection.

(g) do all the measurements without readjusting the electronics because of any change in the radiation frequency under study.

We may add that microphone shading resulted in better directivity response by equalizing the minor lobes (Sec. 4.5.2 (2)). The shading coefficients are constant as long as the ratio d/λ is unchanged.

Now, we proceed to expound, briefly, our recommendation for future studies on this project.

5.2 Recommendation for Further Studies

1. A new model of an acoustical antenna, the design of which is basically the same as the one that has already been built, is recommended. This new model will feature: (a) easier operation; (b) maximizing the performance in the sense of obtaining higher discrimination (higher angular resolution), same output at input frequency, sharpening the main lobe, suppressing minor lobes, automatic shading, etc., using the same number of acoustic transducers (microphones) if possible; (c) a self-contained portable package which can be used indoors or outdoors; (d) near field measurement capability, as well as far field measurements; and (e) automatic as well as manual steering.

2. Measurement should be done to correlate the acoustical measurements with the density fluctuations in the flow. Optics techniques, probing the flow (looking inside it) are available. These techniques are of two types:

(a) point by point probing, and

(b) interferometric and holographic mapping of the acoustic field. Part III and Appendix A, Sec. IV, deal with these methods extensively.

3. Design a new acoustical antenna, having the general capability of the already designed one (Model 909B), and, in addition, producing an acoustical hologram to be analyzed later on, either by computer or optically, to confirm the noise identification as well as the density fluctuation, simultaneously.

BIBLIOGRAPHY

1. Hargest, J. Sound and Vibration 20, 360 (1972).

2. D. A. Bies, "Investigation of the feasibility of making model acoustic measurements in the NASA Ames 40x80 foot wind tunnel." Bolt-Beranek & Newman, Report #2088 for NASA Contract NAS 2-6206, July 1970. NASA-CR 114352.

3. O. K. Mawardi, Reports on Progress in Physics 19, 156 (1956).

4. H. H. Hubbard et al., J. Sound & Vibration 19, 227 (1971).

5. H. von Gierke et al., J. Acous. Soc. Am. 24, 169 (1952); also "Symposium on jet noise", J. Roy. Aeronautical Soc., p.221 (1953).

6. Reference 3.

7. Handbook of Acoustic Noise Control, WADC Tech. Report 52-204, p. 119 (Vol. 1, 1952, Wright Air Development Center, Ohio).

8. Reference 3, p. 169.

9. W. L. Lassiter and H. H. Hubbard, Tech. Notes, NACA 2757 (1952); J. Acous. Soc. of Am. 25, 381 (1953); Tech. Notes, NACA 3187 (1954); J. Acous. Soc. of Am. 27, 431 (1955).

10. M. J. Lighthill, Proc. Roy. Soc. A 222, 1 (1954).

11. I. Proudman, Proc. Roy. Soc. A. 214, 119 (1952).

12. H. S. Ribner, Institute of Aerophysics, Univ. of Toronto, Report #51 (1958).

13. M. V. Lawson, Theoretical Studies of Compressor Noise, NASA CR-1287 (1969).

14. L. L. Beranek et al., J. Acous. Soc. Am. 27, 217 (1955).

15. P. M. Morse, "Vibration and Sound" (McGraw Hill, New York, N.Y., 1936, 1st Edition) p. 320 ff.

16. V. Bolleter et al., J. Acous. Soc. Am. 51, 1439 (1972).

17. H. F. Olson, Broadcast News 28, 32 (1938).

18. H. F. Olson, Jour. Inst. Rad. Eng. 27, 438 (1939).

19. W. P. Mason et al., J. Acous. Soc. Am. 10, 206 (1939).

20. Kurze, Tech. Mitt. PTT 27, 1 (1954).

21. A great deal of information is found in an N.D.R.C. Summary Technical Report, Div. 6, Vol. 13, which renders an account of work performed during World War II at the Howard Underwater Sound Laboratory on this subject.

22. Robert E. Collin and Francis J. Zucker, "Antenna Theory" (McGraw Hill Book Co., New York, N.Y. 1969), Part I, p. 138 ff. In this survey on linear antenna arrays, over 80 articles are cited describing the state of the art on antenna design.

23. C. L. Dolph, Proc. IRE 34, 335 (1946).

24. R. L. Pritchard, IRE Trans. Antennas Propagation, Vol. AP-3, 40 (1955); also Acoustics Res. Lab. Tech. Mem. No. 7 (1950), Harvard University.

25. M. Ryle, Proc. Roy. Soc. (London) A 211, 351 (1952).

26. NASA final report, Contract No. 2-6672, H. M. A. El-Sum.

27. Several textbooks are available now. See for example: "Principles of Holography" by H. M. Smith (Wiley, 1969); "Optical Holography" by R. J. Collier et al. (Academic Press, 1971); "Reconstructed Wavefront Microscopy", by H. M. A. El-Sum (under publication by Pacific Press); "Advances in Holography" by same author (under publication by Plenum Press).

28. L. O. Heflinger et al., J. Appl. Phys. 37, 242 (1966); IEEE J. Quantum Electronics EQ-2, 275 (1966).

29. D. J. Collins et al., J. Appl. Phys. 42, 1109 (1971); Trans. of ASME, J. Appl. Mech. paper #72-APM-PP (1971).

30. C. D. Maldonado, et al., J.O.S.A. 56, 1305 (1966) and 55, 1247 (1965).

31. F. Jahodo, Proc. Opt. Methods in Gas Dynamics Research (May, 1970).

32. B. V. Markevitch, private communication; Aviation Week 94 (March 1, 1971).

APPENDIX A

EARLIER STUDY OF THE PROJECT

The following 29 pages are reproduction of an earlier analysis of the project . This analysis were made by the authors and their associates.

Page intentionally left blank

I. INTRODUCTION

1.0 GENERAL REMARKS

The basic formalism for the aerodynamic generation of noise in its broad outlines was developed a few years ago by Lighthill.[1] He was able to show that the general equations of fluid dynamics, by means of a quasi-linear approach lead to a formal expression for the sound generation, wherein the fluctuating Reynolds' stresses play the equivalent role of acoustic sources. Lighthill himself[2] and several other investigators [3],[4] after him pointed out that the strength of his effective sound sources is in fact the first term of a series expansion in the Mach number for the flow. Since this series diverges for Mach numbers greater then unity, Lighthill's earlier formulation is applicable solely to subsonic flows.

The mechanism of noise aerodynamically generated by a fluctuating supersonic flow is expected to be quite different from the subsonic regime. This is not surprising at all, since fluid elements moving coherently and with supersonic velocity will radiate collectively in a manner reminiscent of the familiar Cerenkov effect. Accordingly, a number of semi-heuristic models [5], [6] have been proposed in which the acoustic effect of the fluctuating flow is represented by virtual sources made up of discrete "eddies" radiating as moving sources (Eddy Mach waves).

In light of the brief discussion mentioned above, we will survey the details of noise generation in the subsonic case separately

from that in the supersonic case. It will be seen that Lighthill's theory is a very powerful tool which allows the treatment of any aerodynamically noise generation mechanism associated with a subsonic flow.

1.1 THE SUBSONIC REGIME

We will find it very convenient from a diagnostic point of view to discuss two subdivisions of noise generated in this flow regime: a) The broad band noise (turbulence), b) the coherent or narrow frequency band.

1.1.1 NOISE FROM TURBULENT FLOWS

Since reference to Lighthill's theory will be made quite often in this section, we will summarize some of its salient features. It is readily shown (Ref. (1)), that the sound field is described by

$$\nabla^2\rho - \frac{1}{c^2}\frac{\partial^2\rho}{\partial t^2} = -\frac{1}{c_o^2}\frac{\partial^2 T_{ij}}{\partial x_i \partial x_j} \qquad (1)$$

where ρ is the fluctuacting acoustic density, c_o is the velocity of sound in the fluid region which is at rest (i.e., outside the flow) and T_{ij} stands for $(\rho v_i v_j + P_{ij} - c_o^2 \nabla^2\rho\, \delta_{ij})$. The beauty of Lighthill's formulation is that it not only takes into account the effect of the fluctuating Reynolds' stress $\rho v_i v_j$, but also nonlinearities in pressure and densities. In most cases of interest here, the Reynolds' stress are the dominent source terms. Consequently, as was argued by Lighthill the right hand side of the equation are equivalent to quadrupoles.

Now for randomely fluctuating field, the intensity is the essential sound field variable. Hence it is found that the intensity I is derived from

$$I(\underline{x}) = \frac{1}{16\,\pi^2\,\rho_o\,c_o^5} \iint \frac{(x_i-y_i)(x_j-y_i)(x_k-z_k)(x_\ell-z_\ell)}{|\underline{x}-\underline{y}|^2\,|\underline{x}-\underline{z}|^2} \cdot$$

$$\cdot \overline{\left[\frac{\partial}{\partial t^2} T_{ij}\left(\underline{y}, t - \frac{|\underline{x}-\underline{y}|}{c_o}\right) \frac{\partial^2}{\partial t^2} T_{k\ell}\left(\underline{z}, t - \frac{|\underline{x}-\underline{z}|}{c_o}\right)\right]}\, d\underline{y}\, d\underline{z} \qquad (2)$$

The domain of integration is carried over the whole region of the flow. From eq. (2), it is clear that $\frac{\partial^2}{\partial t^2} T_{ij} \frac{\partial^2}{\partial t^2} T_{k\ell}$ is akin to a correlation. Hence a contribution will only come from the region of the fluid which is moving coherently. If one defines a characteristic dimension L within which the velocities are correlated, one can divide the field into an imaginary set of non-overlapping regions of volume of the order L^3. The intensity given by (2) is now visualized as the contribution of a distribution of point quadrupoles localized in these non-overlapping regions. The problem of exactly estimating the strength of these quadrupoles requires an *a priori* knowledge of the fluctuating flow field (i.e. turbulent field).

By taking the Fourier transform of (2) one obtains an expression for the spectral intensity evaluated from a knowledge of the spectrum of the turbulence (i.e. of $\frac{\partial^2}{\partial t^2} T_{ij}$). This has been calculated for a turbulent field with no mean flow (Proudman[7], Mawardi[8]). When the flow has a mean flow, the eddies move, so the radiation field causes the sound pattern to become

distorted (from that of a stationary quadrupole). But it is clear that the tensor T_{ij} is strongly affected by the presence of shear. Now the shear in the flow may be brought about either by a layer of fluid moving against a fluid at rest (case of a jet) or by a layer of fluid moving in the vicinity of a solid boundary. These two cases will now be looked into in some detailes

a) Free Jet

It was argued by Lighthill that the boundary layer in the jet tends to polarize the quadrupoles, thus establishing a stronger coherence and a consequent reinforcement of the sound radiated. By means of dimensional argument, one finds that the acoustic power radiated at a distance is given by

$$\underline{P} = K \frac{V^5}{C_o^5} \left(\frac{\rho_o V^3}{2} d^2 \right) \qquad (3)$$

where the coefficient K is a very slowly varying function of the Reynolds number. Typical experimental findings are:

i) The efficiency of conversion of mechanical to acoustical energy follows the predicted value M^5 fairly well, (where $M=V/c_o$). Typical values of K are 0.3 to 1 x 10^{-4}.

ii) The sound spectrum is very broad and has an ill defined maximum which seems to vary as V/d.

iii) The polar distribution of the sound has a "butterfly" type configuration in which almost all the sound radiated is encompassed in an acute angle with the jet. The theoretical directivity of

of $(1 - M \cos 0)^{-6}$ seems to be reasonably verified. Indeed Hubbard and Lassiter[9] find a 5.5 power dependence (instead of 6) for a 3/4 inch (1.9 cm) jet, 7.0 for a 3 inch (7.6 cm) jet and 6.3 for a 12 inch (30.5 cm) jet. Westley and Lilly[10] confirm the 6.3 law over a wide range of diameters.

It is interesting to note that after a considerable accumulation of experimental observation [11] over the intervening past twenty years, there seems little doubt as to the validity of the Lighthill's theory for the noise from a subsonic jet.

b) Effect of Solid Boundary on Noise Production

Lighthill's expression [2] can still be applied here, provided that one uses for T_{ij} the fluctuating shear stresses existing in the boundary layer in the vicinity of the solid body. Now, in a boundary layer, it is the motion in the region of fully developed turbulence outside the viscous sublayer which sets a distribution of velocity gradients responsible for the shear stress at the walls[12]. In a fully turbulent region there is a whole assembly of eddies which move with the different convection velocities. Since the motion in the region outside the viscous sublayer is governed mainly by inertia forces, the frequency scale is defined by

$$f^2 \sim \frac{\bar{v}_x^2}{v_o^2} \left(\frac{\partial V}{\partial x_2}\right)^2 \qquad (4)$$

V is the mean flow velocity. Phillips was able to show that the portion of maximum influence is 1/10 of the thickness of the layer and that the acoustic power radiated is approximately

$$P \sim \frac{K}{\left(1 - M_c^2\right)^2} \frac{\rho_o V^6}{c^3} \qquad (5)$$

K is a slowly varying function of the Reynolds number of the order of 10^{-7} and M_c is a mean Mach number.

It is worthwhile to note that the sixth instead of the eighth power dependence for the velocity in (5) is indicative of noise radiated from a distribution of dipoles instead of quadrupoles. This is not surprizing since a quadrupole in front of a solid boundary radiates like a dipole (i.e. the quadrupole plus its mirror image).

1.1.2 THE COHERENT NOISE CASE

The generation of acrodynamically produced sound of single frequency (or of very narrow band) is invariably found wherever some solid boundary allows the possiblity of some feedback which tends to stabilize the fluctuation in the flow around a particular mode of oscillation of the system (edge tone, vortex shedding, etc.). There again we find Lighthill's equation (2) of use, provided we use in addition an expression for the acoustic feedback on the flow. The essential point of interest from a diagnostic point of view is the complete description of the flow mechanism if one can determine the spatial distribution of the velocity fluctuations.

1.2 THE SUPERSONIC CASE

The very nature of the acoustic radiation from an element of fluid moving with supersonic velocities makes it very unlikely to obtain sound generation with narrow band spectra (or coherent). Accordingly only the free jet and the effect of solid boundaries will be considered.

1.2.1 THE FREE JET

The theory of supersonic jets has been considered theoretically by Ffowes Williams[5] and by Ribner [6]. Ffowes Williams has shown that for this case the sound emission is analagous to the Mach wave emission from supersonically moving eddies, the latter behaving very much like solid bodies. The sound source is hence equivalent to simple source and the source strength is estimated from a density correlation by an expression of the form

$$\text{Acoustic Power} \approx \frac{1}{16\,\pi^2} \int \frac{(x_i-x)^2(x_j-x)^2}{|\underline{x}_i - \underline{x}|^2} \left(\frac{\partial \bar{u}}{\partial y}\right)^2 T_{ij}(\underline{x})\, d\underline{x}$$

$$\text{where} \quad T_{ij}(\underline{x}) = \int \left\langle \frac{\partial \rho}{\partial t}\left(\underline{x}, t - \frac{|\underline{x}_j - \underline{x}|}{c_o}\right) \frac{\partial \rho}{\partial t}\left(\underline{x} + \xi, t - \frac{|\underline{x}_i - \underline{x} - \xi|}{c_o}\right)\right\rangle d\xi$$

$\bar{u}$ is of course the mean value of the flow.

The effect of the shear appears as an amplifying factor.

Now it was pointed out by Nagamatou et. al.,[14] that an important property of a supersonic jet is that the flow contains

a region that is supersonic, a transition region and finally a subsonic fully developed turbulent region .

The noise generation accordingly is different for the different regions. In the supersonic region the sound power radiated follows a $M^{3/2}$ dependence (Ffowes Williams); Nagamatou on the other hand, suggests that the formula be replaced by $M^{7-\alpha}$ near the jet exit and $M^{7-\beta}$ at the end of the supersonic region. Experimental values yield $\alpha \approx 6.2$; $\beta \approx 2.4$. It appears, however, that the α, β coefficients are sensitive functions of temperature, velocities and atomic weights of the gas so that the theory is still far from being settled.

In summary we find the table shown below very helpful for the discussion.

AUTHOR	FLOW REGIME	NATURE OF SOURCE	IMPORTANT PARAMETER
Lighthill	subsonic jet	quadrupole	velocity correlation
Phillips	subsonic boundary layer	dipole	velocity and/or correlation
Ffowes Williams, Ribner Nagamatou et. al,	supersonic jet	monopole	density correlation
- - - - -	supersonic boundary layer	dipoles	pressure correlation

II. FREE FIELD VS. REVERBERANT FIELD MEASUREMENTS

The radiation field from point sources (monopoles, dipoles, etc.) in free space is well known and yields well known directivity pattern as well as divergence dependence ($1/r^{\alpha}$; α = 1 for simple source, α =3 for dipole, etc.). From a mapping of the sound field, all the essential characteristics of the source and in particular its strength can be estimated. If the source is not a point source, but has an extention in space, the far field distribution too can yield the directivity and strength distribution (this is equivalent to inverting a Green's formulation for the radiation field).

When the source radiates in an enclosure of finite dimensions, however, the situation becomes very different for two reasons.

i) The reflected waves from the walls of the enclosure when interacting with the direct waves from the source, will interfere and the resultant sound field is so complicated that it becomes very difficult to infer from the interference pattern the characteristic of the source. If the signal radiated from the source is random, as is often the case in noise from turbulence, the field in the enclosure, the so-called reverberant field, is diffuse. If the acoustic absorption of the walls is known, then classic acoustic theory through the Knudsen's formula yields the strength of the source from the average reverberant field. But in this case no details can be inferred from the reverberant field.

ii) In many instances, the back reaction of the reflected waves on the radiating source can cause the power radiated from the source

in the enclosure to be different from that in free space. In communication theory this is equivalent to stating that because the source is not a constant current source, then the power radiated is a function of the effective impedance of the enclosure.

In our case, it will be assumed that the source acts as a constant current source, since it is reasonable to state that the sound field will not alter the strength of the turbulence in the jet. In order for the sound to interact with the turbulence (i.e., a third order effect in magnitude) one would need extremely intense sounds of an energy level comparable to the energy level of the turbulence. Now in subsonic flow it was seen that the efficiency of mechanical to acoustic energy conversion went like M^5. Typically the efficiency was of the order of 10^{-3} % and under extreme conditions could approach one per cent. For supersonic flows it is still of the order of a per cent. Hence the interaction is ruled out.

One has to point out, however, that for coherent noises (edge tones, etc.) the noise generation mechanism is very sensitive to feed back, consequently the reflected waves can be very important (because of phase effects). It is not easy to generalize the case of the narrow band noise produced aerodynamically and each case has to be studied individually. The only remark one can make, however, is that if the wave length is much smaller than the size of the enclosure and the walls are efficient absorbers, hopefully, we can approach the free field conditions.

In the next section on diagnostics we will describe three methods which will be able to allow one to obtain information on the acoustic properties of the source from reverberation field measurements.

III. METHODS OF MEASUREMENTS AND INSTRUMENTATION TECHNIQUES

3.1 IMPORTANT PARAMETERS NEEDED

In the light of the previous discussion on aerodynamic noise the field parameters of interest are of two categories. The first refers to the source, the second to the field radiated at a distance. The state of the theory is such that we can deduce the second (i.e. the noise field) from a knowledge of the first (for a few cases e.g. subsonic flow); but not the inverse.

The source is described by means of:

i) Strength of velocity fluctuations (turbulence level)

ii) Spectrum of velocity fluctuations

iii) Characteristic dimension for coherence (correlation length) and under certain conditions.

iv) Strength of fluctuations of the fluid density

The radiated sound field is described by

i) Directivity (in free space) of source

ii) Frequency spectrum for sound (pressure, or velocity in free space)

iii) Acoustic power radiated. This can be inferred from (ii) above if measurements are in free space, if not one has to make use of methods described in VI to deduce the free space equivalents.

3.2 SURVEY OF KNOWN DIAGNOSTIC METHODS

The measurement of the fluctuating velocity field in a turbulent field has been obtained directly by hot wire anemometers [5] and by velocity microphones. Unfortunately, either of these two instruments have to be immersed in the flow with a consequent disturbance of the mean value of the flow.

Several methods have been developed in which the magnitude of the fluctuating velocities and/or densities are measured by detectors which are outside the flow. Now two general procedures have been used according as to whether a tracer material is or is not introduced in the flow field. To prevent the tracers from separating from the bulk of the fluid it has to be present in extremely small quantities.

3.2.1 NO TRACER-METHODS

In these methods, the interaction of the light (e.m. wave) with the sound field is brought about via the modulation of the index of refraction (for e.m. wave) by the fluid fluctuations. This interaction has been detected in a number of ways.

a) Funk and Cikanek[16] correlate the output from two optical signals, originating from two lasers and which have been transmitted through the gas. Although their paper does not state it, the correlation they observe is directly related to the density fluctuation.

b) Gruber and Marhic[17] have conducted the above experiment much more carefully. They also work out the theory. They show that the spectrum of the signal is proportional to

$$\left(\frac{\nu_o}{kc}\right)^2 \frac{1}{2\pi} \int_{-\infty}^{\infty} e^{-ik\xi} T_{ij}(\xi)\, d\xi \quad .$$

ν_o is the frequency of the e.m. wave, $k = \omega/U$ is the wave number corresponding to the acoustic frequency ω, U is the mean flow velocity and T_{ii} $\langle n(\underline{x},t)\, n'(\underline{x}', t+\tau)\rangle$ is the cross correlation for the density.

3.2.2 TRACER-METHODS

If a tracer gas is introduced in the field, the sensitivity of the diagnostic techniques can be improved. This is because the index of refraction (real and/or imaginary part) for the tracer is usually more sensitive to the fluctuations then that (i.e. index) for the host gas. In most cases the hot gas is air. A typical application of this method is described below.

Wilson et. al., have used a crossed beam optical method to detect the influence of the fluctuations on the absorption of the traces of CO_2 that are already present in the air.

The transmission loss for each beam is directly related to the local fluctuation of the density in the mechanism. Hence the correlation of the outputs from the two beams yields directly the cross correlation for the density. This has been denoted by T_{ii} in 3.2.1(b). Wilson et. al., assume that the CO_2 is so diffused in the host gas, that it is reasonable to consider the density of the tracer to be directly proportional to that of the host gas.

It is interesting at this point, to observe that a great deal of work on holographic and optical investigations in other fields seem to be unfamiliar in acoustics as they are rarely referred to. For instance, it was shown by Buchshaum and Gsanastein[19], Bekefi[20]

C2

and others that if a mild glow discharge is struck in a gas flow the very weakly ionized gas yields an electron gas which can be treated as a tracer gas. Since the ionized gas is completely collision dominated, there is no question but that the local fluid velocity as well as the local density of the electron gas is that of the host gas. A great advantage of this method is that the chemical composition of this tracer is independent of that of the host gas i.e. it will always be an electron gas, unlike the case of Wilson et.al., where they had to concentrate on CO_2, etc. Now, for most of these weakly ionized gases one can easily obtain densities of 10^{11} to $10^{13}/cm^3$ which brings them within the reach of many readily available detection techniques, in particular

i) Laser interferometric techniques: Ashby-Tephcott[21] and Hooper[22]

ii) Holographic interferometric technique: Jahodo[23]

iii) Thomson scattering[24]

Another advantage of these methods, is that whereas in the methods described in 3.2.1(a) and (b) only, the correlation of the density is measured, the techniques of (i) to (ii) yields the density, while (iii) yields the velocity.

3.2.3 LASER INTERFEROMETRIC TECHNIQUES

The laser cavity is coupled, in series, to another cavity which contains the turbulent region of interest. This region is now outlined by a glow discharge so that the region is filled with diffuse electrons. A mirror at the end of turbulent region is now made to rock to and fro. Consequently, the cavity containing the turbulent region goes through resonances and anti-resonances and

the corresponding output from the laser is directly proportional to the "load".

It is shown that, the electron density and hence that for the gas is proportional to the slope near the anti-resonance. By using a separate path (as a reference path, one can obtain the auto-correlation for the density. Limiting resolution times of 0.1 μsec have been obtained with this method.

3.2.4 HOLOGRAPHIC INTERFEROMETER

The advantage of this method is that one can obtain a map for the autocorrelation of the density. Unlike 3.2.3 where the auto-correlation function is measured point by point. The arrangement for this method is shown in Fig. 1 which is self explanatory. (After Jahodo, Ref. 23.)

It is known from holographic theory that in fact the intensity of the signal received is directly related to the auto-correlation density for the electrons and hence for that of the gas.

3.2.5 INTENSITY OF OPTICAL LINE

This method does not rely on lasers. It follows directly from the fact that whereas the density of electrons is proportional to that of host gas, so also is the density of the excited atoms (because the gas is collision dominated). Consequently the intensity of the light emitted at a given optical wavelength is proportional to the density of the gas.

When one monitors the light emitted, one measures directly a quantity proportional to the density. A correlation of the light output hence yields the correlation of the density directly as was shown by Bekefi et. al.

Fig. 1. Holographic Interferometric Arrangement of F. Jahodo (23)
to Map the Autocorrelation of the Density.

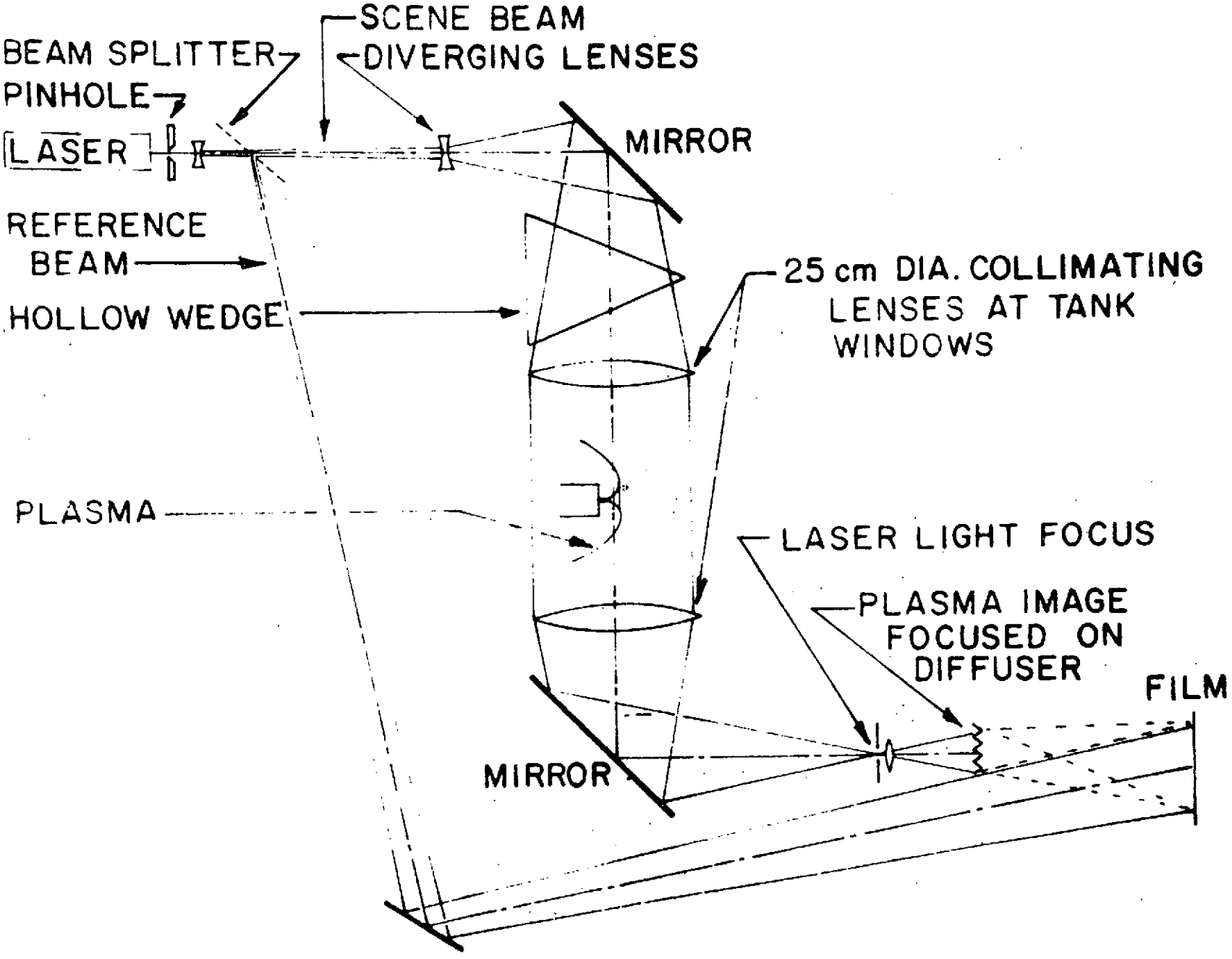

3.2.6 THOMSON SCATTERING

Sometime ago Salpeter[24] showed that the Thomson scattering from the ions in an ionized gas yields a direct measurement of their local temperature. Since the ions, here, are cold, it is reasonable to assume that their fluctuating energy (mainly turbulent energy) is greater than their thermal energy. Consequently, the scattering energy in a Thomson scattering experiment should be directly proportional to the auto-correlation of the ions velocity (and hence of that of the neutral gas).

This experiment, which has been very successful in plasma investigations is difficult to perform and not conceivable to be completed in one year. Because of the low intensity of the scattered signal (since the ion density is so low) one would have to use substantial optical energy as obtained from a Ruby laser. The experiment is feasible in principle and should be considered in long range planning.

IV. HOLOGRAPHY AND VISUALIZATION OF SOUND FIELDS

We discussed in section (3.2.4) a tried technique utilizing holographic interferometry to record a map of the autocorrelation of the density of a gas. In this section we shall explain other methods of holography which transduce the sound field to an optical one and hence revealing visible images of the sound sources.

4.1 BRIEF INTRODUCTION TO HOLOGRAPHY

The principle of holography in brief is that when a wavefront (emitted from or scattered by an object is attended by a coherent background (reference wave), the resultant record of the two waves, known as the hologram, contains all the information about the object. Hence, when the hologram is re-illuminated the original object is

reconstructed in its true original form [29],[30],[31]. The reconstructed image can be a scaled up or down 3-dimensional replica of the object, depending on the linear scaling of the hologram and the wavelength of the reconstructing wave relative to the object wave. A hologram can be made with acoustic radiation and reconstructed with an optical one and hence transducing the acoustic object or source to a visible one[32], [33].

4.2 REFERENCE WAVES IN ACOUSTICAL HOLOGRAPHY

The reference wave is an essential component in recording a hologram. Such a reference wave in acoustical holography, however, need not be a physical one. It can be simulated electronically[32] or temporally[34]. The electronically simulated reference hologram is made by mixing (before recording), electronically, the object signal with another one from a local oscillator tuned to the same frequency as that of the object, and properly phased to simulate the required wave form. The temporal reference, on the other hand, has a frequency that differs from that of the object by an amount Δf. Both types are made by either a scanning detector or a properly arrayed detectors (linear or mosaic configuration) properly phased to introduce the off-set angle θ that separates the object wave from the simulated reference wave, according to the equation $\sin \theta = (\Delta f/f) \cdot (c/v)$ where v and c are the scanner and sound propagation velocities.

4.3 DIRECT SOUND-LIGHT INTERACTION

A pseudo-acoustical-holography approach is based on the direct interaction between coherent light and the sound field[35]. Such

interaction results in Bragg diffraction of the light wave which provides a real-time visualization of the sound field. The Bragg angle is governed by the ratio of the light to sound wavelengths. The reconstructed image is demagnified by the ratio of the two wavelengths and furthermore, its resolution is influenced by the size of the light source. It has been shown analytically that this technique is useful for visualizing single frequency sound sources of medium frequencies range, (outside that of aerodynamic noise) and hence will be considered no further.

4.4 HOLOGRAPHIC INTERFEROMETRY

It is well known and has been demonstrated that a single hologram can store several wavefronts, e.g. at different times. Hence, if a conventional doubly exposed, pulsed, optical hologram is made of the flow, its reconstruction may reveal the change that took place in the flow during the interval between the two exposures. Careful analysis of such technique in order to locate and define the sound sources in the flow may prove to be quite beneficial.

4.5 DIFFICULTIES OF HOLOGRAPHY AND HOW TO OVERCOME THEM

Holograms have been made so far in a quiet environment with monochromatic radiation. Both of these conditions may not be satisfied in the 40 x 80 foot wind tunnel: the aerodynamic noise sources are broad band and the wind tunnel is reverberant. Furthermore, the source of noise may not be stationary. To overcome these

difficulties, we must use very narrow band detectors, well-focussed on a specific plane, and more or less near-instantaneous type recording. With such detectors one can make a temporal reference type hologram (the unknown signal is mixed with a known fixed frequency one before recording) the construction of which will reveal the sources of that particular band. On the other hand, if the detectors have a wide band characteristics, then the construction of a temporal reference hologram is expected to reveal one of the following:

a) If the noise sources are stationary and have the same single frequency, they will be reconstructed optically with their relative positions preserved.

b) If the noise sources are stationary, monochromatic but of different frequencies, they will be reconstructed, with distorted relative positions, (equation of section 4.2). The exact relative positions can be determined by repeating the experiment with different reference waves of different frequencies, and comparing the various reconstructions from the various holograms.

c) If there is only one stationary noise source having a broad continuous band, its image will be revealed as a defocussed image. The intensity distribution in the image is a function of the power spectrum of the source.

d) Discrete sources of the above (c) type can be similarly analyzed. The degree of overlap of the reconstructed images depends on the band width of each source and their relative distribution in space.

e) Moving sources of narrow spectral band width produce streaks of constant intensity, while broad band sources produce streaks of variable intensity in directions other than the direction of migration of the source. This is the most difficult of all cases and require further theoretical analysis to determine both the degree of accuracy in interpreting the results, and the experimental implementation.

f) Other configurations are possible and require the analysis of different holograms taken with different reference waves and also, taken in different locations.

The detectors in this approach can be either

(i) A single detector

(ii) A linear array of detectors scanning in a direction perpendicular to their arrangement

(iii) A mosaic of detectors in a two dimensional lattice, or

(iv) A series of piezoelectric crystals probed with an electron beam, after a fashion similar to Sokolov tube (36).

The choice of the appropriate configuration depends mainly on the stability of the sound sources.

Another problem that may be encountered is the effect of turbulence. This, however, can be overcome by making a conventional type hologram with the reference wave penetrating the same turbulent flow. Experimental verification of this approach has been demonstrated by Aoki [37].

V. ANTENNA THEORY AND ACOUSTIC NOISE MEASUREMENT

Measurement of the coherence of the pressure variation between pairs of points at various vectorial separation is the tool that is useful in the study of noise radiation from extended sources in other subjects, for example radio astronomy [28]. While undoubtedly the same statistical theory holds true in acoustics, there are differences in practice arising from the necessary proximity of the sources to the measuring instruments and from the special character of the instruments themselves, that require attention before an experimental investigation of this tool can be recommended.

The coherence measurements concept is independent of the hardware implementation, applying equally to any acoustic sensor whose output follows the time-varying pressure.

From a study of this approach, we should arrive at theoretical limitations on the resolution with which noise sources can be localized by measurements made well outside the main flow, where the problems of perturbations are at a minimum.

Data processing of information obtained by multiple probes is fortunately well advanced and covers a number of configurations such as variable-spacing and arrays of various kinds, all of which should be examined for possible application to, or modification for, the noise problem.

VI. DISCRIMINATION AGAINST REVERBERATION NOISE

It was mentioned in our general remarks that three methods can be used to discriminate against the reverberant signals. These are

1) The use of a pulsed flow

2) The use of correlation techniques

3) The use of highly directional microphones

We discuss these briefly.

6.1 THE USE OF PULSED FLOW

If the flow is pulsed, with characteristic times less than 30 millisecs (corresponding to time of travel of sound over the smallest dimension of tunnel i.e. $\sim$40 ft (12.2 m)), that a discriminating circuit gated over the same period will only receive the direct sound. For large jet engines this may not be practical.

6.2 THE USE OF CORRELATION TECHNIQUES

Correlation techniques has been used with great success in a number of applications. The basic idea is based on the use of two microphones. The output of these two microphones is correlated. The signal received from one consists of the direct signal plus signals which have suffered many reflections from the walls. If the signal to each microphone is written as

$$S_d(r,t) \quad \text{and} \quad S_i(r,t)$$

i.e. direct and indirect, then the correlation of the two outputs is

$$F(r,r',\tau) \approx \int_{-\infty}^{\infty} [S_{d,1}(r,t) + S_{i,1}(r,t)][S_{d,2}(r',t+\tau) + S_{i,2}(r',t+\tau)]\, dt$$

Since the reverberant signals usually suffer several random reflections and changes of phase specially if the walls act as diffuses, then beyond a correlation length of the order of a wave length $F(r,r',\tau)$ has contribution only from the two coherent signals which are the direct signals, i.e.

$$F(r,r',\tau) \approx \left\langle S_{c,1}(r,t)\ S_{d,2}(r',t+\tau) \right\rangle$$

The disadvantage of this method is that it is very laborious, as the field is plotted point by point, and furthermore the correlation is made in time, which requires special long delay instruments such as magnetic recorder.

6.3 THE USE OF HIGHLY DIRECTIONAL MICROPHONE

The most direct method is to discriminate against the reverberant noise by means of direction signals. There are two types which are specially recommended

1) The tubular microphones
2) Shaded line microphones

The art of designing directional microphones is very old and dates from the decade of the 40's. The characteristics of such instruments are very well known.

Tubular microphones orginally due to Mason and Marshall[25] and later refined by Olson[26] have a directivity which is very sensitive to frequency. In fact it is expressed by

$$\text{Directivity} \quad \alpha \frac{1}{n} \frac{\sin \phi}{\sin \phi n}$$

where $\phi = \frac{\pi L}{\lambda} (\cos \theta - 1)$.

" n " is the number of tubes in the bundle. L the length of the longest tube, θ the angle of view and λ is the wave length of sound. A fifty tube microphone yields a 60° lobe with a discrimination of 30 db for $L/A \approx 0.5$. Of course the directivity improves

with increasing frequency. Since aerodynamic noise, however, has a wide band character it is important to cover a fairly large range of frequency.

In the shaded line array of microphones, the line consists of microphones not necessarily equally spaced and phase and/or amplitude compensated.

For the particular case considered here, the simplest array considered is a cross array made of two lines containing m and n microphones each seperated by distance d_1, d_2 respectively. The directivity for such an array is given by [27]:

$$\text{Directivity} = \frac{\sin\{(\cos\alpha)(m\pi d_1/\lambda)\}\sin\{(\cos\beta)(n\pi d_2/\lambda)\}}{m\sin\{(\cos\alpha)(\pi d_1/\lambda)\}.n\sin\{(\cos\beta)(\pi d_2/\lambda)\}}$$

α, β are the zenith and azimuth angle of view.

REFERENCES

(1) Lighthill M.J., Proc. Roy Soc. A 211, 564, (1952).

(2) Lighthill M.J., Camb. Phil Soc. 49, 531 (1953), Proc. Roy Soc. A 222, 1, (1959).

(3) Kraichnen R.H., J. Acoust. Soc. Am. 25, 1096, (1953), Ibid 27, 438, (1955).

(4) Mawadi O.K., J. Acoust. Soc. Am 27, 442, (1955).

(5) Ffowes Williams, J.E. et. al., F. Fluid Mech. 24, #4, (1965).

(6) Ribner H.J., Advances App. Mech. 8, 103, 1964 (See also Proceedings Basic Aerodynamic Noise Research NASA SP-207, 1969).

(7) Proudman, F. Proc. Roy Soc. A 216, 119, (1952).

(8) See Ref. 4.

(9) Hubbart, H.H. et. al., NACA TN 2 757 (1952), J. Acoust. Soc. 25, 381, (1952).

(10) Westley, R.M. et. al., Rep. Coll. Aero, Cranfield 53, (1952).

(11) See in particular NASA SP-207.

(12) Townsend A.A., Proc. Camb. Phil Soc. 47, 375, (1951).

(13) Phillips, O.M. Proc. Roy Soc. A. 234, 327, 1956.

(14) Nagamatsu, et. al. see in particular NASA SP-207 p. 17 ff.

(15) A very good summary of the state of the art found in L.L. Beranck Acoustic Measurements (J. Wiley & Son, New York).

(16) Funk, B.H. et. al., NASA TM X-53850, 1969.

(17) Gruber S., et. al., (In Press) J. Acoust. Soc. Am.

(18) Wilson, A.N. et. al., NASA SP-207 p. 147.

(19) Buckshaum S.J., et. al., Brill. Am. Phys. Soc. 10, 605, (1965).

(20) Bekefi A., et.al., Proc. 5th International Conf. on ionized gases (Munich) (1961).

REFERENCES (Cont.)

(21) Ashby, D.E., et. al., J. Appl. Phys. 36, 29, (1965).

(22) Hooper, E.B. et. al., J. Appl. Phys. 37, 4083, (1966).

(23) Jahodo, F., Proc. Optical Methods in Gas Dynamics Research (May 1970).

(24) Salpeter, E.E., Phys. Res. 122, 1663 (1961).

(25) Mason W.P., et. al., J. Acoust. Soc. Am. 10, 206 (1939).

(26) Olson H.F., Elements of Acoust. Eng. (van Norstrand, N.Y. 1967).

(27) Sterzel H., Leitfaden zur Berechnung von Schallvorganger (Springer Verlog, Berlin 1939).

(28) Bracewell, R.N. et. al., Sky and Telescope, 42 (July 1971).

(29) Gabor, D. Nature 161 777 (1948); Proc. Roy. Soc. A 197 454 (1959) and B64 244 (1951).

(30) El-Sum, H.M.A., Ph.D. Dissertation (Stanford Univ., 1952).

(31) Leith, E.N. and Upetnicks, J., J.O.S.A. 51 1469 (1961), 52 1123 (1962).

(32) El-Sum, H.M.A., Et. Al., J. Acoust. Soc. Am. 42 1169 (1967).

(33) El-Sum, H.M.A., Acoustical Holography, vol.I, pp. 1-25, (Plenum Press, 1969); SPIE Proceedings 15 137 (1968).

(34) El-Sum, H.M.A., Acoustical Holography, vol. II, pp. 7-22, (Plenum Press, 1970).

(35) Korpel, A.; App. Phys. Letters 9 425 (1966).

(36) Sokolov, S., U.S. Patent 2, 164, 125 (June 27, 1939).

(37) Aoki, Y., Acoustical Holography (vol. I), pp. 244 (Plenum Press 1969).

APPENDIX B

ACOUSTIC ANTENNA
ELECTRONIC STEERING CONTROL, MODEL 909B
OPERATING MANUAL

ACOUSTIC ANTENNA
ELECTRONIC STEERING CONTROL
MODELS 909 & 909B

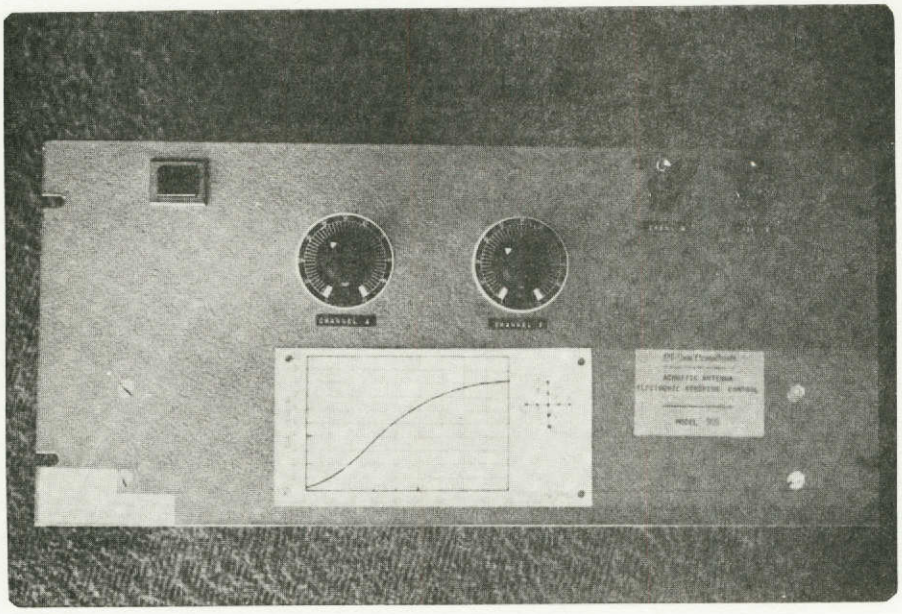

FRONT VIEW

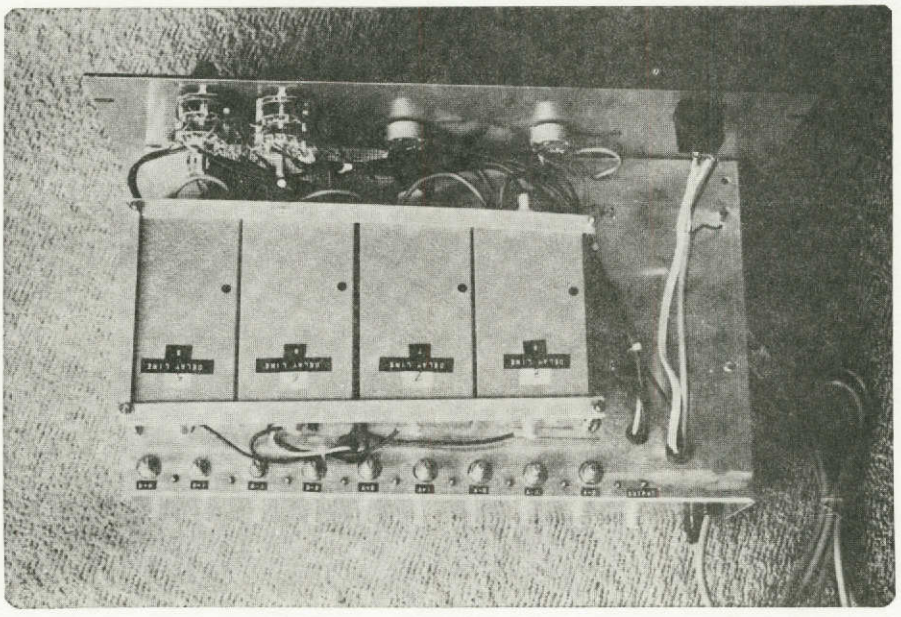

BACK VIEW

ACOUSTIC ANTENNA

ELECTRONIC STEERING CONTROL

MODEL 909B

TABLE OF CONTENTS

Front and back view of the instrument ---------- ii

Introduction ---------- 1

Specifications ---------- 2

Design features of model 909B

- Measured output ---------- 3
- Steering of antenna ---------- 4
- Shading (Tschebycheff correction) ---------- 7

Calibration and Testing procedure ---------- 9

Block circuit diagram ---------- 5

Positions of electronic phase shift selector switches ----- 6

Calibration curve (Dial reading vs. steering angle) ------- 8

ACOUSTIC ANTENNA
ELECTRONIC STEERING CONTROL

MODEL 909B

INTRODUCTION

Model 909B electronic steering control is a unique instrument capable of steering two crossed linear arrays of acoustic transducers (microphones) around any chosen axis in space withount mechanically disturbing the transducers in any way. In other words, with two simple dials, any position of the plane of the acoustic antenna may be chosen.

The maximum number of transducers which can be used with this model is nine, arranged in two groups (A & B) of five each. Each group is placed along a straight arm, and the two arms form, preferably, a right-angle cross. The plane of the transducers can be made to rotate clockwise or anticloskwise around a vertical axis, out of,or into its own plane around a horizontal axis, or tilt in any direction by the combined rotation around the two axes. Thus,linear, two dimensional, as well as helical scanning are possible. All this can be accomplished , simply, by appropriate positioning of two switches and properly controling two dials. The dials control the necessary phase shifting of the transducers in order to induce the eqivalence of mechanical rotation. The phase shifting is independent of the frequency of the detected radiation. Provision is made for high directivity as well as improved discrimination against unwanted background noise, such as reverbration and echoes, through Dolph-Tschebycheff shading.

SPECIFICATIONS

Maximum number of transducers (microphones)per arm ----- 5
Number of linear arrays ---------- 2
Maximum number of transducers (total) ---------- 9
Possible steering of one array independent of the other- yes
Possible steering of both arrays simultaneously ------- yes
Phase shift at 1 KHz (per delay line) ---------- 4.7 radians
Steering angle of any linear array ---------- 0^0 to 360^0
Steering dependence on radiation frequency ---------- none
Suggested optimum value of (d/λ) ---------- 0.75
Half angular resolution ---------- 10^0
Maximum input per channel ---------- 30 mv
Power supply ---------- 110^V;60∿;1 A
Style ----- rack mount 19"w x 8.75"h x 10"d (48.3 x 22.2 x 25.4 cm)
Weight ---------- 15.25 lb (6.8 Kgm)
Output ----- each linear array (arm) seperately, or
the product of the two arrays.

DESIGN FEATURES OF MODEL 909B

MEASURED OUTPUT

If w (x,y) is the microphone strength distribution in the (x,y) plane, its response to the incident wave (Figure 1) is then given by a quantity proportional to

$$\int w(x,y)\ e^{ik(x\cos\alpha + y\cos\beta)}\,dx\,dy$$

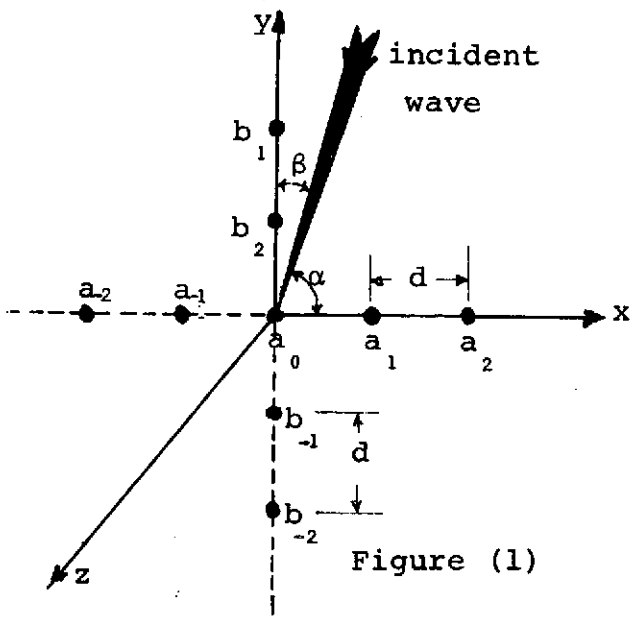

Figure (1)

where $k=(2\pi/\lambda)$, λ being the wavelength of the incident wave.

For a distribution of point microphones along the x & y-axes, the response is proportional to:

$$\Sigma w_n\ e^{ik(x_n \cos\alpha_n + y_n \cos\beta_n)} = \Sigma a_n \text{ in the x-direction, and}$$

$$\Sigma w_m\ e^{ik(x_m \cos\alpha_m + y_m \cos\beta_m)} = \Sigma b_m \text{ in the y-direction}$$

where n & m are the number of microphones in the x & y-directions respectively.

Model 909 (the predecessor of this model) measures $(\Sigma a_n)+(\Sigma b_m)$. This model 909B measures (Σa_n) alone, (Σb_m) alone, or the product $(\Sigma a_n)x(\Sigma b_m)$.

Provision is made to filter (Σa_n) and (Σb_m) before their multiplication operation. This filtering is necessary when the incident wave is noisy or hetrochromatic. If the incident wave is monochromatic (single frequency) no filtering is necessary.

STEERING OF ANTENNA

When the antenna is tilted by α (or β), as shown in Figure (1), there is a phase difference of $\frac{2\pi fd}{c} \cos \alpha$ (for $\beta=0$, say) between neighbouring microphones, where d=distance between microphones, f is the frequency and c is the velocity of sound.

In order to steer the antenna, therefore, we shift the relative phase of the output of microphones by means of electronic means through an angle equal to $\frac{2\pi fd}{c} \cos \alpha$ for horizontal direction and through an equivalent appropriate angle for the vertical direction.

The block diagram for the arrangement is shown below, Figure (2).

The phase shifters are all pass networks designed to provide 4.7 radians (+ or -) shifts at 1 KHz. Since the characteristics of an all pass network is to have constant amplitude and linear phase shift, the electric shift is proportional to the frequency.

Actually, the electric phase shift $\phi = \frac{4.7}{10^3}$ f.a , where a is an adjustable number that controls the RC value and hence the phase shift. Now we see that the phase shift

$$\frac{\omega d}{c} \cos \alpha = \frac{4.7}{10^3} f.a$$

then notice that the actual steering angle α (or β) is given by

$$\alpha = \cos^{-1}\left(\frac{4.7}{d\ 10^3} \frac{ac}{2\pi}\right)$$

It is more convenient to use the steering direction which is (90 - α) or (90 - β). The quantity actually varies between 0 and 1, and is controlled by the dials A & B .

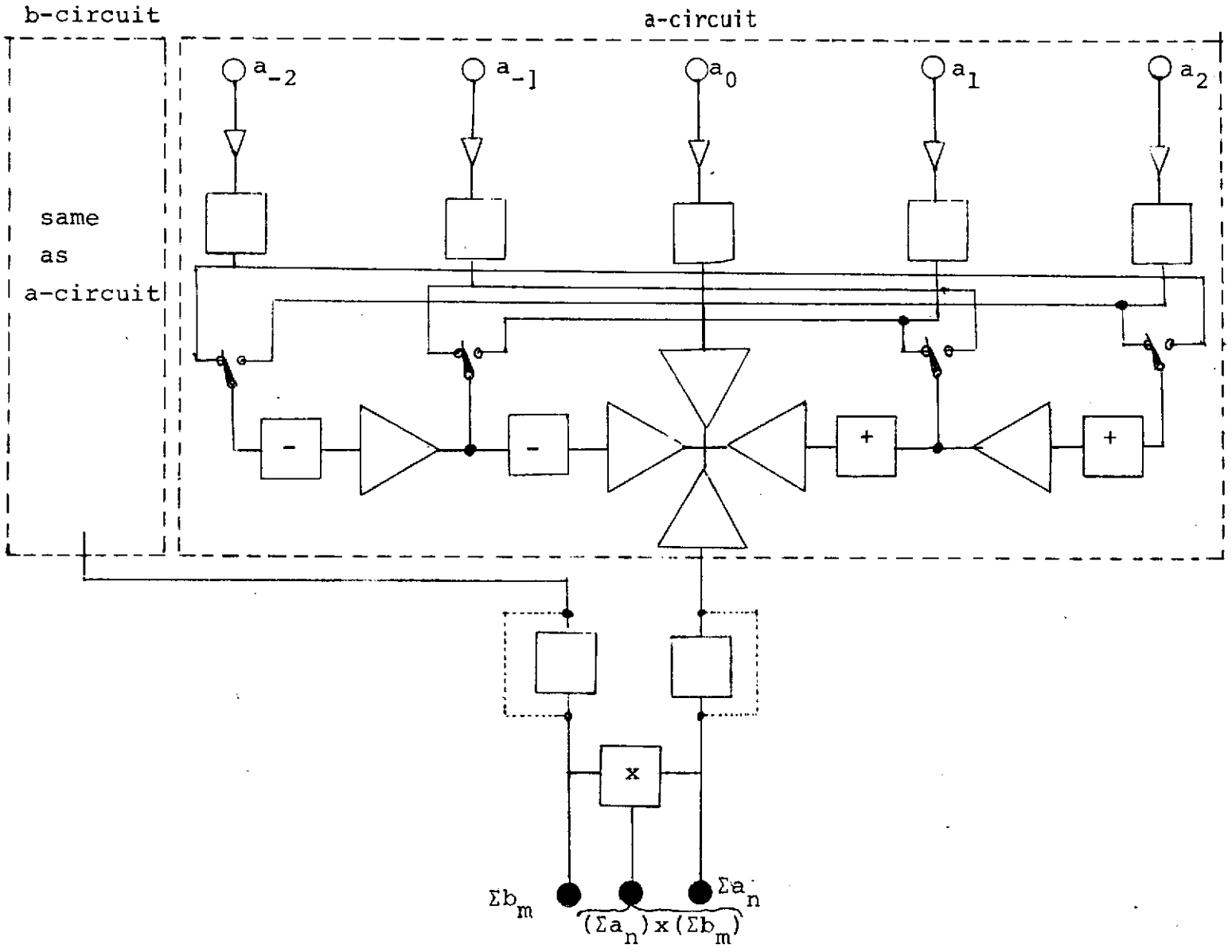

FIG. 2. Model 909B Block Diagram

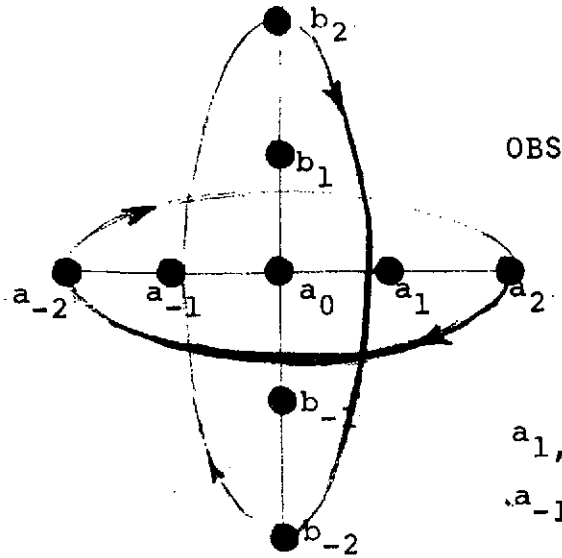

OBSERVER FACES ARRAY

$a_{1,2}$ & $b_{1,2}$ come out of page

$a_{-1,-2}$ & $b_{-1,-2}$ recede into page

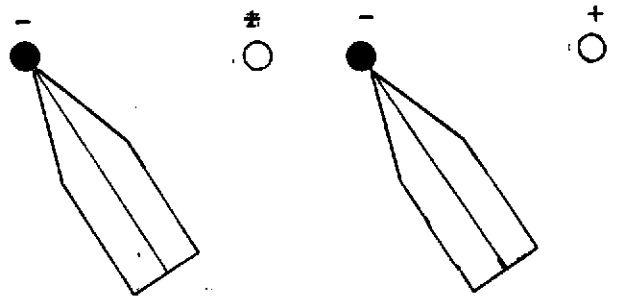

switch in (-),(-) position

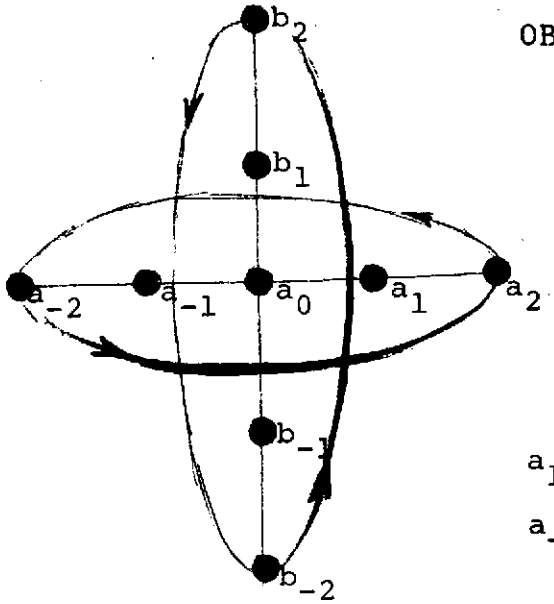

OBSERVER FACES ARRAY

$a_{1,2}$ & $b_{1,2}$ recede into page

$a_{-1,-2}$ & $b_{-1,-2}$ come out of page

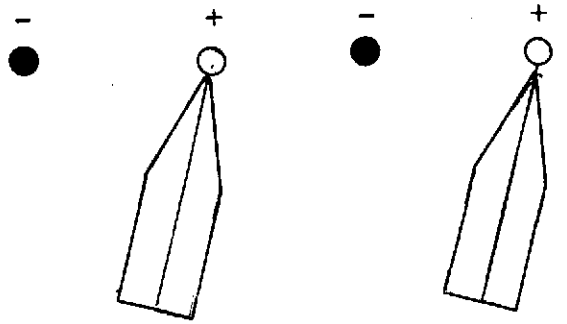

switch in (+),(+) position

FIG. 3 Phase Shift Selector Switch

The crucial point is that the above relation for α (or β) is independent of the frequency and is completely set by the design parameters (absolute phase shift and d).

The calibration of the instrument (dial reading vs. steering angle) is shown in Figure (4)

SHADING (TCHEBYCHEFF CORRECTION)

For five transducers per arm, the weight of the coefficients are as indicated below. The value of d/λ is 0.75 .

b_{-2}	----------	0.46
b_{-1}	----------	0.82
b_{+1}	----------	0.82
b_{+2}	----------	0.46
a_{-2}	----------	0.46
a_{-1}	----------	0.82
a_{0}	----------	1.00
a_{+1}	----------	0.82
a_{+2}	----------	0.46

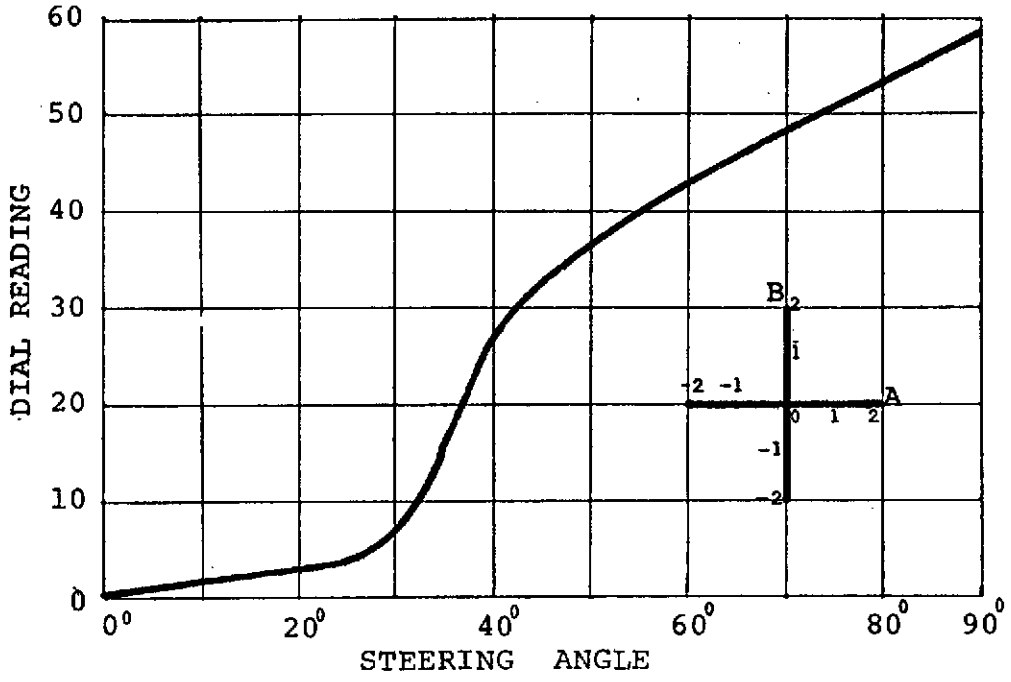

Figure (4)

Instrument Calibration Curve

CALIBRATION AND TESTING PROCEDURE

Calibration is preferably done in an anechoic chamber.

(1)- For $(d/\lambda)=0.75$ and f=500 Hz the microphones are seperated by d=19" (48.6 cm), (where d is the distance between adjacent microphones).

(2)- Mount the nine microphones on a right angle cross (Figure (1)). Each arm of the cross consists of five microphones. Label the arms, "A" for the horizontal and "B" for the vertical. Label the microphones, a_n and b_m where n & m are 0 to 2 . Set the antenna to face a loud speaker 20 ft (6 m) away (or more).

(3)- Tune the loud speaker to 500 Hz and the output of any microphone to not more than 30 mv .

(4)- Short circuit the filters connections at the A & B output terminals (found at the back), as long as only one frequency is being used.

(5)- Switch on the power supply to model 909B .

(6)- Connect all nine microphones to their corresponding terminals at the back of model 909B .

(7)- Measure the input to each microphone using its marked tap at the back of the instument. Adjust this input to reasonable value (e.g. 12 mv), not more than 30 mv , using the adjusting screws above the microphone terminals .

(8)- Turn both dials of channels A & B (located at front) anti clockwise until they click. The antenna is now in the (0,0) position with its plane parallel to the incident palne wave front.

THE INSTRUMENT IS NOW READY FOR TESTING WITHOUT SHADING

IF SHADING IS REQUIRED THEN INSTEAD OF STEP (7) THE INPUT TO THE MICROPHONES SHOULD BE WEIGHED BY TSCHEBYCHEFF CORRECTION FACTORS FOUND IN THE TABLE ON PAGE 7.

(9)- Connect the output of the instrument (found at the back) to a chart recorder.

(10)- With the antenna in the (0.0) position (step 8, above) turn both arms A & B mechanically through 360° and record the output.

(11)- Repeat step (10) while dial A is turned to a reading corresponding to a specific steering angle (using the calibration curve, mounted on the instrument, and also reproduced in Figure (4) of this manual. The recorded output should be the same as in step (10) rotated through the steered angle. Notice any discrepancy and make necessary correction.

(12)- Repeat step (11) using dial B alone.

THE INSTRUMENT IS NOW READY FOR USE.

The following steps may be made if desired.

(13)- Check the output of a_n & b_m ; each one should be equal to the sum of the output of the microphones in the corresponding arm. If not, check the individual microphone circuits.

(14)- Compare the output of each arm alone with the output of their product, using a CRT. The product has an amplitude less than the amplitude of each arm alone, and a frequency which is double the input frequency.

A NEW MODEL 909C provides an output frequency , same as the input.

IT IS VERY IMPORTANT TO CONNECT APPROPRIATE VARIABLE FILTERS TO THE OUTPUTS OF Σa_n & Σb_m WHEN THE INPUT IS NOISY OR NOT-MONOCHROMATIC, THESE FILTERS MUST BE TUNED TO THE PROPER FREQUENCY UNDER TEST.